

SEPARATION AND ANALYSES OF PETROLEUM RESIDUES

J. F. McKay, P. J. Amend, P. M. Harnsberger, T. E. Cogswell, and D. R. Latham

Laramie Energy Research Center
Energy Research and Development Administration
P. O. Box 3395, University Station
Laramie, Wyo. 82070

INTRODUCTION

Petroleum residues are a valuable raw material for the production of fossil fuels. The efficient utilization of this resource requires knowledge of the chemical composition of the residue. The composition work described here is an extension of previous work involving the separation and analyses of high-boiling petroleum distillates (1) and residues (2). The purpose of this paper is 1) to describe the separation of residues, using modifications of techniques previously developed for the separation of high-boiling distillates, 2) to obtain compositional data on the residues, and 3) to compare the composition of the residues and high-boiling distillates.

Much of the characterization work on petroleum residues and asphalts has been performed on unseparated samples (3-6). The separation of these high-molecular-weight mixtures became possible as chromatographic techniques were developed. Kleinschmidt (7) developed a method to separate asphalts into fractions of asphaltenes, water white oils, dark oils, and asphaltic resins. The separation of asphalts using the method of Corbett (8) produces fractions of saturates, naphthene-aromatics, polar aromatics and asphaltenes. The "SARA" method developed by Jewell and co-workers (9) separates petroleum residuals into fractions of saturates, aromatics, resins, and asphaltenes. Bungler (2) modified the separation techniques developed by API Project 60 (1) to separate both tar sand bitumens and petroleum residues.

This paper describes the separation of petroleum vacuum residues that do not distill at a boiling point of 675 °C (corrected). The residue was separated into acids, bases, neutral nitrogen compounds, saturate hydrocarbons, and aromatic hydrocarbons, using ion exchange, complexation, and adsorption chromatography. Acids and bases are removed from the residue with ion exchange resins. Neutral nitrogen compounds are isolated by complexation with ferric chloride adsorbed on Attapulugus clay. Saturate and aromatic hydrocarbons are separated using silica gel. These separations have been applied to residues from four crude oils. Elemental analyses of the major fractions obtained from these separations are discussed. The composition of residues from four oils are compared, and the composition of a residue is compared with the composition of high-boiling distillates from the same crude oil.

EXPERIMENTAL

Reagents

Amberlite IRA 904 and Amberlyst 15, the anion- and cation-exchange resins, were obtained from Rohm & Haas. The Attapulugus clay (LVM, 50/80 mesh) was obtained from Engelhard Minerals and Chemicals Corp., and the silica gel (grade 62, 60/200 mesh) came from Davidson Chemical Co. Reagent-grade ferric chloride hexahydrate and potassium hydroxide were obtained from Baker and Adamson Co. Cyclohexane and n-pentane (99%, Phillips Petroleum) were purified by flash distillation and by percolation through activated silica gel; benzene, methanol, and 1,2-dichloroethane (reagent grade, Baker and Adamson) were flash distilled; isopropyl amine (reagent grade, Eastman) was used as received.

Apparatus

The separations were made on a liquid chromatographic column 1.4-cm i.d. by 119-cm long. The column was water jacketed and contained a recycling arrangement that permits the continuous elution of the sample without the need for large quantities of solvent. Solvent was removed from the fractions using a rotary evaporator followed by a nitrogen gas sweep at steam-bath temperature until a constant sample weight was obtained.

Preparation of Petroleum Residues

Petroleum residues representing portions of crude oils that did not distill at a boiling point of 675 °C (corrected) were prepared at the Bartlesville (Okla.) Energy Research Center (10). The residues were prepared by vacuum distillation of crude oils in a wiped-wall still at 5×10^{-3} torr and 296 °C. Thermal exposure of the oil to heated surfaces was minimized by short residence time, and no decomposition was detected during these distillations. Vacuum residues from four crude oils--Wilmington (Calif.), Gach Saran (Iran), South Swan Hills (Alta.), and Recluse (Wyo.)--were prepared.

Preparation of Resins and Adsorbents

Anion-Exchange Resin. - Amberlite IRA 904 resin (1000 g) was placed in a glass column and activated by the following procedure. The initial washes were made with 1 N hydrochloric acid (7.8 liters) and distilled water (2.0 liters), using a flow rate of 8 bed volumes per hour. The resin was activated using 1 N sodium hydroxide (7.8 liters). This washing sequence was repeated, starting with hydrochloric acid. The resin was then washed with distilled water (2.0 liters). Final preparation of the resin was made by washing with the following solvent sequence: 75% water-25% methanol (1.0 liter); 50% water-50% methanol (1.0 liter); 25% water-75% methanol (1.0 liter); methanol (2.0 liter); benzene (3.0 liter); cyclohexane (3.0 liter). The resin was stored under cyclohexane. (Important: Do not allow resin to dry or to be exposed to heat.)

Cation-Exchange Resin. - Amberlyst 15 resin was prepared in the manner described for the anion resin with the exception that the acid-base washing sequences were reversed.

Ferric Chloride on Attapulgus Clay. - Ferric chloride hexahydrate (10 weight percent in methanol) was contacted with Attapulgus clay for 1 hour. The ferric chloride-Attapulgus clay was filtered, washed several times with cyclohexane, extracted with cyclohexane for 24 hours in a Soxhlet extractor to remove nonadsorbed metallic salt, and dried at room temperature. The material contained 0.7 to 2.0 percent by weight of iron.

Silica-Gel Adsorbent. - The Davidson Chemical Co. grade 62 silica gel was used as received.

Separation Procedure

The separation procedure is shown in Figure 1. The residues are separated into five fractions: acids, bases, neutral nitrogen compounds, saturate hydrocarbons, and aromatic hydrocarbons. Acids are isolated using anion-exchange resin, bases with cation-exchange resin, and neutral nitrogen compounds by complexation with ferric chloride adsorbed on Attapulgus clay. The remaining hydrocarbon fraction is separated on silica gel to produce saturate and aromatic hydrocarbon fractions.

Anion-Exchange Chromatography. - A sample of residue (20 g) was dissolved in cyclohexane (250 ml) and charged to the resin (60 g) that had been wet-packed in the column. Unreactive material was washed from the resin with cyclohexane (200 ml) for approximately 12 hours, using the recycling arrangement of the column. After removal of the unreactive materials, the reactive compounds (acids) were recovered by successive 12- to 24-hour elutions with benzene, followed by 60% benzene-40% methanol (azeotrope). The resin was then removed from the column and placed in a Soxhlet extractor. A final elution was then made with 80% benzene-20% methanol saturated with carbon dioxide. These three solvents remove compounds of increasing acid strength, and the fractions can be analyzed separately or combined to give a total acid fraction. The data reported in this paper were obtained on the total acid fraction.

Cation-Exchange Chromatography. - The procedure for the removal of the bases was similar to that used for the removal of acids. The sample of acid-free residue was dissolved in cyclohexane and charged to the A-15 resin that had been wet-packed in the column. Unreactive material was washed from the resin with cyclohexane (200 ml) for approximately 12 hours. The reactive material (bases) was removed from the resin by successive 12- to 24-hour elutions with benzene, followed by 60% benzene-40% methanol. A final elution was made in a Soxhlet extractor using 54% benzene-38% methanol-8% isopropyl amine. The three base fractions were combined to give a total base fraction.

Ferric Chloride Coordination Chromatography. - Ferric chloride-Attapulugus clay (280 g) suspended in cyclohexane was wet-packed in a column. A sample of acid- and base-free residue (10 g), dissolved in cyclohexane, was slowly percolated through the column. The entrained oil was removed by 24-hour elution with cyclohexane. The first fraction was desorbed from the clay by 60- to 72-hour elution with 1,2-dichloroethane. The nitrogen compound-ferric chloride complexes in this fraction were broken by passing the 1,2-dichloroethane solution over anion-exchange resin contained in a second column. The ferric chloride salt was retained on the resin, and the nitrogen compounds were recovered in the eluate. A second fraction was removed from the clay by 60- to 72-hour elution with 45% benzene-5% water-50% ethanol (1000 ml). The solvent was removed, and the organic compounds were redissolved in benzene and then filtered; the solvent was again removed to eliminate traces of water and ethanol. The organics were redissolved in benzene and passed over anion-exchange resin to remove ferric chloride. The nitrogen compounds were recovered in the eluate. The two subfractions were combined to give a total neutral nitrogen fraction.

Silica Gel Chromatography. - A portion of the acid-, base-, and neutral nitrogen-free residue (300 mg) was dissolved in n-pentane (10 ml) and was placed¹ on a silica gel column (90 g) that had been wet-packed with n-pentane. The column was eluted with n-pentane (600 ml) to remove the saturate hydrocarbons. Aromatic hydrocarbons were eluted from the column, using 85% n-pentane-15% benzene (400 ml), and 60% benzene-40% methanol (300 ml). The two aromatic subfractions were combined to form a total aromatic hydrocarbon fraction. Ultraviolet analyses of the saturate fraction indicated that trace amounts of aromatic hydrocarbons were present. The amount of saturates in the aromatic fraction, if any, is unknown.

RESULTS AND DISCUSSION

The four crude oils used in this work were obtained through a sampling program conducted by API Research Project 60 and were selected for study because they represent crude oils having different geological classifications (11). The separation and analyses of the residues from these particular oils allows us to 1) demonstrate the applicability of the separation scheme to the separation of 675 °C residues predicted to have large differences in composition and 2) compare the composition of the 675 °C residues with the composition of high-boiling distillates from the same oils.

Table 1 shows the weight percent of the crude oils that does not distill at a corrected boiling point of 675 °C. The amount of residue is different for each crude oil, reflecting differences in composition of the crude oils. For example, the Wilmington crude oil contains 22 percent residue and the South Swan Hills crude oil contains 3 percent residue. The percentages of residual material in some of the crude oils are an indication of the large potential amounts of fossil fuel contained in the residue portion of the oils.

TABLE 1. - Weight percent of 675 °C residue in crude oils

Crude oil	Wt. percent
Wilmington, Calif.	22
South Swan Hills, Alta.	3
Gach Saran, Iran	16
Recluse, Wyo.	4

Table 2 shows the results of the separation of the four residues. The residues have large differences in composition. For example, the Wilmington and Gach Saran residues contain large amounts of polar materials--acids, bases, and neutral nitrogen compounds. In contrast, the South Swan Hills and Recluse residues contain smaller amounts of these compounds and larger amounts of hydrocarbons. The residues having a large polar compound content have more aromatic than saturate hydrocarbons; residues that are low in polar compound content have more saturate than aromatic hydrocarbons. The data in the table also show that the total amounts of acids and bases are variable from oil to oil and the amounts of acids are equal to or less than the amounts of bases. The duplicate separation of the Gach Saran residue indicates that the separation is reproducible. In general, the recovery of material after separation was 90 percent or better.

TABLE 2. - Composition of 675 °C petroleum residues

Crude oil	Weight percent					Recovery
	Acids	Bases	Neutral nitrogen compounds	Saturate hydrocarbons	Aromatic hydrocarbons	
Wilmington, Calif.	18	19	41	4	15	97
Gach Saran, Iran						
Run #1	17	25	14	8	30	94
Run #2	16	23	16	7	25	87
S. Swan Hills, Alta.	12	13	10	34	27	96
Recluse, Wyo.	9	10	8	44	26	97

The information in tables 1 and 2 shows that when a crude oil has a high 675 °C residue content most of the residue will be composed of acids, bases, and neutral nitrogen compounds. Conversely, when a crude oil has a low 675 °C residue content the composition of the residue will be mostly hydrocarbons.

Table 3 shows elemental analyses data for the total Wilmington residue and the separated fractions. Carbon and hydrogen ratios (C/H) are shown in the first column. The polar fractions show a C/H of from 0.72 to 0.74, and the saturate hydrocarbon fraction shows higher hydrogen content with a value of 0.56. The value of .66 for the aromatic hydrocarbons indicates the larger degree of unsaturation of this fraction relative to the saturate hydrocarbon fraction. The acids

are high in nitrogen and oxygen, and the bases are high in nitrogen. The neutral nitrogen compounds are lower in nitrogen than either the acid or the base fractions and may contain compounds other than nitrogen compounds. The separation scheme was effective in removing nitrogen compounds in the polar fractions--only 6 percent of the original nitrogen remained in the hydrocarbon fractions. The saturate hydrocarbons are essentially free of heterocompounds. The aromatic hydrocarbons contain small amounts of nitrogen and oxygen compounds and larger amounts of sulfur compounds. Sulfur is rather evenly distributed in polar and aromatic hydrocarbon fractions, indicating that sulfur compounds have not been concentrated in any of the fractions. The amount of nitrogen, oxygen, and sulfur in the total residue was compared with the sum of the nitrogen, oxygen, and sulfur in the fractions. The nitrogen and sulfur in the total residue equalled the sum of the amounts found in the separated fractions. The analyses for oxygen appear to be in error because 50 percent more oxygen was found in the fractions than was found in the total residue (oxygen analyses on small samples have not been reproducible).

TABLE 3. - Elemental analyses of Wilmington 675 °C residue and residue fractions

Sample	C/H	Percent carbon	Percent hydrogen	Percent nitrogen	Percent sulfur	Percent oxygen
Total residue	.72	84.50	9.73	1.62	2.57	1.46
Acids	.74	80.23	9.09	2.33	2.53	5.53
Bases	.72	83.17	9.64	1.96	2.31	2.67
Neutral nitrogen compounds	.74	83.02	9.36	1.78	2.71	1.30
Saturate hydrocarbons	.56	85.48	12.69	0.11	0.82	0.81
Aromatic hydrocarbons	.66	85.34	10.76	0.63	2.37	0.74

Table 4 shows a comparison of the composition of the residue with the composition of two high-boiling distillates from Wilmington crude oil. The data for the distillates were reported in an earlier publication (12). The weight percent of acids, bases, and neutral nitrogen compounds increases with the increase in boiling range. The weight percent of saturate and aromatic hydrocarbons decreases with increasing boiling range.

TABLE 4. - Composition of Wilmington residue and distillates

Sample	Weight percent		
	370-535 °C distillate	535-675 °C distillate	675°C residue
Acids	5.6	9.3	18.0
Bases	6.8	12.7	19.0
Neutral nitrogen compounds	4.2	21.3	41.0
Saturate hydrocarbons	36.9	20.8	4.0
Aromatic hydrocarbons	46.5	36.0	15.0

CONCLUSIONS

The separation procedure described in this paper can be used to separate 675 °C residues having large differences in composition. The procedure provides useful information concerning the composition of the residues. For example, the South Swan Hills residue, which contains small amounts of acids and bases and large amounts of hydrocarbons relative to the Wilmington residue would be predicted to be more easily refinable than the Wilmington residue. The separation of the residue into chemically meaningful fractions lays the groundwork for further characterization according to compound type.

SUMMARY

Vacuum residues from four crude oils have been separated into fractions of acids, bases, neutral nitrogen compounds, saturate hydrocarbons, and aromatic hydrocarbons. The separation scheme was a modification of a separation scheme originally developed for separating high-boiling petroleum distillates. Elemental analyses were obtained for the residue fractions. The compositions of four residues were compared, and the composition of the Wilmington residue was compared with the composition of Wilmington high-boiling distillates.

REFERENCES

1. D. M. Jewell, J. H. Weber, J. W. Bunker, H. Plancher, and D. R. Latham, *Anal. Chem.* 44, 1391 (1972).
2. J. W. Bunker, Preprints, Div. of Fuel Chemistry, Amer. Chem. Soc., 19 (2), Los Angeles, Calif., April 1974, p. 231.
3. R. V. Helm and J. C. Petersen, *Anal. Chem.* 40, 1100 (1968).
4. J. W. Ramsey, F. R. McDonald, and J. Claine Petersen, *Ind. Eng. Chem. Prod. Res. and Devel.* 6, 231 (1967).
5. F. E. Dickson, B. E. David, and R. A. Wirkkala, *Anal. Chem.* 41, 1335 (1969).
6. D. Burton and E. Beitchman, *J. of Res. Nat. Bur. Stand.* 63A (2), 189 (1959).
7. L. R. Kleinschmidt, *J. Res. Nat. Bur. Stand.* 54, 163 (1965).
8. L. W. Corbett, *Anal. Chem.* 41, 576 (1969).
9. D. M. Jewell, E. W. Albaugh, B. E. Davis, and R. G. Ruberto, *Ind. Eng. Chem. Fundam.* 13 (3), 278 (1974).
10. H. J. Coleman, J. E. Dooley, D. E. Hirsch, and C. J. Thompson, *Anal. Chem.* 45, 1724 (1973).
11. J. F. McKay, T. E. Cogswell, J. H. Weber, and D. R. Latham, *Fuel* 54, 50 (1975).
12. Haines, W. E., and C. J. Thompson, ERDA Rept. of Inv., LERC/RI-75/5 and BERCI/RI-75/2, July 1975, 30 pp.

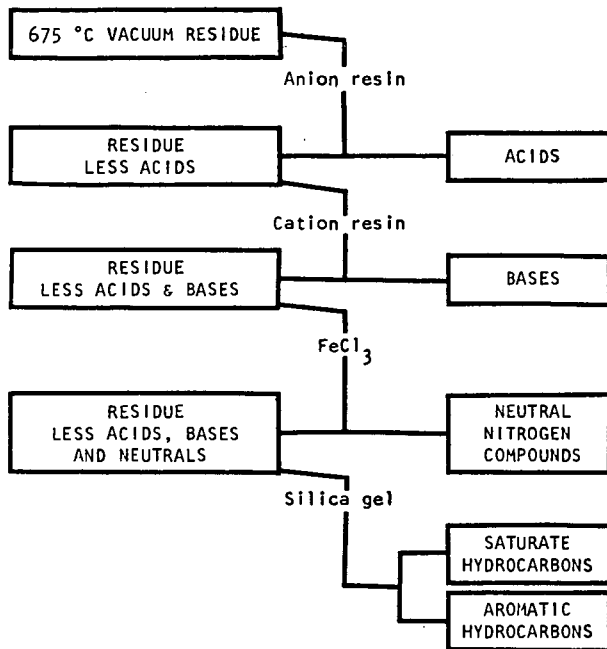


Figure 1. - SEPARATION SCHEME

COMPETITIVE HYDROGENATION OF MODEL HETEROCYCLES AND OF POLYNUCLEAR AROMATICS

Louis D. Rollmann

Mobil Research and Development Corp.,
Central Research Division
P. O. Box 1025, Princeton, N. J. 08540

Comparison of hydrodesulfurization catalysts is generally complicated by the presence of diffusion effects and by the problems associated with laboratory trickle bed reactors (1). The importance of diffusion is underscored by the numerous patents and publications dealing with effects of pore size distribution (2), diffusivity (3), and porosity (4). Contacting effectiveness in trickle bed reactors was recently reviewed both in terms of liquid hold-up and of catalyst wetting characteristics (5).

In order to eliminate the effects of diffusion and of reactor design and to examine the chemistry and the relative rates of the reactions associated with commercial hydrodesulfurization, conversion of a series of model feed mixtures was studied over a conventional CoMo catalyst (6). Components of the feeds were chosen to be representative of the various chemical types found in petroleum, in shale oils, in coal oils, and the like. For sulfur species, sulfides and fused ring thiophenes were studied (7); for nitrogen, quinolines and indoles (8,9); and for oxygen, phenols, fused ring furans, and carboxylic acids (8,10).

For a conventional CoMo catalyst (6) it was found that NSO compounds could be grouped by chemical type, both with respect to the relative rates and to the mechanisms of heteroatom removal. More important, the behavior experienced with these model feed mixtures closely paralleled that known for actual heavy petroleum charge stocks. The hydrogen consumed in the "hydrodesulfurization" of coal oils, shale oils, and petroleum residua could be estimated from their heteroatom content and from the mechanistic data provided by the models.

In the following pages, these phenomenological studies on model feeds are extended to other catalysts, to NiMo as well as CoMo, to Mo-only catalysts. Again a comparison is drawn between the behavior of model feeds and that observed with actual charge stocks.

Experimental

Four catalysts were used in these experiments and are described in Table I. All were commercial samples, HDS-2 (CoMo, American Cyanamid), HDS-1441 (SiO₂-stabilized CoMo, Amer. Cyanamid), HDS-3 (NiMo, Amer. Cyanamid), and Mo-1201T (Mo-only, Harshaw). Each was sized to 60/80 mesh for testing.

Details of the hydrogenation apparatus, a high-pressure trickle bed reactor, were given earlier (6). Presulfiding was at 180°C, 2 hours, in a 20% H₂S in H₂ stream. Reaction conditions were 344°C, 700 psig, WHSV=2, H₂/feed=8. (~6500 SCF/bbl.)

Table I
Selected Hydrodesulfurization Catalysts

Catalyst	<u>HDS-2</u>	<u>HDS-1441</u>	<u>HDS-3</u>	<u>Mo-1201T</u>
Weight Percent				
CoO	4.5	2.8	-	<0.1
NiO	<0.1	-	2.8	-
MoO ₃	12.7	10.3	12.2	10.1
SiO ₂	<0.1	4.9	-	0.0
Surface Area, m ² /g	280	280	190	150
Pore Volume, cc/g	0.58	0.57	0.60	0.37
Part. Density, g/cc	1.15	1.13	1.09	1.48
Real Density, g/cc	3.40	3.19	3.15	3.29
Pore Diam., Å	82	83	128	98
Pore Distribution (N ₂),%				
<25Å radius	18	17	7	13
25-50	27	32	13	21
50-100	19	27	19	22
100-200	12	16	23	13
200-300	3	2	10	4
>300	21	6	27	27

Table II
Feed Compositions

Standard feed:	<u>Moles</u>	<u>Weight Percent</u>
Dibenzothiophene	1.0	10.4
Dibutylsulfide	1.0	8.2
Quinoline	1.0	7.3
Dibenzofuran	1.0	9.5
Naphthalene	1.0	7.2
2-Methylnaphthalene	2.0	16.0
2,3-Dimethylnaphthalene	1.0	8.8
Hexadecane	1.5	19.1
1,2,4-Trimethylbenzene	2.0	13.5
Substitute components:		
Benzothiophene	p-Cresol	
Indole	4-Propylphenol	
2,3-Benzofuran	2-Ethylphenol	
2-Phenylphenol		

Both elemental and gas chromatographic analyses were obtained on all samples, as described earlier (6). Hydrogen consumption values were calculated from elemental analysis.

Results

Rate data. The feed compositions are detailed in Table II and represent an attempt to simulate the chemical composition of petroleum-type charge stocks while maintaining equimolar ratios of individual reactants. The standard feed contained 3.61% sulfur, 0.79% nitrogen, 0.90% oxygen, 8.79% hydrogen and 85.91% carbon. In general, only one feed component was changed at a time when comparing the relative rates and mechanisms of heteroatom removal. The total number of moles in the feed was held constant.

In the present study conversion data were determined at 344°C and at fixed hydrogen partial pressure (640 psia), a detailed examination of the effects of process variables on the relative first-order rate constants having been reported earlier (6). Under the above reaction conditions, naphthalene conversion to tetralin approached an equilibrium value of 96.9% (11). Decalin was not produced.

Initial conversion of the various components changed rapidly with time on stream as shown by the example in Figure 1 but reached a stable level after several days on stream. In the time required to reach a "stable" behavior each catalyst was unique. The SiO₂-promoted catalyst for example exhibited a stable conversion almost immediately. The important observation is contained in Table III, where it is shown that all three CoMo and NiMo catalysts, once stable, were remarkably similar in their behavior. The relative rate constants for conversion of the various NSO compounds never differed by more than a factor of two.

The Mo-only catalyst on the other hand was unique. In the absence of Co or Ni, deN activity was maintained but aromatics saturation and, particularly, deS activity declined markedly. Relative to those observed with a CoMo catalyst (HDS-2), rate constants over Mo-1201T were 0.8, 0.2 and 0.02 for the reaction of quinoline, of naphthalene, and of dibenzothiophene respectively.

Product distributions. The similarity in rate of the CoMo and NiMo catalysts was further reflected in the products of heteroatom removal. Desulfurization reactions require little discussion, all stable CoMo and NiMo catalysts converting benzothiophene to ethylbenzene and dibenzothiophene to biphenyl in over 90% selectivity. Mercaptan sulfur in the products rarely approached 100 ppm indicating that the initial thiophene ring opening, and not thiol hydrogenation, was rate-limiting. This suggestion is supported by the high reactivity of thiophenol (6).

Nitrogen and oxygen removal are more complex reactions, reactions nevertheless common to this group of catalysts. Both indole and quinoline produced the corresponding alkylcyclohexanes in over

Table III

Relative Rate Constant for Conversion700 psig, H₂/feed = 8, 344°C

	<u>HDS-2</u>	<u>HDS-1441</u>	<u>HDS-3</u>
Rate Constants ^a			
2-Methylnaphthalene ^b	1.0	1.1	1.0
2,3-Dimethylnaphthalene ^b	1.4	1.2	1.3
Dibenzothiophene	3.6	6.3	5.0
Benzothiophene	3.4	6.2	6.0
Indole	0.9	0.9	1.2
Quinoline	1.3	1.7	2.2
2,3-Benzofuran	1.0	1.1	1.0
o-Ethylphenol	1.2	-	-
Dibenzofuran	0.4	0.3	0.3
2-Phenylphenol	1.4	1.4	1.8
p-Cresol	5.2	7.2	-
4-Propylphenol	-	7.6	-

a--Relative to naphthalene; reproducibility, ±20%

b--Assumes equilibrium conversion is 97% at 344°C

90% selectivity. In both cases the rate determining step was saturation of the aromatic ring in the o-alkylaniline intermediate, as evidenced both by gas chromatography and by analysis for basic nitrogen, indole being non-basic (9).

Oxygen removal proceeded with similar saturation of the aromatic ring. Benzofuran and the various alkylphenols all yielded alkylcyclohexanes in over 90% selectivity. Phenol analysis of the benzofuran products identified phenol hydrogenation, not furan ring opening, as the rate determining step.

Commercial feeds. Such uniformity of catalyst behavior makes possible an extension of these results to feeds which are not well characterized. The summary in Table IV shows that the hydrogen consumed in removal of any given heteroatom can be estimated without a detailed knowledge of the chemical form of the undesired species. Thus, sulfur removal requires ~110 SCF/bbl of H₂; nitrogen, ~650; and oxygen (phenolic as in coal oils), ~400.

In Table V these projections are tested with actual commercial feeds, a resid (high S), a shale oil (high N), and a coal oil (high O). Two comments are appropriate to these data. First, although the quantitative distribution of heteroatom types in these feeds is not known, the relative reactivities of the NSO-species generally reflect the behavior observed with model feeds.

Table IV

Summary of Behavior CoMo and NiMo Catalysts344°C, 700 psig, H₂/feed = 8

<u>Chemical Species</u>	<u>Relative Rate Constant^a</u>	<u>Moles H₂/heteroatom</u>	<u>Hydrogen Consumed^b</u>
Sulfides	>50	2	90 SCF
Benzothiophene	5	3	130
Dibenzothiophene	5	2	90
Indole	1.1	6	600
Quinoline	1.7	7	700
p-Alkylphenol	6	4	350
o-Alkylphenol	1.5	4	350
Benzofuran	1.1	6	530

a--Relative to naphthalene, ±20%

b--Hydrogen consumed for each 1.0% heteroatom removed, assuming a change stock density of 1.0g/cc

Table V

Commercial Feed Data for CoMo, NiMo, NiW Catalysts

<u>Feed</u>	<u>Arab Light atm. resid^c</u>	<u>Shale Oil, NTU-type (12)</u>	<u>Utah Coal Oil (13)</u>
N, %	0.2	2.0	1.0
S, %	3.6	0.9	0.3
O, %	0.1	a	6.6
Pressure, psig.	700	3000	2500
H ₂ circ., SCF/B	9500	6000	15000
Temp., °C	399	375	397
LHSV	2.3	0.5	1.0
deS	80	89	99 ⁺
deN	36	65	67
deO	-	-	80
H ₂ Consumption, SCF/B	520	1000	2240
Calculated H ₂ ^b , SCF/B	370	870	2290

a--Not given

b--From NSO removal and data in Table IV

c--Present work

More important, over 70% of the hydrogen consumed in the processing of these three commercial charge stocks could be accounted for in terms of NSO removal. The remainder is primarily associated with the saturation of polynuclear aromatics.

Conclusions

Studies with model feed mixtures, mixtures selected to reflect the NSO-content and chemical type distribution found in resids, shale oils, and coal oils, showed that the behavior of a series of CoMo and NiMo catalysts became increasingly similar as the catalysts aged. As is known in the literature (14-18), desulfurization and aromatics hydrogenation activity were substantially reduced in the absence of Co or Ni. Nitrogen removal, however, was little changed.

The results showed that NSO-compounds can be grouped according to reactivity in the order:

Sulfides >> p-alkylphenols > benzothiophenes > quinoline ~
o-alkylphenols ~ indoles ~ benzofurans ~ naphthalenes > dibenzofurans
>> mononuclear aromatics.

Examination of the products of hydrogenation indicated that these NSO-compounds fall into two categories in terms of the mechanism of heteroatom removal. Sulfur compounds (sulfides, fused ring thiophenes) were readily cleaved to give H₂S and alkane or aromatic respectively. With N- and O- species, saturation of any aromatic ring attached to the heteroatom was required prior to C-N or C-O bond scission.

Hydrogen consumption values were determined for NSO- removal from the model compounds, and the values were projected onto the observed behavior of atmospheric resids, coal oils and shale oils.

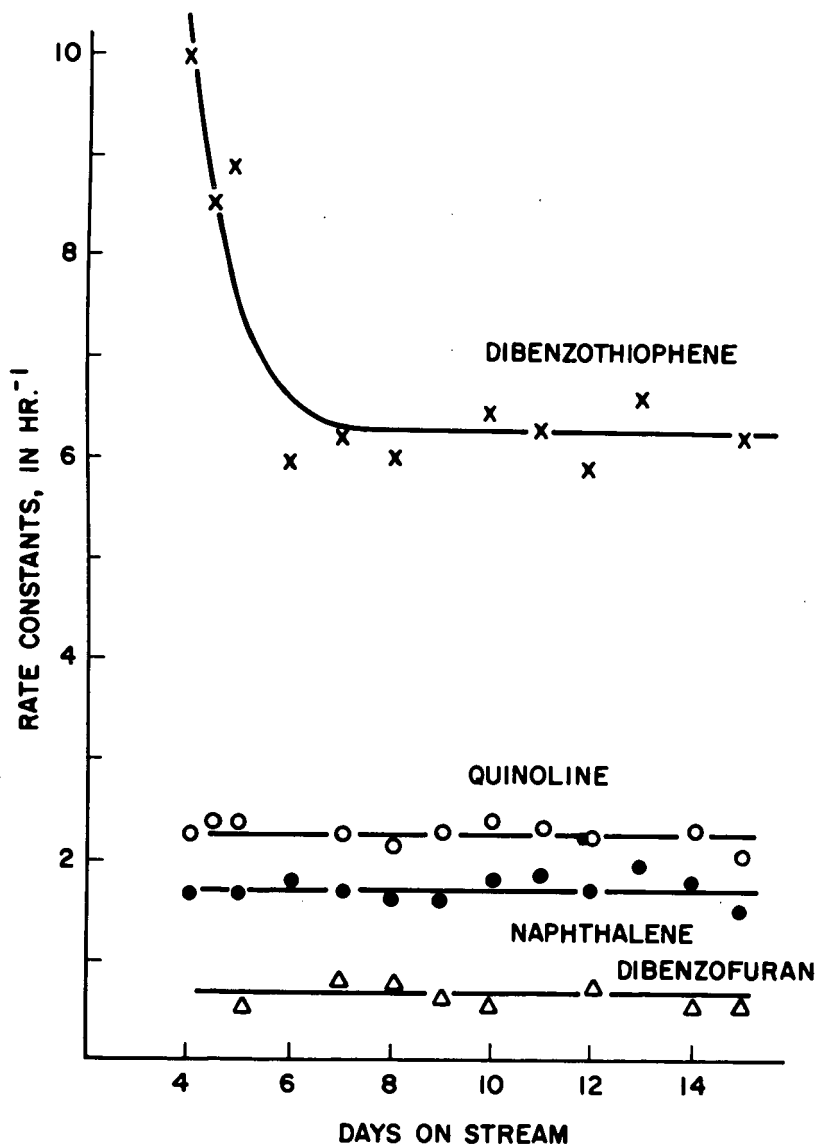
Acknowledgement

The helpful suggestions of D. Milstein and R. H. Fischer, Mobil's Paulsboro Laboratory, and the technical assistance of R. R. Jones, Mobil Central Research Laboratory, have been greatly appreciated.

References

1. O. Weisser and S. Landa, Sulphide Catalysts, Their Properties and Applications, Pergamon Press, 1973.
2. H. Beuther and B. K. Schmid, Sixth World Petroleum Congress, Section III, Paper 20-PD7, 1963.
3. R. R. Cecil, F. X. Mayer, and E. N. Cart, Jr., 61st AIChE Meeting, Los Angeles, December, 1968.
4. D. Van Zoonen and C. Th. Douwes, J. Inst. petroleum, 49, 383 (1963).
5. C. N. Satterfield, Third Intl. Symp. on Chem. Reaction Eng., Northwestern, August, 1974.
6. L. D. Rollmann, submitted for publication.
7. H. V. Drushel, ACS Preprints, Division of Petroleum Chem., 15 (2), C13 (1970).
8. L. R. Snyder, *ibid.*, 15 (2), C44 (1970).
9. F. P. Richter, P. D. Caesar, S. L. Meisel, and R. D. Offenbauer, Ind. Eng. Chem., 44, 2601 (1952).
10. T. J. Palmer and M. Vahrman, Fuel, 51, 22 (1972).
11. T. P. Wilson, E. G. Caflisch, and G. F. Hurley, J. Am. Chem. Soc., 62, 1059 (1958).
12. W. M. Smith, T. C. Landrum, and G. E. Phillips, Ind. Eng. Chem., 44, 586 (1952).
13. J. F. Jones, M. R. Schmid, M. E. Sacks, Y-C. Chen, C. A. Gray, and R. T. Eddinger, OCR Tech. Rept., NTIS PB-173 916, Oct., 1965.
14. G. C. A. Schuit and B. C. Gates, AIChE Journal, 19, 417 (1973).
15. A. Aoshima and H. Wise, J. Catalysis, 34, 145 (1974)
16. P. Grange and B. Delmon, J. Less-Common Metals, 36, 353 (1974).
17. H. Beuther, R. A. Flinn, and J. B. McKinley, Ind. Eng. Chem, 51, 1349 (1959).
18. E. Furimsky and C. H. Amberg, Can. J. Chem., 53, 2542 (1975).

FIGURE 1
 RATE CONSTANTS FOR HYDROGENATION
 HDS-2, 700 PSIG, 344°C, H₂/FEED=8



AROMATICITY DETERMINATION OF COAL, OIL SHALE AND THEIR DERIVATIVES BY X-RAY DIFFRACTION

Jonathan T. Kwan and T. F. Yen

University of Southern California
Chemical Engineering Department
Los Angeles, California 90007

INTRODUCTION

X-ray diffraction has been proven to be the most direct and non-destructive analytical method for the structural study of solid samples. The x-ray scattering pattern of coal at the medium and low angle regions reveals two unresolved peaks (1,2). The diffuse peak shifts more to the position of the most prominent graphite-peak (002) as the carbon content of coal increases. This suggests that coal contains small graphite ring clusters, which become more graphite-like as coalification proceeds. Suitable interpreted, the area and shape of the bands will provide insight into certain interesting structural features. By using a blend of low crystallinity polyethylene and carbon black, it demonstrated that aromaticity can be determined semiquantitatively by resolving the two peaks in the x-ray scattering pattern (3). The experimental results have led to the characterization of the structural parameter-- aromaticity in coal, oil shale and their derivatives.

EXPERIMENTAL

A. Instrumentation

The General Electric XRD-6 X-ray Diffractometer unit with copper as the x-ray target was used. The x-ray energy was set at 35 KV and 18 ma for each run. A scanning speed of $4^\circ/\text{min}$ covering the range of 2θ from 5° to 90° was selected. All samples were ground to a 200 mesh size and pressed on a aluminum sample holder. The chart recorder was calibrated to read an exact count per second from the proportional counter.

To achieve monochromatic radiation from the copper source, a balance filter comprised of nickel (Ni) and cobalt (Co) at a thickness of 0.0068 mm and 0.0075 mm respectively, was used. The standard method employed running the experiment first using the Ni filter and then repeating the experiment using a Co filter so that a pass band could be made on the difference of data obtained from each of the runs. The exclusion of wavelengths outside the pass band can be considered practically complete.

B. Procedure

The data from the recorder must be corrected for polarization effects, normalized to electron units, corrected for incoherent scattering, and examined for the effects of background radiation (4,5). In summary, a usable procedure for handling the data is the following:

1. Obtain data values from the differences between Ni and Co filter experiment.
2. Adjust data for polarization by dividing each intensity by $(1 + \cos^2 2\theta)/2$.
3. Adjust the data to electron units by normalizing the amplitudes in the region $0.40 \leq \sin\theta/\lambda \leq 0.50$ is equal to the sum of the coherent and incoherent scattering expected in that range.
4. Subtract tabulated values of incoherent scatterings C.
5. Divide each value by the proper value of the independent coherent scattering E (Figure 1).

The data calculations above were performed by an IBM 360/44, and the results then plotted in analog form.

C. Method

The interpretation of the x-ray diffraction results obtained from non-crystalline carbon compounds is based largely on the fact that one can put together some graphite and some paraffin or polyethylene and get an x-ray pattern that relates to

their composition (6). In the development of quantitative methods, some assumptions were involved; e.g. carbon atoms were regarded as either belonging to aromatic ring clusters or randomly distributed; and ring clusters were presumed to be perfect in their internal structure. There are also some problems in defining the two peaks in the range of $\sin \theta / \lambda < 0.2$, namely, the (002) peak and the gamma peak. This region of the x-ray spectrum has not been sufficiently investigated on a theoretical basis, and hence, the interpretation involves the superimposition of diffraction spectra from substances only supposedly understood.

1. The (002) peak

The (002) band is attributed to the interplanar spacing of condensed aromatic rings. In natural graphite, the spacing corresponding to the (002) band is 3.35 Å, (Figure 2) which corresponds to $\sin \theta / \lambda = 0.15$. Different compounds will have different interplanar spacings as shown in Figure 3. The shifts observed in the (002) band in some compounds are shifts toward larger spacings and are attributed to actual changes in interatomic spacing or to the buckling of planes due to substitutions of heteroatoms.

Blayden et al. (7) studied carbonization products of various coals and their banded constituents as well as pure organic compounds. They contended that the asymmetry of the (002) peak was due to the gamma peak even if the gamma peak was absent at its position. Therefore, the peak was resolved into a symmetrical (002) band and a gamma band.

2. The gamma band

The band centered around the spacing of 4.0-5.5 Å is observed in hot paraffin (Figure 4). It is attributed to the spacing between disordered aliphatic chains or alicyclic rings. There seems to be no published criterion for distinguishing between saturated rings and saturated chains based on the shape of the gamma band. The gamma band has been found to be symmetric (3). This becomes a very important point when one tries to separate the gamma band from the (002) aromatic band on the basis of arguments that defend this symmetry.

Aromaticity, f_a , is the fraction of the total carbon atoms in the sample present in aromatic rings (Figure 5). Implicit in the equation is the assumption that the area under the peaks is proportional to the concentration of each type of structure. The most convincing evidence for the usefulness of this computed aromaticity is from the experiment (6), in which a mixture of half polyethylene and half carbon black was to have an aromaticity of 0.50 ± 0.02 (6).

DATA ANALYSIS

The four coal samples in our study show a reasonable correlation with the coalification process (Sample source and their f_a values are shown in Table I). As carbon number increases with coal ranking, the f_a number also increases (Figures 6a and 6b). More samples will have to be acquired in order to make a more complete correlation. The two domestic oil-rich shales--the Green River Oil Shale (Eocene Shale, 60 million years ago) and Appalachian Black Shale (Ordovician Shale, 400 million years ago) show an increase in f_a number due to its degree of maturation acquired through geological aging. Because of high inorganic interference, for example iron fluorescence from pyrite, both samples must go thru a special treatment process in order to achieve a better form. Acid treatment (50:50 mixture HCl:HF) was used for Green River Oil Shale to remove the inorganic matrix, and LiAlH_4 was used to remove the pyrite from the Appalachian Shale. Another oil shale under investigation is the Torbonite from Australia which is a marine deposit. Its formation age is approximately 250 million years (Permian). It is difficult to compare between lacustrine and coastal oil shale due to the different deposition environment which may be evolved. The next set of data were obtained from the two coal liquids process from FMC-CCED and Synthoil. For analytical reasons, asphaltene was separated from the coal liquid (8). To further fractionate the product, asphaltene was loaded on a SiO_2 glass column, and eluted with ethyl ether and benzene respectively. Polar molecules or aromatic compounds are retained by the column better. The results of x-ray dif-

TABLE I. - Aromaticity of Coals, Shales, and Their Derivatives

Sample	Source	f_a
<u>Coal</u>		
Anthracite	Pennsylvanian	0.86
Low Volatile Bitumenous	West Virginian	0.83
High Volatile Bitumenous	Dorchester	
	Wise Co., Va.	0.64
Lignite	Montana	0.60
<u>Oil Shale</u>		
Torbanite	Coolaway Mtn., New So. Wales	0.12
Green River	Colorado, HF-HCl treated	0.15
Appalachian Black Shale	Plymouth, Ohio LiAlH ₄ treated	0.50
<u>Coal Liquid Asphaltene</u>		
Synthoil (crude)*	U.S.B.M.	0.49
Benzene fraction**		0.43
Ethyl ether fraction**		0.36
COED (crude)*	FMC	0.45
Benzene fraction**		0.43
Ethyl ether fraction**		0.41
<u>Shale Oil Asphaltene</u>		
Synfuel***	Parahoe	0.46
Residual Oil****	Parahoe	0.49

*The crude asphaltene is obtained by n-pentane precipitation, the residue dissolved in benzene, filtered, and freeze-dried.

**Evaluated from SiO₂ column

***Same as (*), oil sample originated from DEI.

****Have been through delayed coking process.

fraction analysis shows lower f_a number for the solvent eluted fraction. Finally, the shale oil asphaltene are listed. Notice that both crude and residual (after coking process) have much higher aromaticity values ($f_a=0.5$) when compared to the original Green River Oil Shale having an $f_a=0.1$. The additional aromaticity naturally originates from the retorting operation.

DISCUSSION

Probably the most difficult separation is the resolution of the (002) and the gamma band. The high angle side of the broad peak is used as a guide to delineate the unresolved slopes of the (002) band, and the remaining intensity is attributed to the gamma band. However, in addition to the use of the high angle side as a guide, it is also necessary to determine a peak for the (002) band. This can be done completely at random, or through fixing a location for the peak. The (002) peak has been fixed as $\sin\theta/\lambda = 0.140$ provided that there is no definite and clear break in the combination of (002) and gamma peaks at a different point. If aromaticities were determined randomly, the error would be approximately 20%. This points out the fact that aromaticities determined by x-ray may be relative and will vary according to the particular location chosen. Further errors may be involved when converting scattering from arbitrary into electron units. Increases in the spacing for the small stacks would give rise to an enhancement of the low angle side of the (002) band at the expense of the high angle side. Thus, the interlayer spacing cannot be regarded as constant. The discrepancy of determination of aromaticity may be attributed to a sim-

plifying assumption involved in the above method that carbon atoms in coals or coal derivatives are either in the aromatic ring clusters or otherwise distributed randomly. It appears that arrangements of organometallics and non-hydrocarbons will lead to the production of a diffuse x-ray interference pattern which may affect the curves. This is a very important consideration since it is extremely difficult to remove the last traces of iron (in pyrite or organic form) from coal or oil shale samples. The fluorescent radiation that is produced forms a considerable proportion of the total x-ray scattering. In some cases, like the Black Appalachian Shale which has a high iron content, the spectrum is masked completely. This is the reason for the treatment of Appalachian Shale samples with LiAlH_4 as a method for the removal of pyrite.

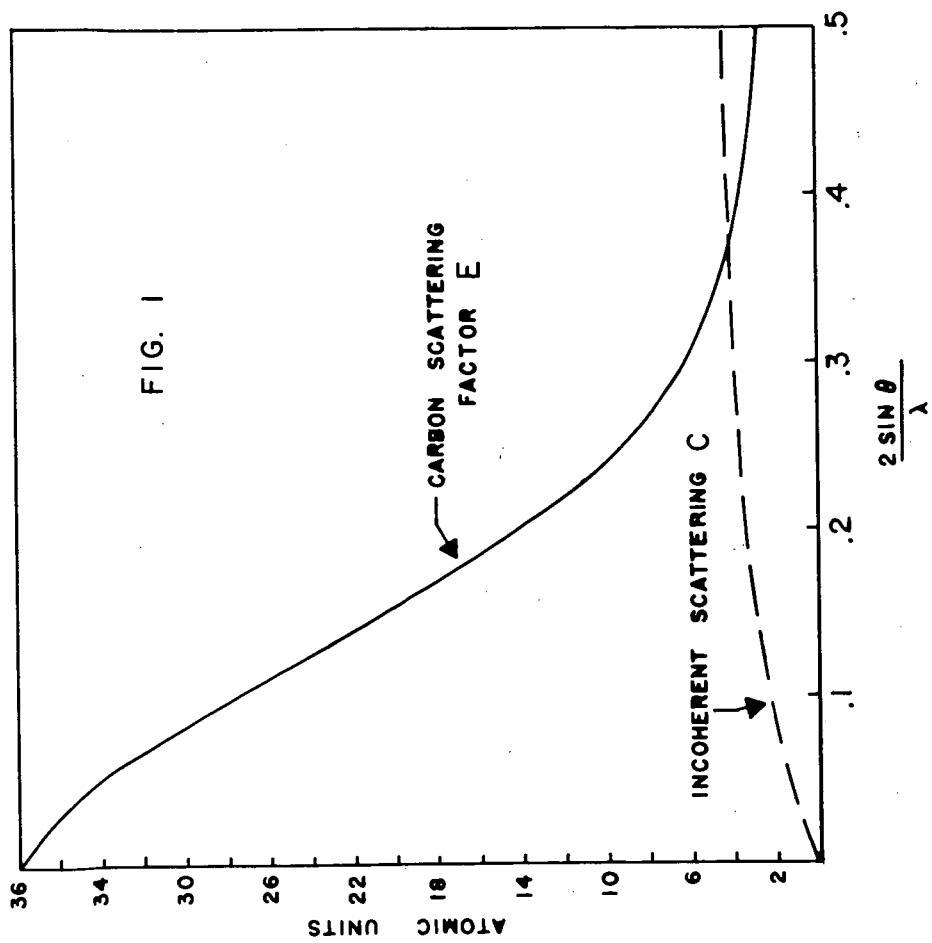
A better understanding of the structure of coal and oil shale and the development of more valid quantitative methods of interpretation of x-ray scattering patterns are more or less interdependent. Investigation of the structure of these materials by other physical and chemical methods (IR, UV, H^1NMR , C^{13}NMR , ESR, chemical oxidation, etc.) will also provide additional information which would improve the techniques and interpretation of amorphous scattering.

ACKNOWLEDGEMENTS

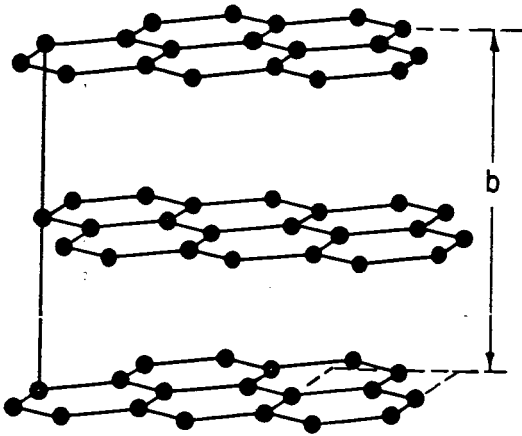
The work described here was sponsored by ERDA, E(49-18)2031 and AGA, BR-48-12, to whom the authors wish to express their appreciation.

LITERATURE CITED

1. Van Krevelen, D. W., Coal Typology--Chemistry, Physics, Constitution, Elsevier Publishing Co., 1961, p. 326.
2. Ergun, S., Fuel, v. XXXVII, Oct., 1958.
3. Yen, T. F., Erdman, J. G., and Pollack, S. S., Anal. Chem., 33(11), Oct., 1961.
4. Warren, B. E., J. Chem. Phys., 2(9), 551, Sept. 1934.
5. Franklin, R. E., Acta Cryst. 3, 107 (1950).
6. Yen, T. F., Erdman, J. G., in Encyclopedia of X-Ray and Gamma Rays, (G.L. Clark ed.), Reinhold, New York, 1963, p. 63.
7. Blayden, H. E., Gibson, J., and Riley, H. L., Proc. Conf. Ultrafine Structure of Coals and Cokes, British Coal Utilization Research Assoc., London, 1944, p.176.
8. Schwager, I. and Yen, T. F., Preliminary Examination of Coal Liquefaction Products, ACS, San Francisco Meeting, Aug., 1976.



GRAPHITE



Hexagonal Unit Cell

$$a = 2.46 \text{ \AA}$$

$$b = 6.70 \text{ \AA}$$

$$d_{002} = b/2$$

$$a/\sqrt{3} = r$$

$$d_{100} = \frac{\sqrt{3}}{2} a = \frac{3}{2} r = 2.1 \text{ \AA}$$

$$d_{110} = \frac{\sqrt{3}}{2} r = 1.2 \text{ \AA}$$

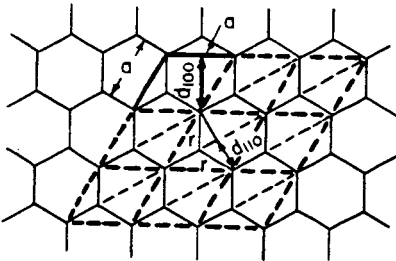


FIG. 2

INTERLAYER DISTANCES

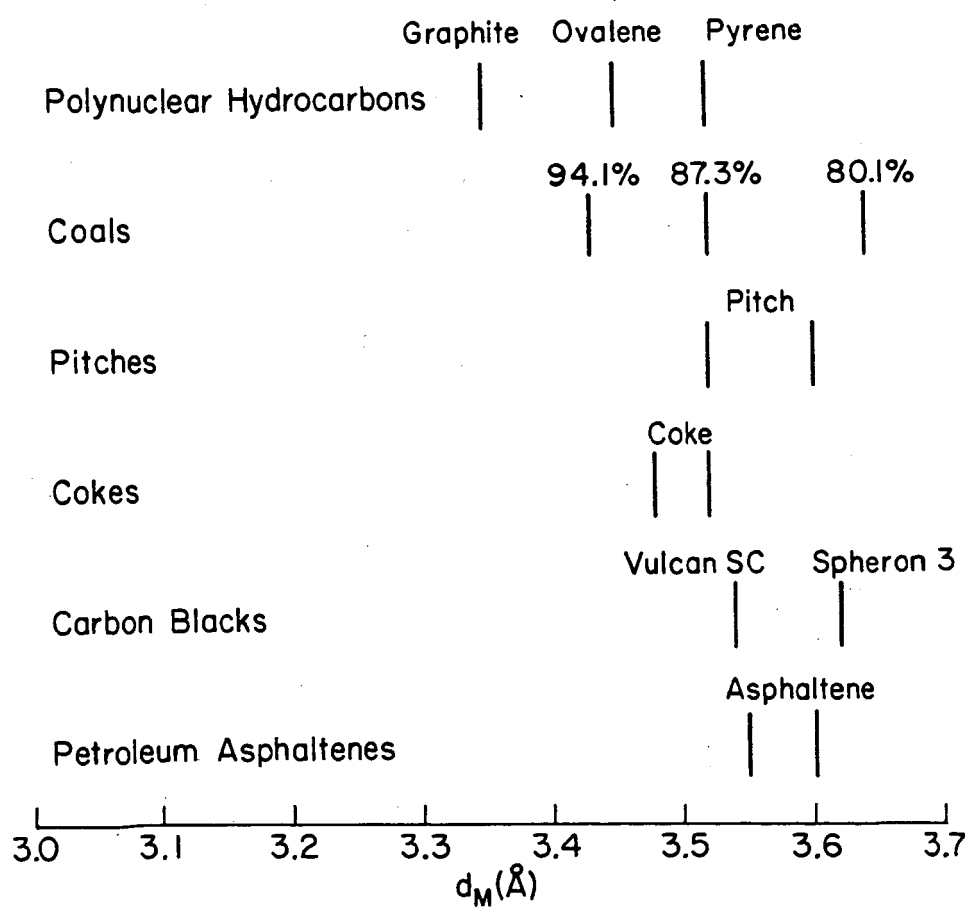
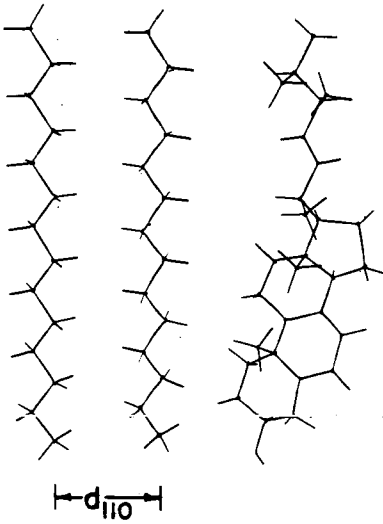


FIG. 3

PARAFFIN



Othorhombic Unit Cell

$$a = 7.40 \text{ \AA}$$

$$b = 4.93 \text{ \AA}$$

$$d_{200} = a/2$$

$$d_{020} = b/2$$

$$d_{110} = \frac{\sqrt{a^2 + b^2}}{2} \sin \left(2 \tan^{-1} \frac{b}{a} \right)$$

$$= 4.1 \text{ \AA}$$

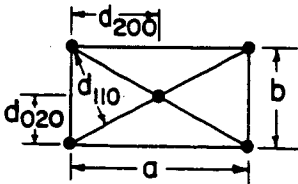


FIG. 4

AROMATICITY, f_a

$$f_a = \frac{C_A}{C} = \frac{C_A}{C_A + C_S}$$
$$= \frac{A_{002}}{A_{002} + A_\gamma}$$

C_i = No. of i th Type Carbon
Atoms per Structural Unit

i = A, Aromatic

i = S, Saturated

A_i = Integrated Intensities

Under the i th Type Bands

i = 002, Bands at $2\theta = 26^\circ$

i = γ , Bands at $2\theta = 18^\circ$

FIG. 5

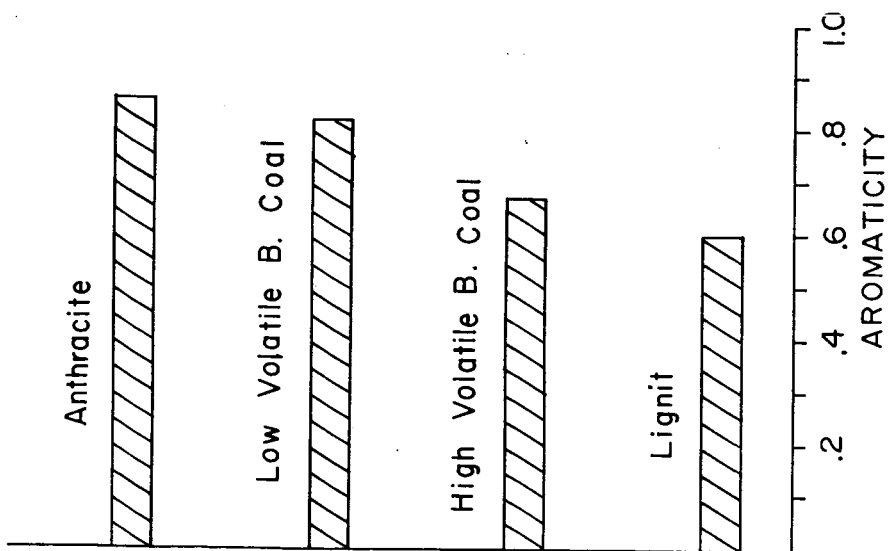


FIG. 6a

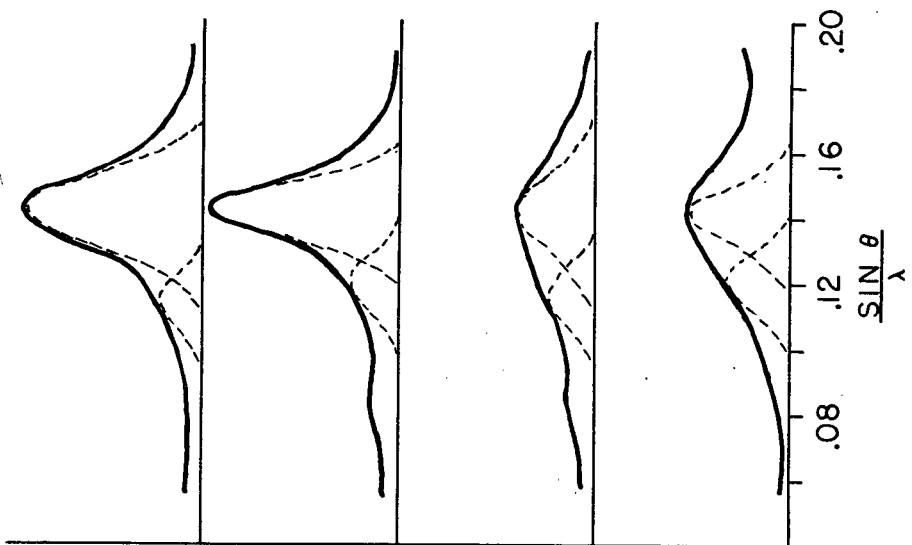


FIG. 6b

Chemical Structure of Heavy Oils Derived from Coal Hydrogenation

S. Yokoyama, David M. Bodily and Wendell H. Wiser

Mining, Metallurgical and Fuels Engineering Department, University of Utah
Salt Lake City, Utah 84112

Introduction

Structural characterization using high resolution nuclear magnetic resonance, NMR, and elemental analysis was first applied to coal pyrolysis products by Brown and Ladner¹. Other investigators 2-5 have extended these studies to coal hydrogenation products and coal extracts. Parameters such as the fraction aromaticity, f_a , the degree of substitution on aromatic rings, σ , the hydrogen to carbon ratio in a hypothetical unsubstituted aromatic ring system, H_{ar}/C_{ar} , the ring index, R_a , the length of alkyl substituents on aromatic rings, $H_o/H_{\alpha} + 1$, and the molecular weight of the unit structure, M_u , can all be calculated. In this study, heavy oils from coal hydrogenation using $ZnCl_2$ catalyst have been characterized by structural analysis techniques.

Experimental

Hiawatha, Utah coal (45% VM, d.a.f.b.) was hydrogenated at 950°F and 1800 psi H_2 pressure. Three (3) samples with catalyst concentrations of 1.5, 3.0 and 6.0 percent zinc as zinc chloride were hydrogenated. The heavy oils were extracted with NaOH and H_2SO_4 to produce neutral oils. The neutral oils were separated into a hexane-soluble fraction and an asphaltene fraction by extraction and the hexane-soluble oil was separated into saturated and aromatic oils by liquid chromatography using a silica gel column. Yields of various products are shown in Table 1. The asphaltene and aromatic oil fractions were further separated by gel permeation chromatography, GPC. GPC elution curves are shown in Figure 1.

Proton NMR spectra were measured for each GPC fraction at 100 M Hz. Molecular weights were determined by vapor pressure osmometry and elemental composition by C, H and N analysis.

Results and Discussion

The GPC elution curves shown in Figure 1 show a shift to smaller molecules as the catalyst concentration increases. (Larger molecules elute first in GPC). Molecular weight measurements verify that the larger molecules are eluted first in all cases.

The NMR spectra show a continuous shift in the properties of the molecules with elution volume. The larger molecules for both the aromatic oil and asphaltene samples have a large fraction of the hydrogens bound to aliphatic carbons β or further from aromatic rings, H_o . As the elution volume increases, hydrogens bound to aromatic carbons, H_{α} , and hydrogens bound to carbons α to aromatic rings, H_{α} , increase. Structural analysis was performed using the equation of

Brown and Ladner¹⁻². Results of these calculations are shown in Figures 2-4. Molecular weights are also shown in Figure 4.

The aromatic oil fractions show a large change in the carbon aromaticity and in the length of alkyl substituents on the aromatic ring. The degree of substitution of ring carbons varies from 0.5 to 0.2. The average number of aromatic rings in the unit structure is 1.5 to 3. The molecular weights calculated for the unit structure agrees with the measured values. The larger molecules, eluted at low elution volumes, appear to be composed of small ring systems with long aliphatic substituents. As the elution volume increases, the alkyl side-groups become shorter resulting in larger values of fa and lower molecular weights.

The asphaltene fractions show a similar trend as the aromatic oils except that the aliphatic branches are much shorter and Ra and fa are higher. The molecular weight of the unit structure is significantly less than the measured molecular weight, indicating that the actual molecules are dimers or trimers of the unit structures determined by structural analysis.

The effect of increasing the concentration of the zinc chloride catalyst is to decrease the yields of asphaltene and benzene-insoluble heavy oil with a corresponding increase in the yields of hexane-soluble oil. The average molecular weight of asphaltene and aromatic oils is also decreased. There is no other major structural change in the heavy oil product of coal hydrogenation. Fractions eluted at the same elution volume show the same properties independent of the catalyst concentrations used to produce the oils.

References

1. J. K. Brown and W. R. Ladner, *Fuel*, **39**, 87 (1960).
2. S. Yukoyama, N. Ounishi, and G. Takeya, *J. Fuel Soc. Japan*, **52**, 906 (1973).
3. Y. Maekawa, S. Ueda, Y. Hasegawa, Y. Nakata, S. Yokoyama and Y. Yoshida, *Preprints Fuel Div. Am. Chem. Soc.*, **20** (3), 1 (1975).
4. G. Takeya, *Gakujustu Geppo*, **25**, 719 (1973).
5. T. Katoh, H. Itoh, K. Ouchi and J. Sohma, *J. Fuel Soc. Japan*, **54**, (12), 11 (1976).

Acknowledgement

This work was supported by the United States Energy Research and Development Administration under Contract No. E (49-18) - 1200.

Table 1
 Products from Extraction of Heavy Oil

	Percent Yield		
	Sample 0.015	Sample 0.03	Sample 0.06
Heavy Oil (% of coal)	25.6	31.8	31.3
Asphaltene (% of heavy oil)	17.3	6.6	6.0
Oil	34.0	63.6	62.2
Saturates	8.9	11.9	6.9
Aromatic	91.1	88.1	93.1
Acidic (% of heavy oil)	9.5	17.4	12.9
Basic (% of heavy oil)	1.5	1.8	2.2
Residue (% of heavy oil)	28.4	5.3	3.3
Loss	9.3	5.3	12.9

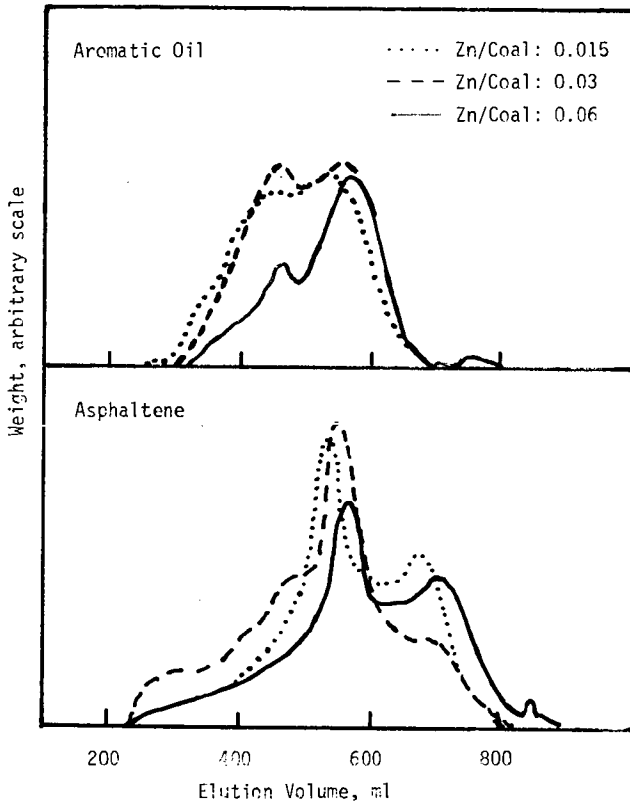


Figure 1. GPC Chromatograms

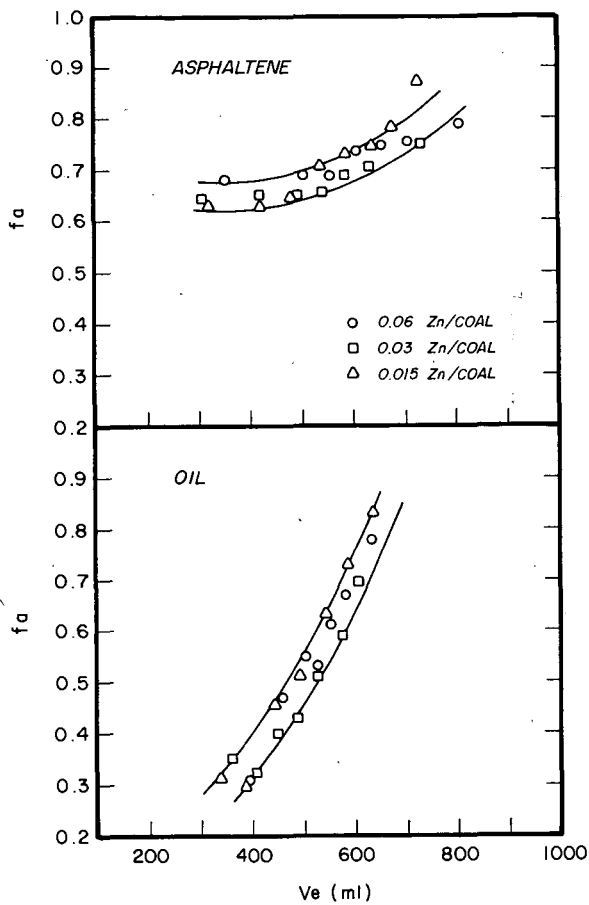


Figure 2. Carbon aromaticity vs. elution volume for oils and asphaltenes.

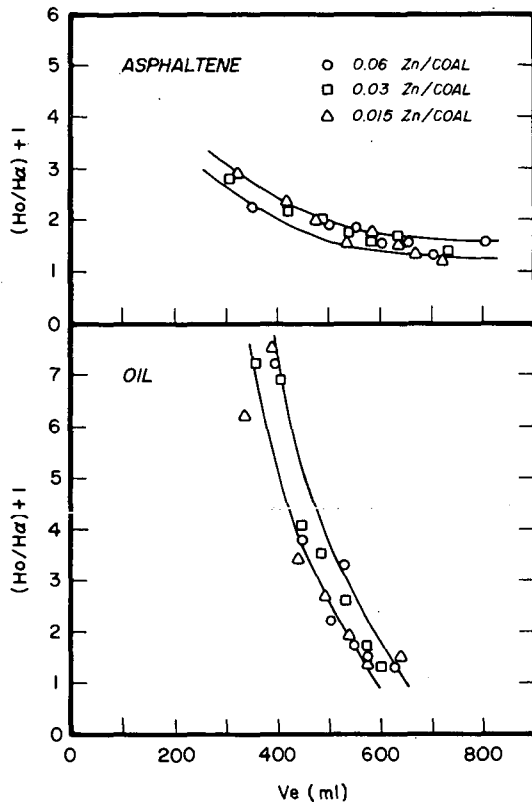


Figure 3. The average length of aliphatic carbon chain vs. elution volume for oils and asphaltenes.

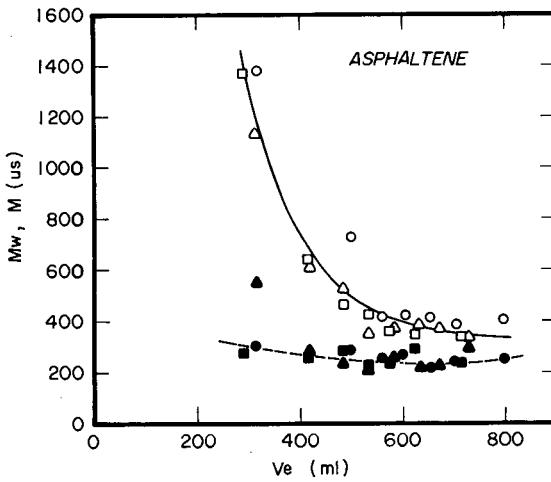
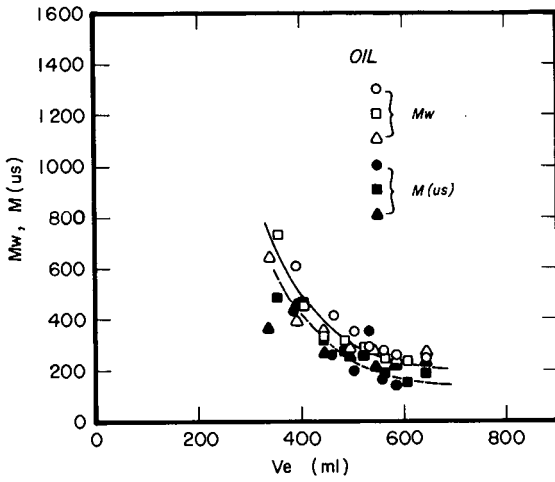


Figure 4. Experimental and calculated molecular weights vs. elution volume.

Structural Characterization of Coal Oils by Proton and Carbon-13 Nuclear Magnetic Resonance

S. Yokoyama, David M. Bodily and Wendell H. Wiser

Mining, Metallurgical and Fuels Engineering Department, University of Utah,
Salt Lake City, Utah 84112

Introduction

The technique of structural analysis based on proton NMR and elemental analysis has been applied to heavy oils derived from coal and petroleum¹⁻³. This approach utilizes the hydrogen types to determine information about the carbon skeleton. Friedel and Retcofsky have applied ¹³C NMR to coal-derived products to obtain structural information directly⁴. The new technique of pulse Fourier-transform (PFT) spectroscopy has helped overcome the problem of low sensitivity and proton decoupling has simplified the spectra, making ¹³C NMR more suitable for studies of heavy oils. Structural analysis is still limited by difficulties in making quantitative measurements and in assigning absorption to various types of carbons. Combinations of ¹H and ¹³C NMR have been used to study petroleum liquids^{5,6}. More recently PFT ¹³C NMR has been applied to coal liquids^{7,8}. In this study, ¹H and ¹³C NMR are used for the structural characterization of heavy oils derived from coal by catalytic hydrogenation.

Experimental

Hiawatha, Utah coal (45% V.M., d.a.f.b.) was impregnated with 6% by weight Zn as ZnCl₂ and hydrogenated in an entrained-flow reactor at 950°F and 1800 psi H₂. The heavy oil fraction was extracted with 10% NaOH and 15% H₂SO₄ and separated into a hexane-soluble oil and an asphaltene fraction by extractions. The hexane-soluble oil was separated into saturate and aromatic fractions by liquid chromatography using a silica gel column. The saturate oil, aromatic oil and asphaltene fractions were separated by size by gel permeation chromatography (GPC) using crosslinked polystyrene gels of pore sizes appropriate to each sample. Neighboring GPC fractions were combined to obtain samples of suitable size. The GPC separation and the samples chosen for analysis are shown in Figure 1.

NMR spectra were measured in d-chloroform using tetramethyl silane as a reference material. A Varian Associates XL-100 FTNMR spectrometer operating at 25.16 MHz and 0.4 - 0.8 second pulse interval time for ¹³C NMR and 100 MHz for ¹H NMR was used to obtain spectra. Typical spectra are shown in Figures 2-4.

Results and Discussion

The GPC results shown in Figure 1 are in agreement with molecular weight measurements for the fractions measured by vapor pressure osmometry. The molecular weights of the asphaltenes varied from 1380 for the fraction eluted at lowest elution volume to 410 for the fraction eluted last. The aromatic oil fractions have molecular weights in the range 250-610. The H/C ratios decrease from 0.94 to 0.83 for the asphaltene fractions and from 1.51 to 0.85 for the aromatic oil fractions with increasing elution volume.

The NMR spectra of the saturate oil fractions in Figure 2 show a typical pattern of a long chain aliphatic compound. The ¹³C spectra show resonance lines at 14, 23, 32, 29 and 29.5 ppm corresponding to the α , β , γ , δ and ϵ carbons respectively of n-paraffins. The average chain length was calculated from the

ratio of peak areas for the various carbon types assuming the structure of a normal paraffin. The results are shown in Table 1, with the calculated amount of n-paraffinic structure and the number of carbons estimated from gas chromatography results. The chain length calculated from ^{13}C NMR is greater than that obtained from gas chromatography. This is attributed to branching near the end of the carbon chain which invalidates the n-paraffin model. The low-molecular weight saturate fractions contains considerable isoparaffins.

The NMR spectra of aromatic oil fractions in Figure 3 indicate a gradual change in structural properties with elution volume. The spectra of larger molecules (eluted at smaller volumes) indicate long alkyl groups attached to small aromatic ring systems. The length of the alkyl substituents was estimated from the intensities of resonance peaks with chemical shifts equivalent to n-paraffin carbons. For fraction 0-1, 57% of the saturated carbons are in such alkyl groups and the average length is 28 carbons. For fraction 0-2, the corresponding figures are 35% and 10 carbons. With increasing elution volume, the spectra progressively changes to a complex broad spectra. The spectra for fraction 0-7 indicates a higher fraction of aromaticity, fa, and that almost all hydrogens are bound to aromatic carbons and carbons α to aromatic rings. Examination of the spectra in Figure 4 shows a similar trend for the asphaltene fractions.

The chemical shift assignments of Bartle, et.al.⁷ were used to determine the carbons α to aromatic rings, C_α , and those β or further, C_β , from the ^{13}C NMR spectra. From ^1H NMR spectra, protons bound to each type of carbon, H_α and H_β respectively, were calculated. Values of $\text{H}_\beta/\text{C}_\beta$ (Y) for aromatic oil fractions are reasonable, but values of $\text{H}_\alpha/\text{C}_\alpha$ (X) indicate a possible error in the assignments of chemical shifts.

The fractions of aromatic carbon are plotted versus elution volume in Figure 5 as determined from the ^{13}C NMR spectra and by structural analysis using ^1H NMR spectra². The structural analysis approach assumes that $X=Y=2$. The ^{13}C NMR spectra is complicated by the long relaxation times of aromatic carbons that are not bound to hydrogens. These carbons generally show chemical shifts downfield from 129 ppm while aromatic carbons bound to hydrogens, C_{ah} , show chemical shifts upfield from 129 ppm^{7,8}. C_{ah} can be equated to the aromatic hydrogens and the ratio of aliphatic hydrogen to carbon is given by equation 1.

$$\text{H}_{\text{al}}/\text{C}_{\text{al}} = \text{C}_{\text{ah}}/\text{C}_{\text{al}} \cdot \text{H}_{\text{al}}/\text{H}_{\text{a}} \quad (1)$$

The ratios on the right hand side of equation 1 can be obtained from the ^{13}C NMR spectra, assuming the division at 129 ppm and from ^1H NMR. Values of $\text{H}_{\text{al}}/\text{C}_{\text{al}}$ are listed in Table 2. Figure 6 shows the value of structural parameters calculated by the Brown-Ladner equations² for $X=Y=2$ and $X=Y=\text{H}_{\text{al}}/\text{C}_{\text{al}}$, using the results in Table 2.

References

1. R. B. Williams, ASTM Spec. Tech. Publ., 224, 168 (1958).
2. J. K. Brown and W. R. Ladner, FUEL, 39, 87 (1960).
3. G. Takeya, Gakujutsu Geppo, 25 (1), 51 (1973).
4. H. L. Retcofsky and R. A. Friedel, FUEL, 47, 487 (1968).
5. D. R. Clutter, L. Petrakis, R. L. Stenger, Jr. and R. K. Jensen, Anal. Chem., 44, 1395 (1972).
6. S. A. Knight, Chem. Ind., 1967, 1920.
7. K. D. Bartle, T. G. Martin and D. F. Williams, Chem. Ind., 1975, 313.
8. Y. Maekawa, T. Yoshida, Y. Yoshida and T. Imanari, J. Fuel Soc. Japan, 54 (12), 21 (1975).

Acknowledgement

This work was supported by the United States Energy Research and Development Administration under Contract No. E(49-18)-1200.

Table 1
Structure of Saturate Fractions

Fraction	¹³ C NMR		Gas Chromatography
	Carbon Number	% Normal Paraffin	Carbon Number
1-P	50-60	67	33
2-P	34	86	27
3-P	23-28	54	22

Table 2
Aliphatic Carbon to Hydrogen Ratio

Fraction Number		1	2	3	4	5	6	7
Hal/Cal	Aromatic Oil	2.0	2.1	2.1	4.5	2.2	2.4	2.6
	Asphaltene	1.6	2.3	1.9	1.8	2.4	2.6	2.7

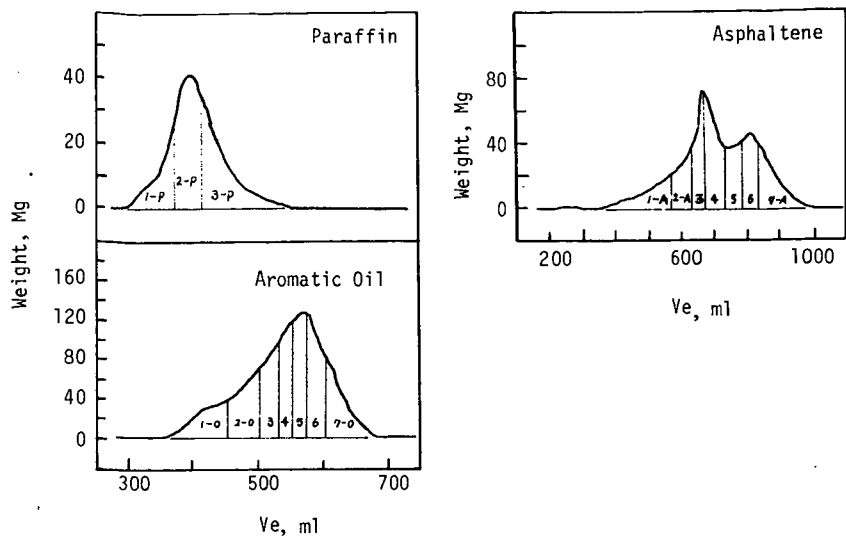


Figure 1. GPC Elution Curves

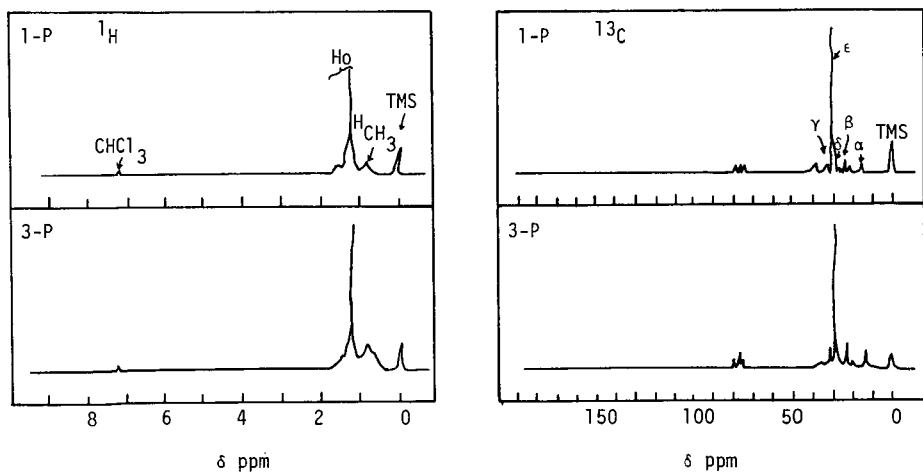


Figure 2. ^1H and ^{13}C NMR spectra of Paraffin Fractions

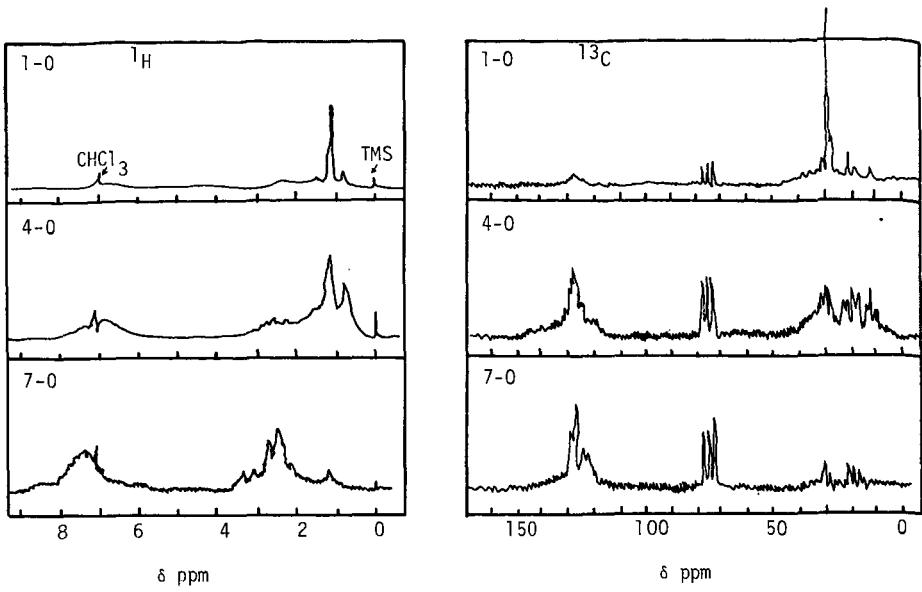


Figure 3. ^1H and ^{13}C NMR Spectra of Aromatic Oil Fractions

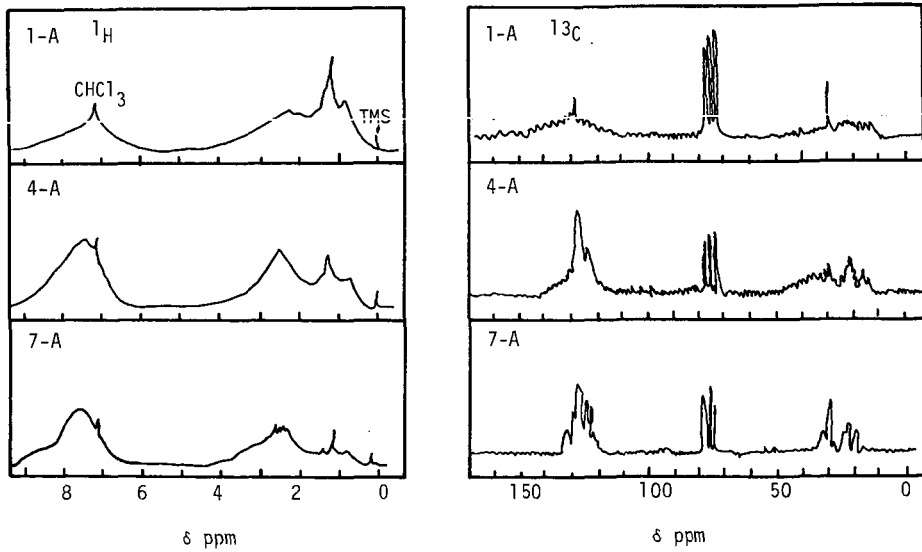


Figure 4. ^1H and ^{13}C NMR Spectra of Asphaltene Fractions

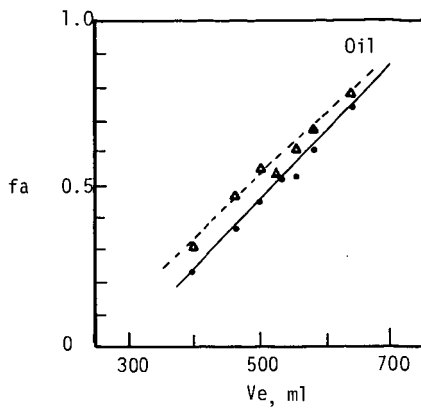
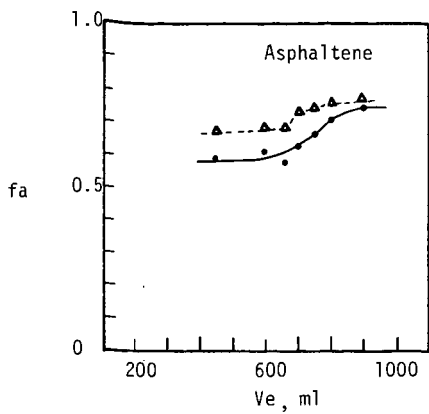


Figure 5. Carbon aromaticity; solid line from ^{13}C NMR, dashed line from ^1H NMR.

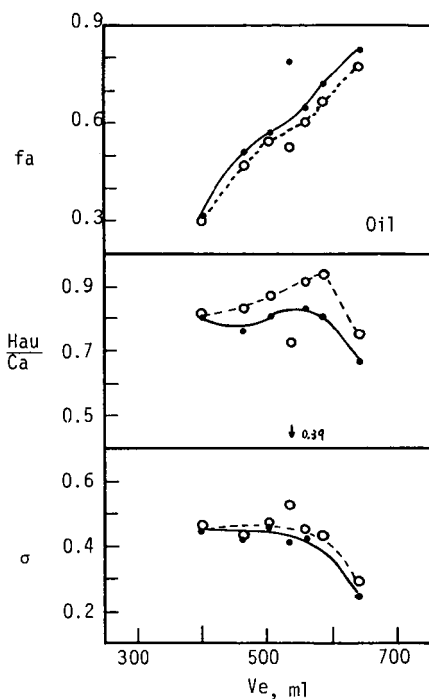
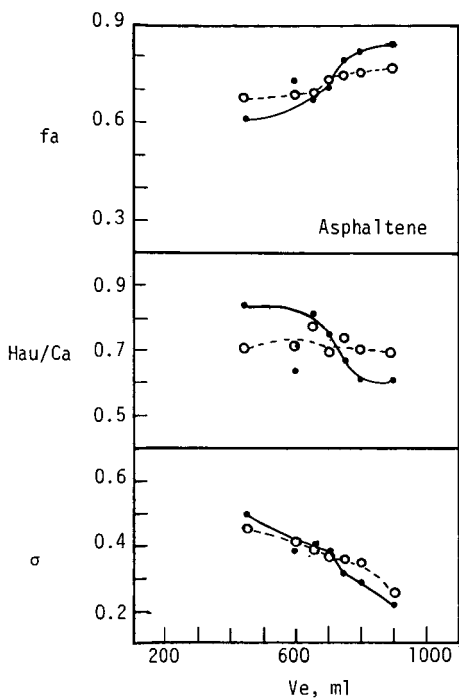


Figure 6. Structural Parameters; solid line from ^{13}C , dashed line from ^1H NMR

OCCURRENCE AND DISTRIBUTION OF TRACE ELEMENTS IN COAL

R. A. Cahill, J. K. Kuhn, G. B. Dreher, R. R. Ruch,
H. J. Gluskoter, and W. G. Miller

Illinois State Geological Survey
Natural Resources Building
Urbana, Illinois 61801

Chemical analyses for nearly 60 elements are reported for 70 whole coal samples, 34 separate fractions of five laboratory-prepared (washed) coals, and 40 bench samples from five different seams of Illinois coal. These data supplement the previously reported (1) analyses for 33 elements made for 101 whole coals. Analytical procedures used in this study are listed in Table 1. The application of instrumental neutron activation analysis has been primarily responsible for the increase in the number of elements reported. Two or more methods were used to assign a best value to many elements.

TABLE 1. Analytical Procedures Used in Coal Analyses

Procedure	Type of sample	Element
Instrumental neutron activation analysis (INAA)	Whole coal	Na*, K*, Rb, Cs, Sr*, Ba, Ga, In, As, Sb, Se, Cl*, Br*, I, Sc, V*, Cr*, Mn*, Co*, Fe*, Ni*, Zn*, Mo*, Ag*, Hf, Ta, W, La, Ce, Sm, Eu, Tb, Dy, Yb, Lu, Th, U
Neutron activation analysis-radiochemical separation (NAA-RC)	Whole coal Low-temperature ash (150°C)	Hg Tet
X-ray fluorescence - wave-length dispersion (XRF)	Whole coal	Na*, K*, Mg, Ca, Al, Si, S, P, Cl*, Br*, Ti, Ni*, Zn*, Fe*
Atomic absorption (AA)	Low-temperature ash (150°C)	Ni*, Cu*, Zn*, Cd*, Pb*, Tl†, Li†
Optical emission-direct reader (OED)	High-temperature ash (500°C)	Be, Sr*, B, Ge*, V*, Cr*, Co*, Cd*, Ni*, Cu*, Zn*, Zr*, Mo*
Optical emission-photographic (OEP)	High-temperature ash (500°C)	Ge*, Pb*, V*, Cr*, Co*, Ni*, Cu*, Mn*, Zn*, Zr*, Mo*, Ag*, Sn†
Ion-selective electrode (ISE)	Whole coal	F

*Elements for which two or more analytical procedures have been applied.

†Elements for which further methods of analysis are being developed.

This paper concentrates on data for 70 coal samples, of which 31 are from the Illinois Basin which includes parts of Indiana, Illinois, and western Kentucky. Fourteen samples are from Eastern states, 22 from Western states, and 3 from Iowa. Cumulative data for the 171 samples analyzed during this and the prior study are reported elsewhere (2).

Table 2 summarizes the analyses for the 70 whole coal samples. For calculation of the mean values, the "less-than" (below limit of detectability) values were considered real values. The number of samples that had "less-than" values is noted in the table. Individual distribution plots for each element are included in the final report (2). The data can be grouped into similar types of distribution, which is more useful than considering a range of values. Elements such as Zn, Ba, As, and Cd showed wide ranges and skewed distributions, which may be explained by the occurrence of discrete mineral phases in the coal mineral matter. Elements associated with the organic material of the coal may show moderate ranges or normal distributions. For the highly dispersed elements, such as the rare earths, moderate ranges and normal distributions are also observed.

TABLE 2. Preliminary Analytical Data For 70 Coal Samples*

Element	Mean	Min	Max	Element	Mean	Min	Max
Al	1.21%	0.31%	3.1%	P	112	16	1500
Sb	1.1	0.01	7.7	K	0.16%	0.01%	0.68%
As	15	0.3	116	Rb	19	<1	63
Ba (1)†	240	20	1600	Se	2.6	0.4	8.1
Be (7)	1.3	<0.1	3.8	Si	2.13%	0.38%	6.30%
B	88	5	<240	Ag	0.03	0.01	0.08
Br	5.2	0.5	27	Na	780	100	6000
Cd (54)	0.44	<0.1	9.3	Sr	126	13	550
Ca	0.96%	0.01%	3.3%	Ta	0.18	1.1	1.5
Cs	1.3	0.04	6.2	Th	2.6	0.6	9
Cl	0.09%	0.01%	0.8%	Sn (57)	0.67	<0.2	11
Cr	20	2.4	52	Ti	0.06%	0.02%	0.16%
Co	3.9	0.6	13	W (1)	0.8	<0.2	4.2
Cu	14	3	92	U (4)	1.5	<0.3	6.1
F	81	19	147	V	25	4.8	90
Ga	3.7	0.8	11	Zn (2)	51	<0.3	645
Ge (15)	3.3	<0.1	18	Zr	35	12	88
Hf	0.8	0.1	2.2	Ce	16	3	46
In (16)	0.16	<0.01	0.6	Dy	1.2	0.3	3.5
I (21)	1.2	<1	14	Eu	0.32	0.07	0.9
Fe	1.46%	0.3%	3.7%	La	8	1.8	23
Pb (17)	8.3	<0.7	79	Lu (10)	0.12	<0.1	0.4
Mg	0.09%	0.03%	0.39%	Sm	1.4	0.3	4.3
Mn	52	1.4	303	Sc	3.0	0.5	9.3
Hg (1)	0.15	<0.05	0.6	Tb	0.3	0.06	0.7
Mo (7)	5.4	<0.1	23	Yb	0.58	0.1	1.5
Ni	13	1.5	51				

*All values in ppm unless otherwise noted.

†() indicates number of samples below the limit of detectability.

One method used to show trends in environmental and geological data is the calculation of enrichment factors, or Clarke values. The ratio is calculated from the concentration of a given element compared to its average abundance in the earth's crust. Elements having a Clarke value greater than 10 are considered highly enriched; those with values less than 0.1 are considered depleted. Table 3 groups the data into four general categories. Only Se shows high enrichment, a condition that was also observed by Ruch et al. (1). Boron, which was shown to be organically combined (1), is only slightly enriched. The depletion of seven elements, largely those associated with crustal rocks, is probably due to dilution by organic matter. The slight enrichment of 9 elements may be due in part to

organic combination of these elements in the coal matrix to their concentration in sulfide minerals, or to uncertainties in the crustal averages used.

TABLE 3. Average Enrichments* in 70 Coals

Elements <0.1	Depleted	Na, Mg, Mn, K, Si, P, Ti
Elements 0.1-2	No trend	Al, Ca, Fe, V, Sn, Cu, Co, Ni, Be, Cr, Sr, Zr, Pb, Zn, Ga, Hg, F, U, Ba, Ce, In, La, Lu, Ag, Rb, Cs, Sc, Sm, Tb, Dy, Yb, Th, W, Eu, Hf
Elements 2.0-10	Slightly enriched	B, As, I, Cl, Sb, Mo, Cd, Ge, Br
Elements >10.0	Highly enriched	Se

*Crustal averages used are from Taylor (3).

Two additional methods are being used to establish the presence of trace elements in coal. Specific gravity separations, which had been made on 4 coals in the previous study (1) were conducted on five coals in this study. Washability curves show some elements (e.g., Ge, B, Be) are associated with the organic phase, some (e.g., Zn, Cd, As) are present in the mineral phase, while other elements demonstrated mixed associations. An acid extraction procedure for preferential dissolution of mineral matter is being used on 25 whole coals to determine the quantity of each element closely associated with the organic fraction of the coal.

The vertical distribution of trace elements was studied in five coal seams from the Illinois Basin. Representative curves are shown for Tb, Br, Sb, and Ge in four different bench sets (Figs. 1-4). A few elements, notably Ge, appear to be concentrated in the upper and lower coal bench samples. Elements such as Tb and Br often show relatively flat distributions. Further work on this phase of the project is being continued to make significant trends more obvious.

Our program is designed to characterize the nature and association of elements within the coal matrix and to approximate the range of concentrations of elements occurring in coal.

This work is supported in part by U.S. Environmental Protection Agency
Contracts 68-02-1472 and 68-02-2130.

REFERENCES

- (1) Ruch, R. R., H. J. Gluskoter, and N. F. Shimp, Occurrence and distribution of potentially volatile trace elements in coal: Illinois State Geological Survey Environmental Geology Note 72, 1974, 96 pp.
- (2) Final Report EPA Contract 68-02-1472, 1976.
- (3) Taylor, S. R., Abundances of chemical elements in the continental crust: *Geochimic et Cosmochimica Acta*, v. 28, pp. 1280-1281, 1964.

BENCH SAMPLE DISTRIBUTIONS

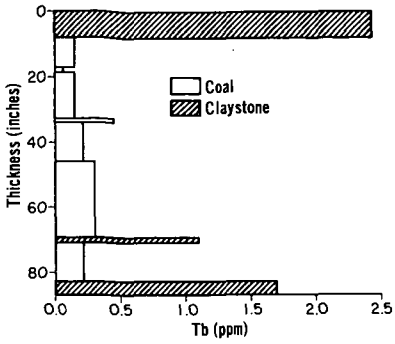


Fig. 1

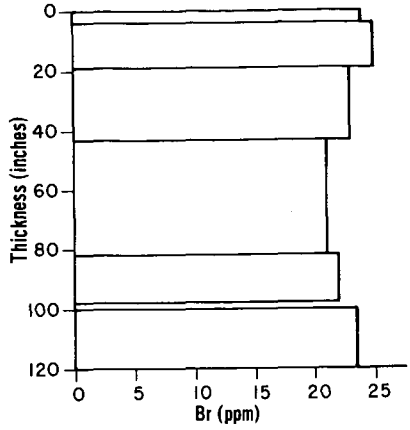


Fig. 2

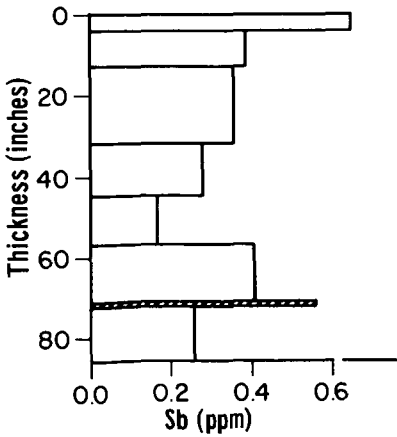


Fig. 3

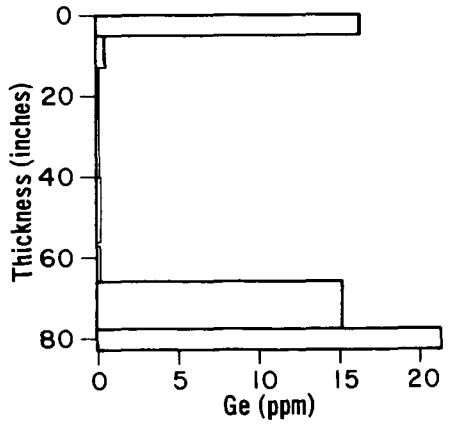


Fig. 4

KINETIC STUDIES OF GAS EVOLUTION DURING PYROLYSIS OF SUBBITUMINOUS COAL^{*}

J. H. Campbell and D. R. Stephens

Lawrence Livermore Laboratory, University of California

Livermore, California 94550

INTRODUCTION

The Lawrence Livermore Laboratory is currently developing a method for in-situ gasification of subbituminous western coals (1,2). One of the most important unresolved questions relates to the amount and type of products obtained during the pyrolysis phase. Wyoming subbituminous coal loses about 40 to 50% of its dry weight during pyrolysis, generating low-molecular-weight gases, light hydrocarbons, and heavy tars. Since such a large percentage of the coal can be removed in the form of pyrolysis products (many of which have a high heating value), the pyrolysis process must be well understood if we are to model in-situ gasification properly.

Unfortunately, the literature contains little quantitative information on subbituminous coal pyrolysis between 383 and 1273 K (110-1000°C). With this in mind, we have carried out our study of Roland seam (Wyodak mine[†]) subbituminous coal. This report describes our analysis of the major gaseous pyrolysis products (H₂, CO, CO₂, CH₄, C₂H₆, C₃H₈, and C₂H₄). These gases account for approximately 25% of the weight of the original coal. The quantity of each gas and the temperature range of evolution were determined. Also, the effective kinetics for the evolution of each species were evaluated using nonisothermal kinetic methods. Effective kinetic parameters are valuable for modeling purposes since they can accurately describe the macroscopic pyrolysis process.

Since coal is such a heterogeneous mixture of compounds, it is only possible to relate macroscopic effective kinetics indirectly to actual specific microscopic chemical and physical processes. Therefore, the results reported here are only generally correlated to the known chemistry of coal, but they provide a good physical picture of the chemical process that may occur during pyrolysis.

EXPERIMENTAL

A 50-g sample was used in the experiments. Sample preparation procedure is described elsewhere (3). Table 1 gives a standard analysis of the coal. Particle diameter distribution was from 1.68 to 3.35 mm. All samples were water-saturated, then dried in vacuum at 383 K (110°C) for 4 h. Following drying, the sample were immediately pyrolyzed. At no time was air allowed to contact the dry samples.

^{*} This work was performed under the auspices of the U.S. Energy Research & Development Administration, under contract No. W-7405-Eng-48.

[†] Reference to a company or product name does not imply approval or recommendation of the product by the University of California or the U.S. Energy Research & Development Administration to the exclusion of others that may be suitable.

The details of the apparatus and procedures are described elsewhere (3). The pyrolysis apparatus consisted of a flow control unit, a reactor, and a sampling system.

The flow control unit provided a constant sweep ($\pm 1\%$) of Ar carrier gas through the system. Thus, we could obtain by mass spectroscopy a quantitative measure of the gaseous product composition relative to the constant background flow.

The furnace, which enclosed the reactor, was programmed to increase the temperature linearly with time ($3.33^\circ\text{C}/\text{min}$). The coal sample was placed in a basket and positioned at the center of the reactor (and furnace) atop a mass of ceramic balls. The ceramic balls preheated the carrier gas to the reactor temperature. A thermocouple at the center of the coal sample monitored the temperature of the pyrolysis reaction zone.

METHOD OF KINETIC ANALYSIS

We have used nonisothermal methods to obtain the gas evolution kinetics. These methods have been described by van Heek *et al.* (4), who show that for a constant heating rate ($dT/dt = C$), the rate of gas evolution for a first-order reaction is given as

$$\frac{dV}{dt} = \frac{AV_\infty}{C} \exp\left(\frac{-E}{RT} - \frac{ART^2}{CE} e^{-E/RT}\right), \quad 1)$$

where E is the activation energy, A is the kinetic frequency factor, C is the heating rate and V_∞ is the total volume of gas evolved.

The rate of gas evolution (dV/dT) for a given constant heating rate is determined experimentally. Knowing the total volume of the material evolved, one can fit Equation 1 to the experimental results and obtain E and A . The closeness of the fit is a good indication of the validity of the assumed reaction order.

As noted in the introduction, coal is such a complicated heterogeneous mixture of different organic and inorganic compounds that the reported pyrolysis kinetics are undoubtedly an average for a vast number of different reactions that give the same product. For this reason, the activation energy and frequency factor for a particular gas evolution process are only "effective" values for the whole process.

RESULTS AND DISCUSSION

Figure 1 gives the experimentally observed gas evolution curves for the major coal pyrolysis gases: H_2 , CO_2 , CO , CH_4 , C_2H_6 , C_3H_8 , and C_2H_4 . These curves were obtained using a heating ramp of $3.33 \text{ K}/\text{min}$ ($3.33^\circ\text{C}/\text{min}$) between 383 and 1273 K (110°C - 1000°C).

The concentrations of product gases were normalized to that of the constant-flow Ar carrier gas. Integration of the evolution envelopes provides the total volume of each gas given off during pyrolysis (Table 2).

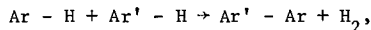
Hydrogen evolution

Figure 1a and Table 2 reveal that H₂ is the major pyrolysis gas. It occurs at twice the mole concentration of any other gas and represents about 40% of the total gas evolved.

Using Equation 1, one can evaluate the activation energy and kinetic frequency factor for pyrolytic H₂ evolution by assuming that it is a first-order process. By numerically fitting Equation 1 to the experimental points in Figure 1a using a standard computer code (5), one can calculate an effective activation energy of 22.3 kcal/mole and a frequency factor of $1.2 \times 10^3 \text{ min}^{-1}$ for dehydrogenation. Figure 2a reveals the closeness of this fit to the experimental data. The activation energy and the frequency factor are the only variable parameters in the code. From the closeness of the computer fit, it appears that H₂ evolution is adequately described as a first-order process.

The observed activation energy for H₂ evolution is unusually low for the temperature at which it took place. The activation energy for a typical C-H bond-breaking process is about 101 kcal/mole. Berkowitz and den Hertog (6) report activation energies of 8 to 15 kcal/mole for pyrolytic dehydrogenation of other coal types between 873 and 1073 K (600-800°C), and their low values are in fair agreement with the results reported here for Roland seam coal. It would appear therefore that the simple bond-breaking picture is inadequate.

It is well known that H₂ evolution in coal results from the fusion of aromatic ring structures (lamellae) in the coal matrix. This reaction can be schematically represented as



where Ar and Ar' represent particular lamellae structures containing n and n' aromatic ring units each (e.g., pyrene and phenanthrene). Berkowitz and den Hertog (6) proposed that the diffusion of two lamellae into some configuration where reaction becomes possible is the rate-determining step. The activation energy observed for H₂ emission would then be a measure of the activation energy associated with the diffusion of the lamellae units.

Since char is such a heterogeneous mixture of materials, it is also possible that H₂ emission occurs from a number of chemically nonequivalent sites, each with its own activation energy. If this is the case, the experimentally observed dehydrogenation curve represents the sum total of H₂ from many different sites. Thus the activation energy for H₂ release from each site could be quite high ($\gg 20$ kcal/mole), and yet the curve (Fig. 2a) would give the appearance of a low activation energy overall. The observed temperature dependence of the total H₂ release (7,8) gives support to this view. As temperature increases, the H₂ release increases, although at each temperature, dehydrogenation goes essentially to completion. This indicates that a number of different H₂ formation reactions take place, each occurring at a different temperature.

Carbon oxides

Carbon dioxide. Carbon dioxide is the first pyrolysis gas to be released in appreciable quantities (Fig. 1b). A trace of CO₂ appears at about 523 K (250°C), goes through maxima at 793 K (470°C) and about 923 K (650°C), and then eventually declines to zero at 1123 K (850°C). The twin peaks seem to indicate CO₂ emission from at least two distinct sources. The first peak may be due in large part to carboxylic acid (COOH) decomposition; the second peak probably results from carbonate decomposition in the minerals. Fitting Equation 1 to the observed evolution curve gives the values of the effective activation energies and frequency factors (Table 2). Figure 2b shows the closeness of the calculated fit.

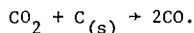
Blom (9) reported the distribution of oxygen functional groups in vitrains of various C and O content. For a vitrain of about 18 wt% O₂ and 73 wt% C, dry and mineral-matter free (a composition similar to that of Roland seam coal as described in Table 1), the amount of O as COOH is about 3 to 4 wt% (i.e., about 17 to 22% of the total O). The amount of O as COOH needed to produce the first peak in Fig. 2b would be ~4.4 wt% of the coal (i.e., 25% of the total O). This approximation is only slightly higher than Blom's results.

The second CO₂ peak occurs at a temperature in the range of carbonate decomposition reactions for a number of minerals. O'Gorman and Walker (10) have carried out an extensive study of mineral matter in U.S. coals. Their work includes data for the original mineral (unheated) and final ash samples from 57 different coals. Samples of Wyoming subbituminous coal with an ash composition similar to Roland seam coal (in terms of constituent oxides) contained ankerite.* Calcite, argonite, dolomite, and siderite were not detected. Thermal analysis work by Kulp *et al.* (11) on ankerite shows that the principal carbonate decomposition occurs at about 923 to 973 K (650-700°C). This is in reasonable agreement with the observed second CO₂ peak in Fig. 2b.

Carbon monoxide. The evolution of CO is similar to that for CO₂ in that two peaks are observed. The first peak is at about 773 to 823 K (500-550°C) and the second is at 973 to 1023 K (700-750°C). A numerical fit to the data in Fig. 1b gives the effective kinetic parameters reported in Table 2. These parameters give an accurate representation of the process, as can be seen from the closeness of the fit in Fig. 2c.

The evolution of CO during coal pyrolysis has been attributed to several sources, primarily ether linkages, ketone groups, and heterocyclics. Fitzgerald and van Krevelen (12) suggest that CO formed at low temperatures [T < 773 K (T < 500°C)] arises from decomposition of ether links and carbonyl groups and that CO at high temperatures [T > 773 K (T > 500°C)] results from degradation of heterocyclic compounds.

However, due to the presence of CO₂ in the pyrolysis gas at high temperatures, some of the CO may be a product of the well-known Boudouard reaction:



* Ca(Mg, Fe) (CO₃)₂.

Yergey and Lampe (13) studied the mechanism of this reaction to determine if CO evolution is a two-step process or a simultaneous release of both CO molecules. Using nonisothermal kinetic methods, they show that oxygenated C resulting from CO₂ reaction (at 1% in flowing Ar) evolves simultaneously (desorbs) at a peak maximum of about 600 K (330°C) for pure C and about 700 K (430°C) for coke from bituminous coal. They also report an activation energy 17.5 kcal/mole for CO desorption from bituminous coke. Probably a portion of the CO evolved in the region of 700 K (430°C) is a result of desorption.

Taylor and Bowen (14) investigated the kinetics for CO₂ reaction with char from Roland seam coal at temperatures above the CO desorption regime (in the region of about 900-1050 K). They report an appreciable rate for the CO₂-char reaction at the higher temperatures. For example, at 1023 K (750°C) and 1 atm CO₂, 25 wt% of the char undergoes reaction in 30 min. So, during pyrolysis at high temperatures (about 1000 K), it is reasonable to expect some CO production from char reaction with evolved CO₂ (particularly CO₂ that may be generated from mineral decomposition at these high temperatures).

Major Hydrocarbon Gases

Ethane, propane, and ethylene. Based on the total amount of pyrolysis gas evolved, C₂H₆, C₃H₈, and C₂H₄ are only minor constituents. However, because their heats of combustion far exceed those of other gas components, they have a large effect on the Btu value of the pyrolysis product gas even at low concentrations (Table 3). The combined concentration of C₂H₆, C₃H₈, and C₂H₄ is only 3.56% of the evolved gas, but these gases provide 14.4% of the total gas heat of combustion.

The pyrolysis peak maxima for the above three gas hydrocarbons are nearly equivalent; i.e., 783 to 793 K (510-520°C). Barker (15) measured the peak maximum for the combined C₁ to C₁₀ hydrocarbon release from a number of vitrinites. A value of 753 K (480°C) was reported for the broad peak observed for Roland-Smith (Wyodak) vitrinites (70.2% C, dry, ash-free). The release of condensible liquid hydrocarbons goes through a maximum of 673 to 723 K (400-450°C) (16).

Table 2 gives the kinetic parameters (calculated using Equation 1) for the release of the three gas hydrocarbons. Figure 2 shows a typical fit for C₂H₆. Van Heek and Jüntgen (4) report an activation energy of about 41 or 42 kcal/mole for C₂H₆ evolution from hard coal. As expected, this value is somewhat higher than the one reported here, since the temperature and activation energy of hydrocarbon release increase with rank.

The source of these light hydrocarbons is thought to be aliphatic side chain groupings and inter-lamellae linkages cracked at higher temperatures. Work on model compounds by Depp *et al.*, shows that methylene and ethane linkages, in particular, are quite weak (17).

A review by Tingey and Morrey (18) states that the amount of C present as aliphatic material is generally high for low-rank coals. The major alkane side groupings are methyl, ethyl, and propyl with small amounts of butyl. Alkane units of C_n , $n > 4$ are rare. On the other hand, the concentration of methyl groups is by far the largest and is usually reported to be greater than one pre-aromatic lamellae (18).

Methane

In terms of heating value, CH_4 is the most important pyrolysis product. It accounts for about half the total heat of combustion of the pyrolysis gases (Table 3). Methane evolves over a rather large temperature range (Fig. 1b). The original sharp increase in CH_4 production occurs at the same temperature as observed for the other light hydrocarbons (Fig. 1c). However, the CH_4 peak tails off slowly at high temperatures and does not reach essentially zero until 1173 K (900°C).

It appears that CH_4 production in the 770 K (500°C) region results from dealkylation, the general mechanism proposed to produce other light hydrocarbons. At higher temperatures [$T > 820$ K ($T > 550^\circ\text{C}$)], CH_4 production is undoubtedly due to another (or many other) reactions. Fitzgerald and van Krevelen suggest that, at these higher temperatures, CH_4 is produced from char autohydrogenation reactions (12). Due to the high-temperature tail on the CH_4 curve, it is impossible to represent gas evolution accurately using a single first-order decomposition mechanism. For this reason, a sum of three curves was used. This is the minimum number that will give a close fit on the experimental data. For modeling purposes, it is reasonable to use more than one curve to fit the data, since accurate representation of the overall process is important. However, on a physical basis, it is difficult to identify the source of each peak.

As discussed above, the first sharp rise in CH_4 evolution (at about 770 K) probably results from dealkylation. Since the kinetic parameters for evolution of C_2H_6 , C_3H_8 , and C_2H_4 are nearly equivalent, the activation energy for the initial production of CH_4 would be expected to be 30 to 35 kcal/mole. By using an activation energy of 31.0 kcal/mole for the first peak, one can accurately represent the initial rise in the CH_4 evolution curve. This agrees with the expected result.

SUMMARY AND CONCLUSIONS

Gas evolution during pyrolysis of Roland seam (Wyodak mine) subbituminous coal was investigated from 383 to 1273 K (110-1000°C) in an inert gas (Ar) environment. The effective kinetic parameters (activation energy and frequency factor) for each major gas evolved were determined using nonisothermal kinetic methods. Effective kinetics provide valuable input for modeling processes involving coal pyrolysis (e.g., in situ coal gasification). Table 2 summarizes these kinetic results.

From the experimental results, a quantitative measure of each major gas evolved was also obtained. The temperature region and temperature maximum for the pyrolytic release of each gas were determined.

The observed gas evolution processes generally correlated with decomposition of known chemical structures in coal. This provided a good physical picture of the possible chemical reactions during pyrolysis.

ACKNOWLEDGMENTS

The author gratefully acknowledges the fine technical support of Howard Washington in carrying out certain phases of this work. Support from the LLL analytical Chemistry Laboratories, particularly the fine work by Virgil Duval and Charles Otto, is appreciated. Finally many helpful discussions with Robert Taylor and David Bowen are acknowledged.

REFERENCES

1. G. H. Higgins, A New Concept for In Situ Coal Gasification, Lawrence Livermore Laboratory, Rept. UCRL-51217 (1972).
2. D. R. Stephens, A. Pasternak, and A. Maimoni, The LLL In Situ Coal Gasification Program, Lawrence Livermore Laboratory, Rept. UCRL-75990 (1974).
3. J. H. Campbell, Pyrolysis of Subbituminous Coal as it Relates to In Situ Gasification (Part I: Gas Evolution), Lawrence Livermore Laboratory, UCRL-52035 (1976).
4. K. H. van Heek and H. Jüntgen, Ber. Bunsenges. Phys. Chem. 71, 113 (1967); 72, 1223 (1968).
5. F. J. Ackerman, GNLS: A Computer Program for General Non-Linear Least Squares Curve Fitting, Lawrence Livermore Laboratory, Rept. UCID-15636 (1970).
6. N. Berkowitz and W. den Hertog, Fuel 41, 507 (1962).
7. W. Idris Jones, J. Inst. Fuel 37, 3 (1964).
8. D. Fitzgerald, D. W. van Krevelen, and J. Schuyer, Coal Science (Elsevier, Amsterdam, 1957), p. 307.
9. L. Blom, Ph.D. thesis, Univ. of Delft, Holland (1960). Data reported in: Chemistry of Coal Utilization, H. H. Lowry, Ed. (John Wiley and Sons, New York, 1963), p. 267.
10. J. V. O'Gorman and P. L. Walker, Mineral Matter and Trace Elements in U.S. Coals, Natl. Tech. Info. Service, Rept. OCR-61-INT-2 (1972).
11. J. L. Kulp, P. Kent, and P. F. Kerr, Am. Mineral. 36, 643 (1951). Data also reported in Differential Thermal Analysis, Vol. I, R. C. Mackenzie, Ed. (Academic Press, New York, 1970), p. 323.

12. D. Fitzgerald and D. W. van Krevelen, Fuel 38, 17 (1959).
13. A. I. Yergey and F. W. Lampe, Fuel 53, 280 (1974).
14. R. Taylor and D. Bowen, Rates of Reaction of Steam and Carbon Dioxide with Chars Produced from Subbituminous Coals, Lawrence Livermore Laboratory, Rept. UCRL-52002 (1975).
15. C. Barker, Fuel 53, 176 (1975).
16. J. H. Campbell, Pyrolysis of Subbituminous Coal as it Relates to In-Situ Gasification (Part II: Characterization of Liquid and Solid Products), Lawrence Livermore Laboratory, to be published (1976).
17. E. A. Depp, C. M. Stevens, and M. B. Neuworth, Fuel 35, 437 (1956).
18. G. L. Tingey and J. R. Morrey, Coal Structure and Reactivity, Battelle Pacific Northwest Laboratories, Richland, Wash., Rept. TID-26637 (1973).

Table 1. Standard chemical analysis of Roland seam coal.

Characteristic	As received	Dry sample
<u>Ultimate analysis</u>		
Moisture	34.67%	—
Carbon	43.61	66.76%
Hydrogen	3.44	5.25
Nitrogen	0.73	1.11
Chlorine	0.01	0.01
Sulfur	0.48	0.74
Ash	5.96	9.13
Oxygen (by difference)	11.10	16.99

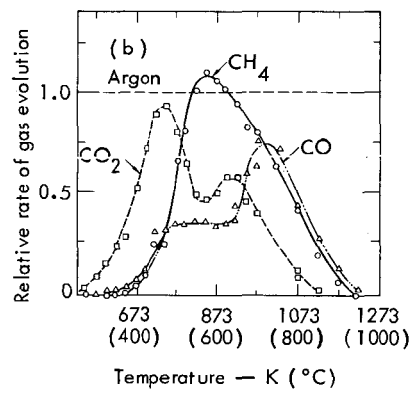
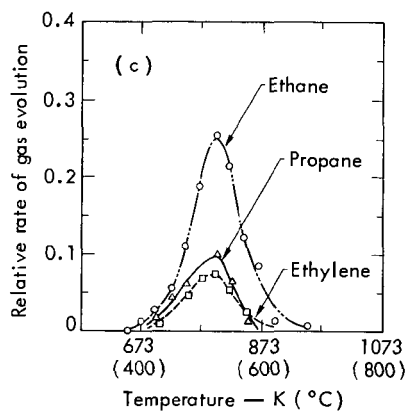
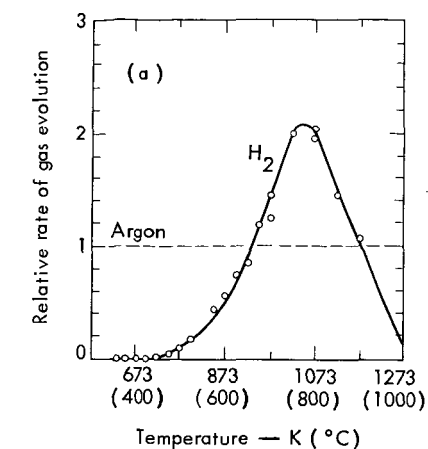


Fig. 1 Effect of temperature of gas evolution during pyrolysis of Roland seam coal. The heating rate is 3.33 K/min (3.33°C/min), the carrier gas is Ar, and the particle diameter is 1.65 to 3.35 mm. The rate of gas evolution is relative to a constant flow of carrier gas. One unit on the vertical axis equals 0.737 cm³/g•min.

NOTICE

"This report was prepared as an account of work sponsored by the United States Government. Neither the United States nor the United States Energy Research & Development Administration, nor any of their employees, nor any of their contractors, subcontractors, or their employees, makes any warranty, express or implied, or assumes any legal liability or responsibility for the accuracy, completeness or usefulness of any information, apparatus, product or process disclosed, or represents that its use would not infringe privately-owned rights."

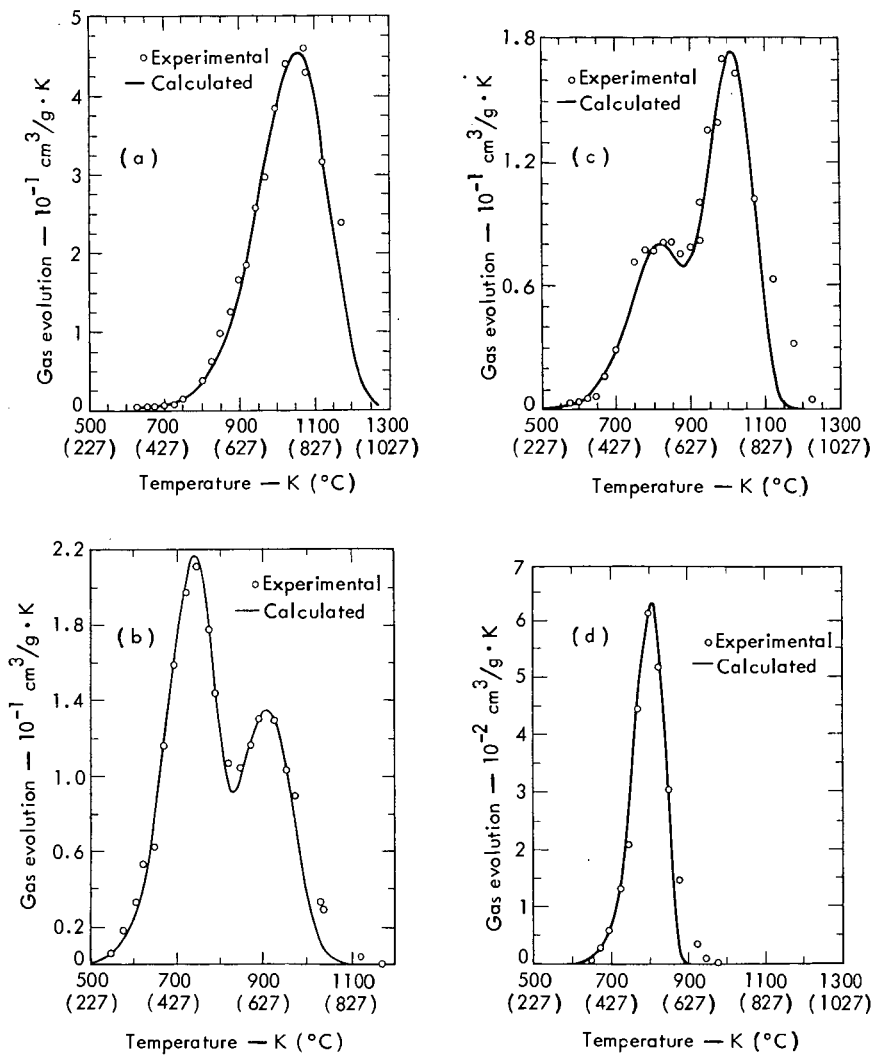


Fig. 2 Numerical fit of Equation 1 to experimental data for gaseous evolution of (a) H_2 , (b) CO_2 , (c) CO , and (d) C_2H_6 . Since the time-temperature scales are coupled, the rate is in units of $\text{cm}^3/\text{g} \cdot \text{K}$. To convert to time units, multiply by the heating rate of 3.33 K/min.

TRANSFORMATION OF SULFUR FUNCTIONAL GROUPS DURING PYROLYSIS OF COAL

Amir Attar^{1*}, Am. H. Corcoran², and G. S. Gibson²

¹Jet Propulsion Laboratory, Pasadena CA 91103

²California Institute of Technology, Pasadena CA 91125

INTRODUCTION

Three classes of sulfur compounds in coal are traditionally considered: (1) the inorganic sulfides, most of which are iron pyrites, FeS_2 ; (2) the inorganic sulfates, most of which are iron and calcium sulfates; and (3) the organic sulfur which includes the sulfur that is bound to the organic matrix of the coal. During processing, transformation of sulfur from one class to another, elimination of sulfur as hydrogen sulfide, or changes in the sulfur functional groups within the same class may occur.

Some of the facts that have been reported on the behavior of the sulfur functional groups during pyrolysis are given as follows:

- 1) Hydrogen sulfide is released.
- 2) Coking at temperatures up to 800°C cannot remove all the sulfur (3)(4). Coking at 1400°C removes up to 95 per cent of the sulfur; however, considerable volatilization of the coal occurs (5).
- 3) The inorganic sulfur remaining in the coke corresponds to 66 per cent of the inorganic sulfur in the original sample. Organic sulfur left in the coke corresponds to 72 per cent of the initial organic sulfur (6). More detailed distribution into classes is given by Given and Jones (7).
- 4) The degree of desulfurization relates to the volatilized fraction (3). The larger the volatilization, the larger will be the desulfurization.
- 5) A larger ash content increases the amount of sulfur that is retained in the coke (7).
- 6) The distribution of sulfur may change during pyrolysis. Inorganic sulfur is incorporated into the organic matrix (4)(8).

From our study, additional conclusions may be developed:

- 7) The release of H_2S at different times of the pyrolysis is due to different processes. Loose FeS_2 crystals, when pyrolyzed with coal, cause release of H_2S by two new processes. The first new H_2S peak is from the FeS_2 that was added to the coal. It has different mass-transfer limitations from the H_2S coming from the FeS_2 that was originally present in the coal. The other new H_2S peak appears at a higher temperature and is from the organic sulfur compounds. The first new H_2S originates in the reaction of H_2 with FeS_2 without mass-transfer limitations. The H_2S from the organic source appears to be by way of catalysis of the hydrodesulfurization of organosulfur compounds by the FeS crystals.
- 8) The total amount of organosulfur compounds of the thiophene class in the tar decreases as a result of adding FeS_2 . The decrease is probably the result of hydrodesulfurization of the compounds, probably catalyzed by the FeS crystals.

EXPERIMENTAL RESULTS

Different samples of bituminous coal were examined. A list of properties is given in Table 1. The coals were crushed to -100 mesh, and variable amounts of iron pyrites, FeS_2 at -170 mesh, were added. The components were thoroughly mixed until a constant total-sulfur reading was obtained for samples of 60-80 mg. The iron pyrites was supplied by Matheson-Coleman and Bell and used as received.

*To whom correspondence should be addressed. Current address: Chemical Engineering Department, University of Houston, Houston, Texas 77004

Experimental System and Procedure

A LECO Model 571-018 resistance furnace was used both to pyrolyze the coal samples and to combust samples for total-sulfur analysis. Pyrolysis was performed at 1300°F in a stream of argon (1250 ml/min) in a standard zirconia boat, LECO Cat. No. 528-051. The gas was bubbled in a chilled solution of $\text{Cd}(\text{BO}_2)_2$ whose pH and $\log[\text{S}^-]$ were followed electrochemically. A radiometer pH meter Model 26 was used with Radiometer electrodes G-202C for pH and F1212S for $[\text{S}^-]$ vs. SCE K401. Carbon dioxide was found to have a small influence on the measurement when it was injected into the argon stream. The aqueous solutions were extracted twice with benzene and then separated. The benzene phase was concentrated approximately 50 times by evaporation and then analyzed by means of an HP Model 5700 gas-chromatograph which was equipped with a flame-photometric detector. Two columns were used. One was 3 ft x 1/8 in. with 1 per cent OV-1 on Gas Chrom Q (Applied Science Laboratories) 80/100 mesh. The other was 6 ft x 1/8 in. 10 weight % diethylene glycol succinate on Gas Chrom Q 80/100 mesh.

Results

Table 2 shows the distribution of the total sulfur between the volatiles and the coke after the carbonization. The sulfur content of the coke increased as a result of adding FeS_2 , but the fraction that remained in the coke did not show an obvious correlation with the content of FeS_2 . In particular, samples C4 and C6 indicate that a smaller fraction of the total sulfur pool was retained when pyrites were added to the sample. The phenomenon can be explained if it is assumed that the iron (or FeS) catalyzes the decomposition of organosulfur compounds.

Figures 1-6 show how the rate of evolution of H_2S and the total amount of H_2S that was evolved vary with the pyrolysis time. Examination of the figures suggests the following points:

- 1) Adding FeS_2 to the samples caused added evolution of H_2S at two points where H_2S was not evolved otherwise. One was between the peaks of the original coal sample and caused them to merge. Compare Figures 1 with 2 and 3 with 4.
- 2) The additional peaks that appeared when FeS_2 was added did not coincide with existing peaks in the H_2S of the evolution.
- 3) The differences between samples C1, C4, and between C2 and C5 was mainly in the particle size and the amount of sulfur. The original microstructure was assumed to stay. When the coarse material was pyrolyzed, however, a third peak resulted which did not appear when the fine coals were pyrolyzed. Mass-transfer may have been controlling.

In Table 3, gas-chromatographic data for the organosulfur compounds that were collected in the solution are given. The peaks of the alkyl-thiophene isomers were lumped together as were the peaks of the alkyl-thianaphthene isomers and the alkyl-dibenzothiophene isomers. Separation was affected by a column with a very low polarity (OV-1), and a sulfur-specific flame-photometric detector was used. Sulfur compounds lighter than methyl thiophene were not analyzed. Moreover, some of the methyl thiophene may have been lost during the concentration by evaporation. The alkyl-thiophene peaks may include also some alkyl and aryl sulfides which are not separated on the column used. When a polar column was used for separation, 2- and 3-methyl thiophene, 2- and 3-ethyl thiophene, smaller amounts of propyl and butyl thiophene, and at least seven thianaphthenes were identified. The chromatograms from a polar column were very much the same as those reported by Martin and Grant (14) who analyzed the sulfur compounds in gas oil. Out of sixteen samples that were analyzed, a moderate increase in the organosulfur was observed for one sample only (#C6).

The data in Table 3 show that the addition of FeS_2 to the coal samples caused a decrease in the amount of the benzene-soluble thiophene derivatives in the oil. This observation is consistent with the result that relatively more H_2S is emitted when FeS_2 is added.

DISCUSSION

The H_2S and the organosulfur compounds that were emitted during the coking of coal were the result of reactions in both the dense phase and in the gas phase. The addition of FeS_2 to the coal was more likely to affect the gas-phase reactions. Such an effect could be either a reaction with components of the gas or catalysis or inhibition of reaction of components in the gas phase.

The following reactions were believed to be the most important in the system of FeS_2 and coal at temperatures below $800^\circ C$.

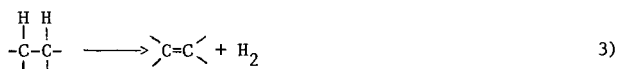
- 1) Decomposition of iron pyrites (7)



- 2) Hydrogen elimination



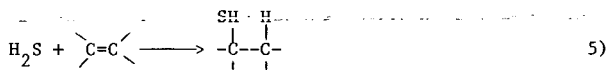
- 3) Production of olefines both in the gas and the condensed phase:



- 4) Desulfurization of iron pyrites by hydrogen (12)



- 5) Incorporation of sulfur via hydrogen sulfide into an organic molecule in the gas or in the condensed phase,

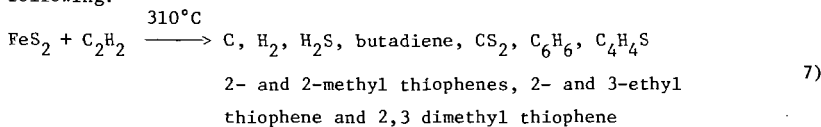


via sulfur by means of crosslinking

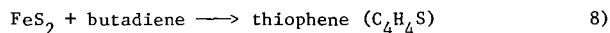


The above reactions can explain the incorporation of sulfur from the pyrites into the char (8).

- 6) Catalysis of ring-closure by reactions among H_2S , S, and unsaturated hydrocarbons. From references 9 and 10 we have reactions in accord with the following:



from reference 10,



Thiophene is a very stable compound and does not thermally decompose in homogeneous media up to temperatures as high as $950^\circ C$. So once formed, it is unlikely that it will decompose at the experimental conditions that were used. In the presence of hydrogen, however, catalytic reduction of the organosulfur compounds may occur even at temperatures lower than $1300^\circ C$. As a result of adding FeS_2 to the coal, the total amount of organosulfur compounds that was produced decreased. One must

conclude that FeS acts to a certain extent like CoS and MoS₂ and catalyzes the hydrodesulfurization of thiophenes. The use of iron in hydrodesulfurization catalysts was mentioned by McKinley (11).

The two additional peaks of hydrogen-sulfide emission that showed as a result of adding FeS₂ to the coal sample are believed to be due to the following:

- 1) The reaction of hydrogen with the FeS₂ crystals that were added to the sample. Such a peak, because of diffusion and mass-transfer limitations, appears a little before the peak of H₂S from the same reaction of FeS₂ that was previously in the coal reactions.
- 2) The hydrodesulfurization of the organosulfur compounds which adsorbed on the FeS crystals at lower temperatures. Hydrodesulfurization on FeS of thiophenic sulfur compounds may be the source of the "organic III" peak reported by Yergey et al. (13). Thiophenic compounds are known to be components of coal tar; however, the mechanisms of their source can be gas-phase or solid phase dehydrocyclation.

The following arguments imply that the thiophenic compounds indeed exist in the coal as such:

- 1) At 300-310°C, FeS₂ reacts with hydrocarbons to form thiophenic compounds; however, FeS₂ decomposes at 450-500°C, and FeS is formed.
- 2) FeS catalyzes the hydrodesulfurization of organosulfur compounds, and when coal is pyrolyzed at 700°C their concentrations in the tar are smaller when FeS₂ is added to the coal than for untreated coal.
- 3) Because thiophenes are found in the pyrolysis tar at temperatures like 700°C, their source must have been the coal itself. Their amounts in the tar will depend on their amounts in the original coal, on the amount of FeS, and on the efficiency of the hydrogenation that takes place which depends on the mass-transfer constraints of the coking reactor.

CONCLUSIONS

Preliminary data on the kinetics of the transformations of sulfur functional groups in coal shows that:

- 1) Hydrogen sulfide from loose FeS₂ crystals evolves at different rates than hydrogen sulfide from FeS₂ that was in the original sample.
- 2) Pyrolysis of coal in the presence of FeS₂ causes a decrease in the benzene-soluble, thiophenic organosulfur compounds in the oil.

The difference in the kinetics of the release of H₂S is probably due to different mass-transfer limitations. This assumption is supported by the fact that the ratio of the amount of sulfur that is released to the gas and that which remains in the char depends on the particular equipment in which the pyrolysis is made.

The reduction in the benzene-soluble organosulfur compounds is probably due to catalysis of the hydrodesulfurization on the FeS surface. Although the H₂ pressure is very small, the rate of reaction may still be large because of the high temperature of the pyrolysis (1300°F).

Since thiophene derivatives are found in the oil, even when FeS₂ is added to the coal, their source must be the organic matrix and not dehydrocyclation reactions on the sulfide surface.

ACKNOWLEDGMENT

Work reported here was supported with funds from a Ford Motor Company Energy Grant and from the Director's Fund of the Jet Propulsion Laboratory. The support is gratefully acknowledged.

REFERENCES

- 1) Powell, A. R., Ind. Eng. Chem., 12 (11) 1069 (1920).
- 2) Powell, A. R., Am. Gas. Assoc., Tech. Sect., 5, p. 244-255 (1920).
- 3) Peet, N. J., Siemon, S. R., and Stott, J. B., Fuel, 48 (1969).
- 4) Cermic-Simic, S., Fuel, 41, 141 (1962).
- 5) El-Koddah, N., and Ezz, S.Y., Fuel, 52, 128 (1973).
- 6) Lowry, H. H., ed., "Chemistry of Coal Utilization," Supplementary Volume, John Wiley & Sons, New York (1963).
- 7) Given, P. H. and Jones, J. R., Fuel, 45, 151 (1966).
- 8) Eaton, S. E., Hyde, R. W., and Old, B. S., Am. Inst. Mine. Met. Eng., Iron and Stee Div. Metal Tech., 19 (7) 343 (1948). Tech. Bull. 2453.
- 9) Steinkopf, W. and Harold, J., Ann., 428, 123 (1922). C.A. 16-3653.
- 10) Schneider, G. G., Beck, H. and Hausser, H., Ber., B70, 425 (1937). C.A. 20-3912.
- 11) McKinley, J. B., in "Catalysis" Volume V, Emmett, P. H. (ed.), p. 405, Reinhold, London (1957).
- 12) Maa, P. S., Lewis, C. R., Hamrin, C. E., Jr., Fuel, 54 (1), 62 (1975).
- 13) Yergey, A. L., Lampe, F. W., Vestal, M. L., Day, A. G., Fergusson, G. J., Johnston, W. H., Snydermass, J. S., Essenhig, R. H., and Hudson, J. E., Ind. Eng. Chem., Proc. Des. Develop, 13 (3) 233 (1974).
- 14) Martin, R. L. and Grant, J. A., Anal. Chem., 37, 649 (1965).

Table 1
Properties of the Coals Used

Coal Source	Supplied By	Notation	Total % S	Pyrites % S	Organic % S	% Volatile	Size Mesh
Jefferson Co., Ohio	U.S. Bureau of Mines	C1	1.698	1.234	0.464	38.0	65-100
Jefferson Co., Pittsburgh Seam		C2	3.233	2.261	0.972	34.3	-100
Washington State	Jet Propulsion Laboratory	C3	0.363	0.363	0.0		-100
As C1 + FeS ₂		C4	3.938				coal -100 FeS ₂ -170
As C2 + FeS ₂		C5	4.650	3.90	0.75		coal -100 FeS ₂ -170
As C3 + FeS ₂		C6	2.689	2.685	0.0		coal -100 FeS ₂ -170

Table 2
Distribution of the Total Sulfur Between the Volatiles and the Coke

Sample	No.	Weight % Volatiles	Weight % Sulfur in Coal	Weight % Sulfur in Coke	mg Sample Size	Fraction of total sulfur weight % in coke in volatiles	
C1	25	33.27	1.698	1.052	49.9	41.34	58.66
C2	23	30.35	3.233	0.724	40.2	15.60	84.40
C3	26	37.58	0.363	0.358	79.3	61.56	38.44
C3*	27	34.36	0.363	0.242	74.5	43.76	56.24
C4	32	30.95	3.938	2.040	33.6	35.77	64.23
C5	28	27.84	4.650	2.009	25.5	31.18	68.82
C6	30	35.04	2.689	0.538	25.4	13.00	87.00

*Coked 24 minutes. All the rest 12 minutes at 1300°F.

Table 3
Organosulfur Compounds in the Pyrolysis Products

Relative amount/mg coal. Note that some of the light sulfur compounds might have been lost.

Sample	No.	C_1-C_2 Alkyl Thiophenes**	C_3-C_4 Alkyl Thiophenes**	Thianaphthenes	Dibenzothiophenes
C1	25-55	0.316	1.97	4.03	3.36
C1*	24-52	0.729	1.42	1.30	0.077
C3	23-54	0.154	0.248	0.204	0.0063
C3*	27-49	0.399	0.77	0.624	0.012
C4	32-56	0.0997	0.459	0.399	0.0399
C5	28-48	0.314	0.251	0.0637	0.0078
C6	30-50	0.0484	0.387	0.436	<0.001

*Deeply carbonized plus mildly carbonized.

**Includes also some non-thiophenic sulfides.

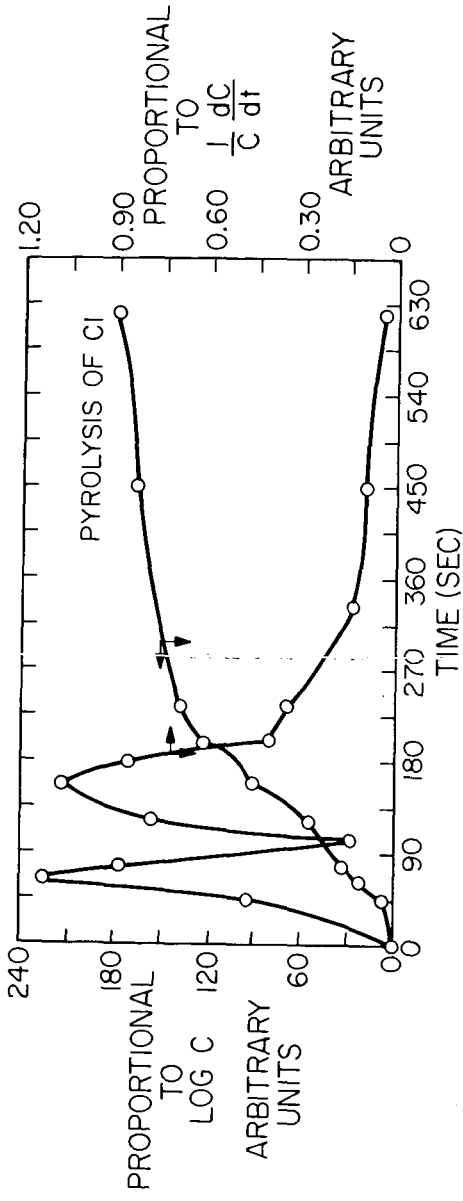


Fig. 1 Relative amount and rate of evolution of H₂S in pyrolysis of coal sample C1

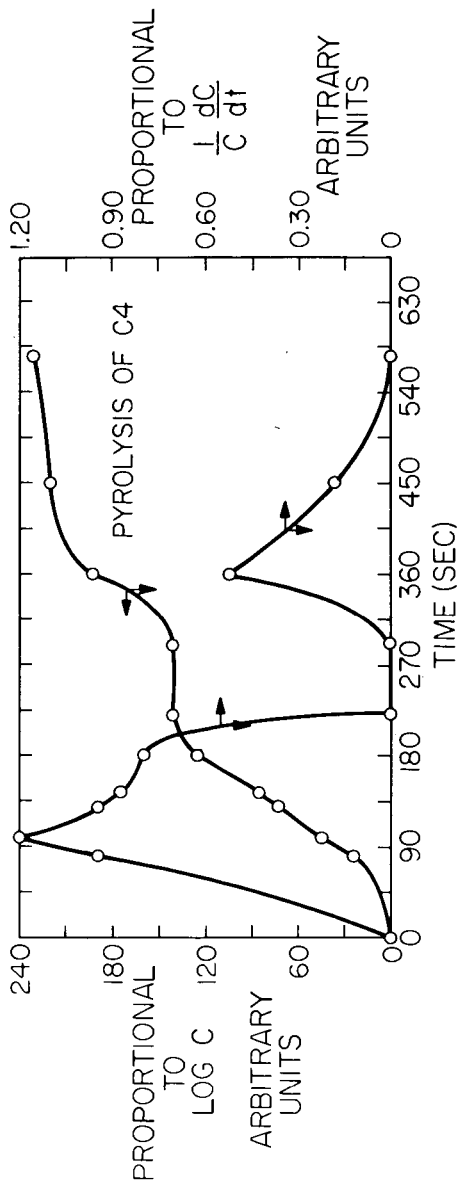


Fig. 2 Relative amount and rate of evolution of H_2S in pyrolysis of coal sample C4

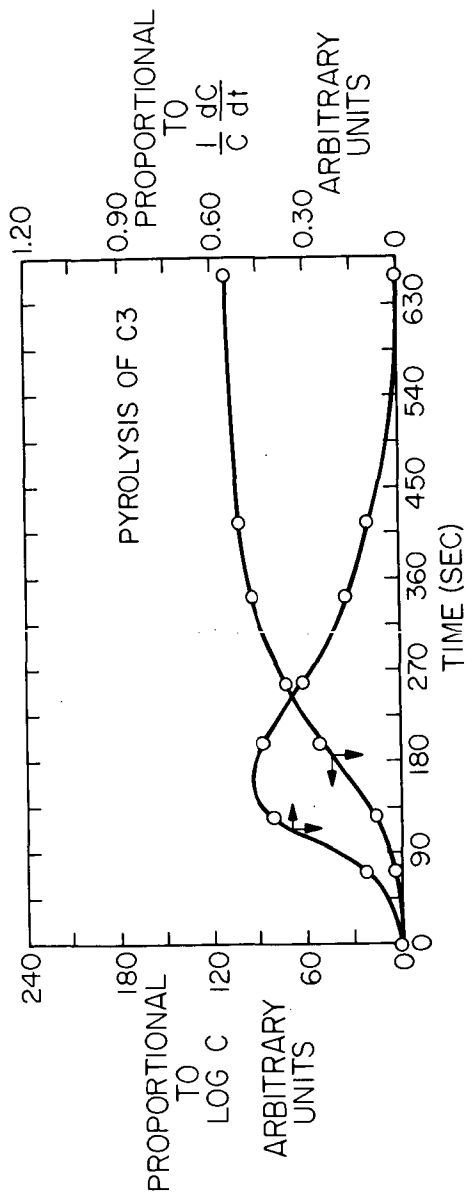


Fig. 3 Relative amount and rate of evolution of H_2S in pyrolysis of coal sample C3

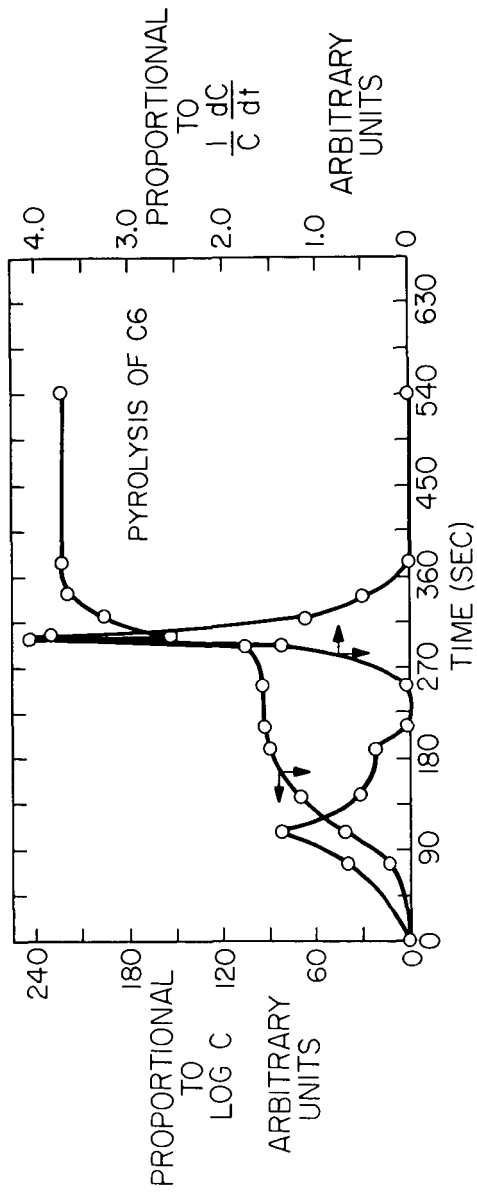


Fig. 4 Relative amount and rate of evolution of H_2S in pyrolysis of coal sample C6

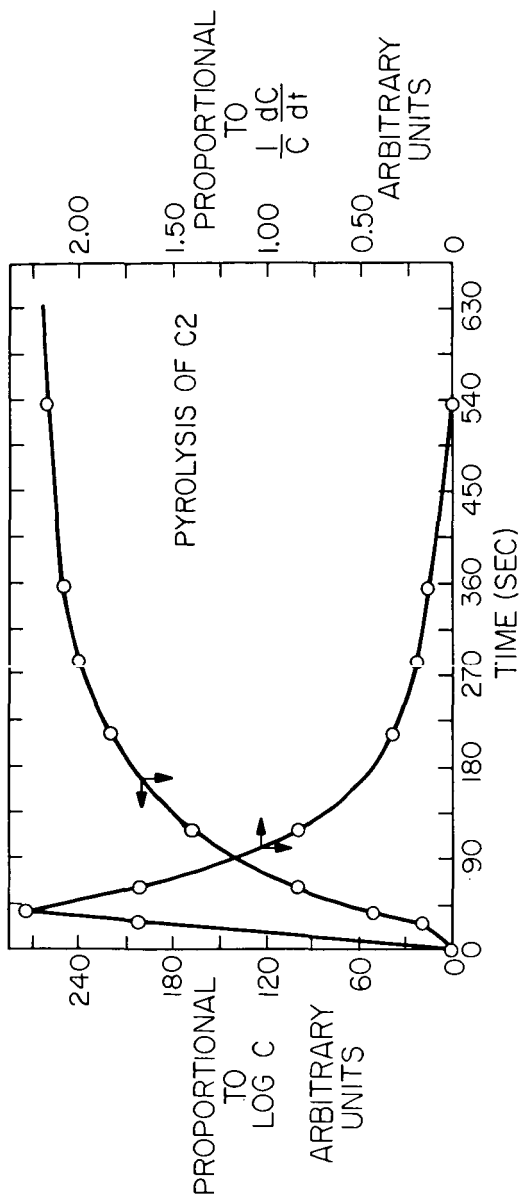


Fig. 5 Relative amount and rate of evolution of H_2S in pyrolysis of coal sample C2

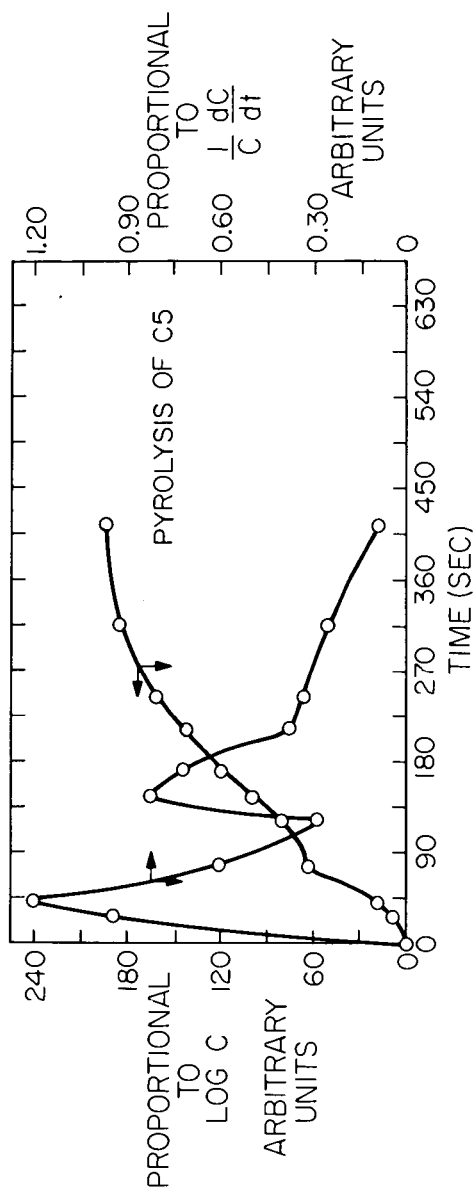


Fig. 6 Relative amount and rate of evolution of H_2S in pyrolysis of coal sample C5

DESULFURIZATION OF COAL BY CHLORINOLYSIS

P. S. Ganguli, G. C. Hsu, G. R. Gavalas*, S. H. Kalfayan

Jet Propulsion Laboratory, California Institute of Technology,
4800 Oak Grove Drive, Pasadena, California 91103

*Professor, Chemical Engineering Department,
California Institute of Technology, Pasadena, California 91125

INTRODUCTION

Since most of the coals, particularly the eastern coals, in this country have high sulfur content, there is a need for an economical process of converting high sulfur coals to clean fuel (<0.7% sulfur by EPA standard) to utilize coal as a source of energy without causing serious air pollution.

Most of the earlier studies^(1,2,3,4,5) on chlorinolysis of coal were conducted to understand the chemistry of the process, to produce a non-caking fuel suitable for burning, and to the possibility of producing chlorohydrocarbons from coal. However, there was a limited amount of work^(6,7) on desulfurization by chlorination of coal in the gas phase and at high temperature (400°C) and elevated pressure. These studies showed that both organic and inorganic sulfurs could be removed to a certain extent but the loss of coal was more than 20%, and because of high temperature chlorination, satisfactory dechlorination was not achieved. A few studies⁽⁸⁾ on the chlorination of coal in the aqueous media at 25°C resulted in poor removal of sulfur.

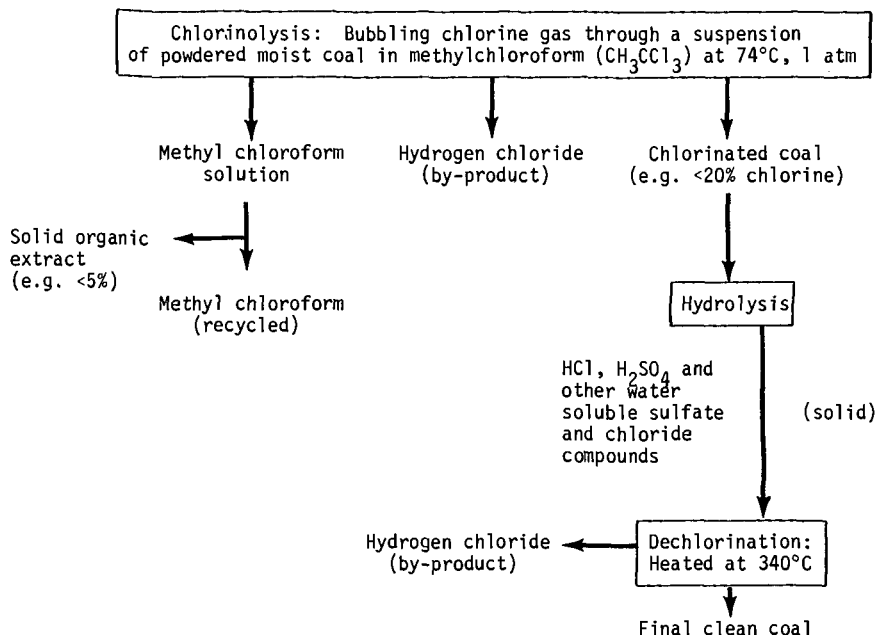
This paper describes some of the experimental results showing the feasibility of removing sulfur particularly organic sulfur from high sulfur coals by a simple method of low temperature chlorinolysis followed by hydrolysis and dechlorination. At first the process concept of this chlorination method will be described. Experiments, results and discussion of this method of desulfurization will be described for two bituminous coals.

PROCESS CONCEPT OF COAL DESULFURIZATION BY CHLORINOLYSIS

Based on the results of earlier studies on chlorination of coal, the experimental conditions were selected in such a way that there should be high degree of organic and inorganic sulfur removal at a low degree of chlorination, and dechlorination of the product would be carried out easily. In the presence of water and at a temperature much higher than room temperature, the S_2Cl_2 formed from FeS_2 chlorination⁽⁹⁾ is readily converted to HCl and H_2SO_4 . However, at room temperature this reaction is slow and S_2Cl_2 reacts with organic compounds to form organo-sulfur compounds. Due to the reactive nature of carbon-sulfur and sulfur-sulfur bonds, chlorinolysis⁽¹⁰⁾ may bring about the scission of these bonds in organic compounds. These reactions are catalyzed by acids or Friedel Crafts catalysts such as $FeCl_3$ and $AlCl_3$. The resulting chlorinated organo-sulfur compounds can be hydrolyzed and oxidized at a relatively high temperature to produce sulfate compounds. Chlorination at a relatively high temperature in an organic solvent is slower than in aqueous media at room temperature, but gives a greater degree of structural loosening of coal and thereby may remove more organic sulfur at a lesser degree of chlorination. Chlorination of coal is mainly a substitution reaction and hydrogen chloride is evolved as a product. Chlorine in coal chlorinated under mild conditions, can be completely removed as hydrogen chloride by heating at 340°C⁽²⁾.

EXPERIMENTAL

Based on the concepts and facts described above, a simple method of coal desulfurization by chlorinolysis was selected as described in the following flow diagram.



In this method chlorine gas is bubbled through a suspension of powdered moist high sulfur coal in methyl chloroform at 74°C and atmospheric pressure for 1 to 4 hours. Methyl chloroform was chosen because it is an economical non-hazardous industrial solvent which cannot be further chlorinated and has a suitable normal boiling point of 74°C. The slurry is filtered and the filtrate is distilled for solvent recovery. The chlorinated coal is hydrolyzed with water at 25°C, and the slurry is filtered. The hydrolyzed chlorinated coal is dechlorinated by heating at 300-350°C and atmospheric pressure.

Several experiments were conducted with a high sulfur bituminous coal from Hillsboro, Illinois. The moisture content in the powdered coal (-100 to +150 mesh) was varied from 0 to 50% with respect to coal. Samples were collected at 1/2 hr., 1 hr., 2 hrs., 3 hrs., and 4 hrs. period. The chlorinated coal was then hydrolyzed and dechlorinated. The results of a typical experiment are presented in Table I. The treated coal samples were analyzed mainly for sulfur forms and chlorine. To find the effect of AlCl₃ as catalyst on organic sulfur removal, a similar experiment was conducted by adding 0.5% AlCl₃ with respect to coal. Chlorinolysis experiment was carried out with a powdered (-200 mesh) moist (30% moisture) bituminous coal with high organic sulfur. The desulfurization results are presented in Table II.

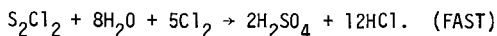
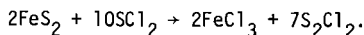
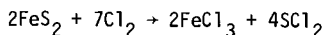
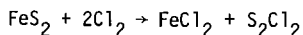
RESULTS AND DISCUSSION

Results of a desulfurization experiment with a high sulfur bituminous coal from Hillsboro, Illinois are presented in Table I. It shows that chlorinolysis of the coal for an hour in the presence of moisture can remove 77% of pyritic sulfur, 70% of organic sulfur, 30% of sulfate sulfur, and 69% of total sulfur. Since sulfate compounds are soluble in hot water, all the sulfate compounds would be removed by improving the hydrolysis step. Chlorinated coal had 22% chlorine before and 11% after the hydrolysis step. After hydrolysis and dechlorination at 300°C for an hour, the residual chlorine in the final treated coal was 2.6%. According to the results of earlier chlorination experiments⁽²⁾, all the chlorine in coal could be removed as hydrogen chloride by heating at 350°C for 2 hours. Results of all the experiments with this coal indicate that removals of up to 60% organic sulfur, 90% pyritic sulfur, 30% sulfate sulfur, and 70% total sulfur have been achieved by current chlorinolysis procedures. Further work is underway to improve the process and to achieve better understanding of the chemistry.

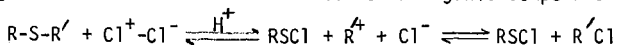
Results of a chlorinolysis experiment with 0.5% AlCl₃ as catalyst indicate that AlCl₃ does not have any noticeable effect on the removal of organic sulfur from coal. Coal contains iron compounds in the mineral matter sufficient to form about 1 to 2 percent of FeCl₃. This quantity would be sufficient to catalyze ionic chlorination reactions.

Results of a chlorinolysis experiment with dried coal and 0.5% AlCl₃ shows that only 18.5% of organic sulfur can be removed. So the presence of moisture has a significant effect on the removal of organic sulfur from coal. An optional solvent extraction step with tetrahydrofuran at room temperature of chlorinated coal shows that it can extract a considerable amount (>20%) of organic matters from coal composition which in turn would be a desirable feed stock for liquid fuel synthesis.

The kinetic data of chlorination and coal desulfurization are presented in Figure 1. The initial rate of chlorination is very fast and the chlorine content in coal is 23% in half an hour and then slowly increases to 26% within the next one and a half hours. Within half an hour period most of the pyritic sulfur and a portion of organic sulfur are converted to sulfate sulfur. In the next one and a half hour period pyritic and organic sulfurs are slowly converted to sulfate sulfur. According to sulfur balance from data, the gain in sulfate sulfur is equal to the combined losses in pyritic and organic sulfurs. This result supports the possible reaction mechanisms for the conversion of pyritic and organic sulfurs to sulfate sulfur as described below.

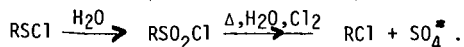


Due to high steric accessibility of bivalent S and electron releasing and electron demanding nature of S atom, the carbon-sulfur (sulfide) and sulfur-sulfur (disulfide) bonds in coal will be highly reactive. Chlorinolysis⁽¹⁰⁾ can bring about the scission of these bonds in organic compounds as follows.





where R and R' represent hydrocarbon groups. The resulting chlorinated organo-sulfur compounds can be hydrolyzed and oxidized in the presence of chlorine at a moderately high temperature to produce sulfate compounds.



Results identify that these sulfate compounds produced are removed from coal in the hydrolysis step.

Heating value of the original coal and that of the final treated coal were 11052 Btu/lb and 10900 Btu/lb, respectively, on an as received and chlorine free basis.

Results presented in Table II show that 57% of organic sulfur can be removed by chlorinolysis of a bituminous coal with high organic sulfur.

CONCLUSION

A simple method of coal desulfurization by chlorinolysis of powdered moist coal in methyl chloroform at 74°C and 1 atmosphere can remove up to 70% organic sulfur, 90% pyritic sulfur, 30% sulfate sulfur and 70% total sulfur from a high sulfur bituminous coal. After hydrolysis, the chlorinated coal is dechlorinated by heating at 300-350°C for two hours.

REFERENCES

1. Macrae, J.C. and Oxtoby, R. Fuel, Lond. 44 (1965) 395.
2. Pinchin, F.J. Fuel, Lond. 37 (1958) 293.
3. Pinchin, F.J. Fuel, Lond. 38 (1959) 147.
4. Oxtoby, R. Fuel, Lond. 45 (1966) 457.
5. Macrae, J.C. and Oxtoby, R. Fuel, Lond. 44 (1965) 409.
6. Sun, S. and Wu, M. Preprint, AIME ANNUAL MEETING at Dallas, Texas, Feb. 1974.
7. Imperial, G.R. and Walker, P.L. Jr., Special Research Report SR-31, The Pennsylvania State University (March, 1962).
8. Mukai, Shigeru et. al. Nenryo Kyokai-shi 48 (1969) 905.
9. Ezbekore, V.I. Trudy Uzbekskogo Gosudarst. Unive., Sbornik Rabot Khim. 15 (1939) 131.
10. Kharasch, N. (ed.) "Organic Sulfur Compounds", Vol, I, Pergamon Press, N.Y. (1961).

Table I. Results* From Preliminary Chlorinolysis Experiments
(A Bituminous Coal from Hillsboro, Illinois)

Reaction Conditions	Composition	Raw Coal	Percent Sulfur Removal (Chlorine free basis)	Finely Treated Coal
Chlorination:				
74°C 1 atm, 1 hr	Pyritic sulfur	1.89%	77	0.43%
Powdered (-100 to 150 mesh)	Organic sulfur	2.38%	70	0.72%
	Sulfate sulfur	0.50%	30	--**
Moist (50% moisture)	Total sulfur	4.77%	69	1.15%
Coal in methyl chloroform				
Before dechlorination	Chlorine			11%
Dechlorination:				2.6%
At 300°C for 1 hr. Chlorine				

* All the chemical analyses were conducted by the Galbraith Laboratories, Inc. at Knoxville, Tennessee.

** The 0.35% sulfate sulfur left is expected to be removed by further water washing.

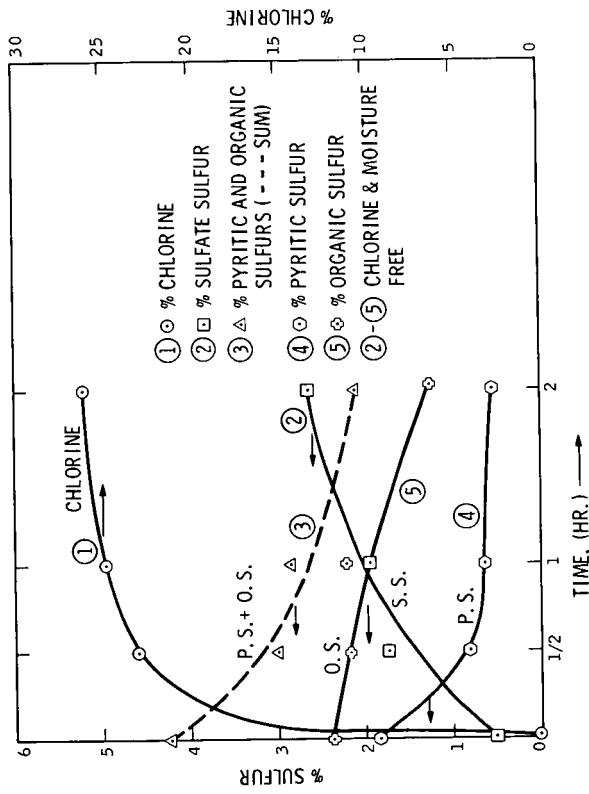
Table II. Results From Preliminary Chlorinolysis Experiments
for a Bituminous Coal (Hamilton, Kentucky)

Chlorination Conditions	Composition	Raw Coal	Finely Treated Coal	Percent Sulfur Removal
74°C, 1 atm, 4 hrs	Pyritic sulfur	0.08%	0.03%	62.5%
Powdered (-200 mesh)	Organic sulfur	2.67%*	1.16%	56.5%
Moist (30% moisture)	Sulfate sulfur	0.15%	0.29%	--**
Coal in methyl chloroform	Total sulfur	2.90%	1.48%	59.0%

* Sulfur in this coal is mostly organic sulfur.

** Sulfate sulfur can be removed in the hydrolysis step.

FIGURE 1. SULFUR AND CHLORINE IN COAL DURING CHLORINOLYSIS



SULFUR AND ASH REMOVAL FROM COALS BY HIGH INTENSITY-HIGH GRADIENT MAGNETIC SEPARATION. C. J. Lin, Y. A. Liu, D. L. Vives, M. J. Oak and G. E. Crow. Department of Chemical Engineering, Auburn University, Auburn, Alabama 36830.

In this paper, the reported experimental data on the removal of sulfur and ash from coals by magnetic separation are reviewed and analyzed. New experimental results obtained on the removal of sulfur and ash from dry, wet and liquefied coals by high intensity-high gradient separation at the Coal Conversion and Magnetic Separation Laboratories, Department of Chemical Engineering, Auburn University, are presented. The effect of operating conditions on the grade and recovery of the separation will be quantitatively discussed. A quantitative assessment of the technical and economic feasibility of applying magnetic separation to the desulfurization and deashing of coals is presented. The needs and opportunities in the future research and development work are also suggested.

EVALUATING SULFUR-PRODUCING FGD PROCESSES

Lawrence H. Weiss

Chem Systems Inc.
747 Third Avenue
New York, N.Y. 10017

Flue gas desulfurization systems can be broadly categorized as throwaway and recovery systems. In the throwaway systems, the sulfur removed from the flue gas is rejected from the process in a waste sludge, usually a wet mixture of CaSO_3 and CaSO_4 . In recovery systems, the sulfur-absorbing reagent is regenerated for recirculation to the flue gas contacting device while the sulfur removed from the flue gas is converted into its elemental form or into sulfuric acid. The dominant choices for commercial installations up to this time have been the wet, throwaway (lime/limestone) systems. Accordingly, the selection of these systems has been well-described in many symposia and other publications. However, the continued development of recovery processes has brought several to the commercial or near commercial status. Thus, this paper addresses the evaluation of such recovery processes for a commercial installation.

PROCESS DESCRIPTIONS

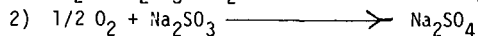
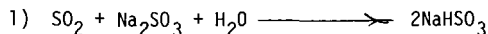
Three processes have been selected for discussion and comparison: Wellman-Lord/Allied Chemical sodium-based (commercial, wet), Catalytic/IFP ammonium-based (near commercial, wet), and Atomics International ACP (developmental, semi-dry). The Wellman-Lord process with Allied Chemical regeneration and the Catalytic/IFP process both require a clean reducing gas to carry out the regeneration of the absorbent and the production of elemental sulfur. Due to the limited availability of natural gas, the use of a medium Btu gas from a coal gasifier has been assumed for the comparison here and a gasifier included in each of these processes. The Atomics International ACP process can utilize petroleum coke or coal for its regeneration and reduction steps with the choice dependent upon their relative cost at a given site.

Wellman-Lord/Allied Chemical Process

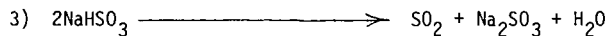
The Wellman-Lord process consists of three major sections for SO_2 recovery: (1) scrubber, (2) evaporative-crystallizer, and (3) sodium sulfate removal. The Allied Chemical SO_2 Recovery Process consists of a catalytic reduction of SO_2 to elemental sulfur.

The chemistry of the Wellman-Lord /Allied Chemical process is as follows:

Absorber:



Evaporator:



Reducer:



Figure 1 shows a block diagram of the coupled scrubbing-regeneration system.

Flue gas from the electrostatic precipitator is adiabatically saturated with water, then contacted countercurrently with the absorbing solution. Sulfur dioxide is absorbed into the solution of sodium sulfite and reacts to form sodium bisulfite as

shown in reaction 1. The scrubbing solution is recirculated through the scrubber to obtain a concentrated solution of bisulfite. Reaction 2 also occurs during scrubbing and recirculation to form the unregenerable by-product, sodium sulfate. Reaction 1 is reversed in an evaporative crystallizer where sodium sulfite is crystallized and SO₂ and water are released as gases (Reaction 3). Steam is used to decompose the bisulfite at the rate of 9-12 pounds of steam per pound of SO₂ recovered. A purge stream is taken to prevent build-up of sodium sulfate. The regenerated sulfite is returned to the scrubber (1).

The product of the Wellman-Lord Process is a stream of concentrated SO₂. The SO₂ may be oxidized to produce sulfuric acid or it may be reduced to elemental sulfur in any number of processes. The Allied Chemical SO₂ Reduction Process (2) can utilize reducing gas to produce sulfur via reactions 4 and 5. These reactions take place at high temperature, requiring refractory-lined reactors.

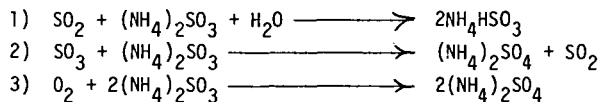
Commercial Status. The Wellman-Lord process is fully commercial with numerous installations world-wide, largely on oil-fired boilers. The Allied Chemical SO₂ reduction process has been operated commercially at a large Canadian copper smelter. A 100 MW demonstration plant has recently been started up at NIPSCO (3).

Catalytic/IFP Ammonia Scrubbing Process

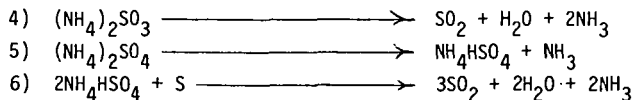
The Catalytic/IFP process consists of five major process sections: (1) scrubber, (2) evaporator-decomposer, (3) sulfur dioxide reduction, (4) reducing gas generation, and (5) wet Claus sulfur recovery. A block diagram of the IFP process is shown in Figure 2.

The chemistry of the IFP process is as follows:

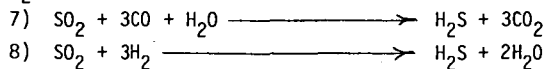
Absorption:



Regeneration:



H₂S Generation:



Claus Reaction:



The flue gases from the electrostatic precipitator are first adiabatically saturated with water in the bottom section of a tray tower. The saturated gases are then contacted with an ammonium sulfite brine to remove sulfur oxides. Reactions 1, 2, and 3 take place in the scrubber. Before the gases are discharged from the scrubber, they are washed in an additional stage with water (or acid) to remove residual gaseous ammonia to prevent its loss. A stream of concentrated

brine is removed from the bottom of the scrubber and sent to an evaporator which separates out ammonium sulfate crystals and decomposes the sulfites to NH_3 , SO_2 , and H_2O by reaction 4.

The sulfate crystals from the evaporator are decomposed in a reducing atmosphere by reactions 5 and 6. The heat for the reduction is supplied by submerged combustion of medium Btu gas with a deficient amount of air. The reduction takes place at 600-700°F.

Additional medium Btu gas is supplied to reduce the stream from the evaporator. Two-thirds of the sulfur dioxide is reduced to hydrogen sulfide by reactions 7 and 8. The hydrogen sulfide produced in the SO_2 reducers and the remaining SO_2 are reacted in the IFP "wet Claus" reactor by reaction 9 to form elemental sulfur. Ammonia is recovered and unreacted H_2S is incinerated or returned to the power plant boiler to be oxidized to SO_2 (4).

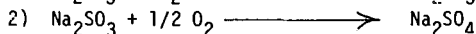
Commercial Status: IFP has studied all the single processing steps on the laboratory and pilot scale at their research center in France. A fully integrated 30 MW demonstration is now operational on an oil-fired utility boiler in France (4). Catalytic is now operating an engineering optimization unit on flue gas from a coal fired utility boiler at an Air Products chemical plant in Kentucky.

Atomics International - Aqueous Carbonate Process (ACP)

The ACP consists of four major sections: (1) scrubber, (2) reducer, (3) carbonator, and (4) Claus plant. Figure 3 shows a block diagram of the ACP.

The chemistry of the ACP is as follows: (5)

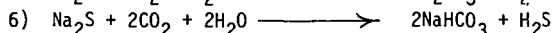
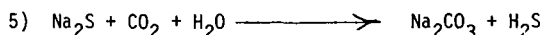
Scrubber:



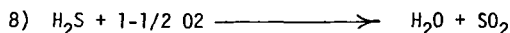
Reducer:



Carbonator:



Claus:



The flue gas leaving the electrostatic precipitator is contacted by sodium carbonate solution to remove sulfur oxides by reactions 1 and 2. These reactions take place in a modified spray drier which is unique to the ACP. The scrubbing solution is dispersed into a finely atomized fog which flows concurrently with the flue gas down the spray drier. The sulfur dioxide from the flue gas diffuses into the liquid phase of the solution and reacts. Water simultaneously evaporates from the tiny fog droplets.

At the bottom of the spray drier, all of the water has evaporated from the "scrubbing" solution and the flue gas has been cooled to a minimum of 20°F above its water saturation temperature (usually 150°F to 200°F). The solids created by the evaporation of the water are collected, first mechanically and then with an electrostatic precipitator. The flue gas is then discharged to the atmosphere through a stack (5).

The solids from the spray drier are conveyed into a molten salt reactor where the reduction reactions 3 and 4 occur. Excess coke or coal is fed to the reducer and the temperature is maintained at 1800°F by combustion of carbon with air. Petroleum coke is presently preferred in the ACP (5), but coal has been successfully tested.

The molten sodium sulfide (Na_2S) product of the reduction is quenched in water and filtered to separate residual solids (carbon and fly ash). The sodium sulfide solution is converted to sodium carbonate by reactions 5 and 6. The CO_2 for H_2S stripping is recovered from the CO_2 rich off-gases from the reducer. The bicarbonate is thermally decomposed and the CO_2 returned to the carbonation step (reaction 7). Sulfur is recovered from the hydrogen sulfide in a standard Claus Plant.

Commercial Status. Atomics International has piloted the spray drier in a 7 ft. I.D. unit with a simulated flue gas and also with a 5 ft. I.D. unit on real flue gas at the Mohave Station. The molten reduction of sodium sulfide and sulfate has been carried out in a 3 ft. I.D. reactor. The A.I., carbonation process has been operated at bench scale. (Equivalent to about 1 MW.) These process steps have not been tested in closed loop operation, but successive use of the product from each individual step through the entire sequence has been carried out.

EVALUATION FACTORS

A review of the detailed flowsheets and material and energy balances (1), for these processes shows differences in energy consumption, type of reducing agent required, and the degree of interaction with the operation of the boiler. In addition, especially for new technology, the extent of technical risk for each process is also a key evaluation factor. Two of these factors are amenable to quantitative evaluation: energy consumption and type of reducing agent. The other two are subjective and can only be quantified by intuitive technical judgement. For example, on a scale from 0 to 10 points, the use of coal as the reducing agent might be given 10 points and natural gas, 0. In another category, a fully commercial process might score the full amount allowed while one under development might only score 20-30% of the full amount. The number of points awarded for the maximum in each category must be determined for each specific site. The availability of the various reducing agents, water, power, land area and intangible attitudes toward technical risk and modifications of normal operations must all be considered. The limitations on the method reflect the uncertainties and risks in evaluating evolving technology. However, the effort and discipline involved in performing such an evaluation can lead to consistent results among independent evaluators.

The amount of energy consumed by an FGD process has a direct impact on the power plant's heat rate (efficiency) and also on the available net electric generating capacity. If a utility must purchase power to offset that consumed by an FGD process it may prefer to select an alternative with higher fuel consumption and lower electrical demand. Such a sacrifice of efficiency for capacity may also be justified where costly peak generating would be required to supply the power consumed by the FGD process. These considerations would be reflected in the choice of maximum score assigned to this factor.

The preferred reducing agent for any process would be the same coal used as boiler fuel. This would ensure an adequate supply and eliminate any requirement for special purchasing, handling and storage. The choice of coal as the preferred reducing agent imposes a direct

penalty for processes unable to use it. It also imposes an indirect penalty in the added technical risk, higher cost, and higher fuel consumption required by a coal gasifier. The extent of such penalties is obviously very site-dependent.

The lesser the extent of interaction between the FGD process and the boiler, the more preferable, because it minimizes operating problems. However, a by-pass for flue gas around the FGD system must be installed and permission obtained to use it when necessary, or this factor is not a valid consideration. Interaction involves the pressure drop through the absorber, as it poses a potential threat of back-pressure in the boiler in case of plugging the absorber or failure of the ID fan. The interaction can also be reduced by providing sufficient intermediate storage to allow limited operation of the absorber while the regeneration section is out of service and vice versa.

The evaluation of technical risk and the weight given to it in the total evaluation is likely to reflect the troubled operating histories of all FGD installations to date, even those which are now successful. The newness of the sulfur-producing processes emphasizes the need to carefully consider redundant components and the materials of construction chosen for the severe service encountered in the regeneration sections. Initial designs are likely to be conservative in attempting to achieve mechanical reliability and minimize the technical risk. The extent to which this is carried out will be limited by cost and by the reliability requirements of the prospective host utility.

Other site-specific evaluation factors are shown in Table 1. The amount of sulfur to be

Table 1

SITE-SPECIFIC EVALUATION FACTORS

% S in coal (% removal required)

% Ash in coal (% removal required)

Other state and local regulations

Waste disposal

Water quality and availability

Geographic factors (elevation, ambient temperature range, etc.)

removed depends upon the sulfur content of the coal and the emissions control requirements. All of the processes under active development should be capable of meeting all current SO₂ emissions limits. The flyash must be removed to prevent operating problems in the FGD system and to meet emissions limits. Unlike the lime/limestone systems, regenerative FGD processes cannot tolerate ash-laden flue gas. Limitations on liquid and solid waste streams can have a major impact on the feasibility of processes such as these with their purge streams. Sufficient water must be available for the consumptive needs of these processes. In addition, it must be of adequate quality to vaporize and disperse into the atmosphere. Local geographic factors influence the size of equipment and the extent of insulation and protective structures required. These all have differing impacts on the evaluation of individual processes.

APPLICATION OF THE EVALUATION METHOD

To illustrate the foregoing evaluation method for the processes described earlier, a hypothetical site for a new 500 MW utility boiler was selected with the characteristics shown in Table 2. The values chosen for the boiler, coal and site are intended to be representative of a wide range of actual conditions. The emissions limitations for particulates must be controlled, since all three regenerable processes require prior

removal of fly ash to prevent interference with process chemistry and process equipment.

The SO₂ removal to meet New Source Performance Standards (NSPS) of 1.2 lb SO₂/MMBtu is about 80%, if all the sulfur in the coal emerges as SO₂. (In many cases 10-15% of the sulfur remains in the bottom ash.) Each of the three processes described earlier should easily meet this requirement.

The assumed plant characteristics of no natural gas and a premium for petroleum coke tend to impose realistic penalties for special reducing agents. For both Catalytic/IFP and Wellman-Lord/Allied Chemical processes, a coal gasifier is required to supply an acceptable reducing agent and fuel. This increases the complexity and cost of these processes. The presence of plentiful water eliminates any penalty for consumptive use in the FGD processes.

The Wellman-Lord/Allied Chemical process with a 60% efficient gasifier consumes about 50,000 Btu/pound of elemental sulfur produced (1). The Atomics International ACP process consumes about 28,000 Btu/pound of elemental sulfur produced (5). An evaluation of the Catalytic/IFP process for this study showed comparable electrical and reheat demands to those for the Wellman-Lord. However, steam and reductant consumption should be lower with the total energy required for Catalytic/IFP intermediate to the other two processes.

For all three processes, coal is the reductant. However, the need for a gasifier in the Wellman-Lord/Allied Chemical and Catalytic/IFP processes adds to their complexity and to their consumption of energy. Thus, the Atomics International ACP process has an advantage for this factor.

Since all three processes use clear solutions as sulfur-absorbing reagents, do not require hot precipitators, and should be capable of responding to boiler load changes, they all show satisfactory independence from the boiler. Nevertheless, the Catalytic/IFP and Wellman-Lord/Allied Chemical processes have relatively high pressure drops through their absorbers, require flue gas reheaters (which have poor reliability records), and use solutions which are more voluminous to store prior to regeneration than the solid product from the Atomics International absorber. Thus, an edge in evaluating this factor would go to the Atomics International ACP process.

As discussed in the preceding section, a prudent evaluation should place heavy emphasis on mechanical and chemical reliability. In this context, a relatively undemonstrated process, such as the Atomics International ACP, is penalized. The Wellman-Lord/Allied Chemical process is the best demonstrated, followed by the Catalytic/IFP process. They would receive correspondingly higher ratings for this factor.

In considering the site-specific evaluation factors (Table 1) for this hypothetical site, the major considerations are waste disposal and the impact of rather severe winters on these three processes.

The production of by-products by an FGD process can be troublesome. Both the Catalytic/IFP and Wellman-Lord/Allied Chemical processes have purge streams of wet flyash from the water used for humidification. The Wellman-Lord process has a further disadvantage in the generation of a sizable purge stream of sodium sulfate. Up to 10% of the SO₂ absorbed is oxidized to the unregenerable sulfate. In considering these factors, the Atomics International ACP process has an advantage, although a small purge of mixed salts will probably be required.

The relatively bulky spray-dryer type of absorber used in the Atomics International ACP process and the more stringent temperature control required for its proper operation will raise its cost for insulation and weather protection relative to the others. The several

solids transport steps required may also be troublesome in severe weather. Thus, both the Catalytic/IFP and Wellman-Lord/Allied Chemical processes should have an edge for this specific site.

Assigning numerical values to all of the pertinent factors described in the preceding section is, itself, a subjective problem. Local preferences and prior experience will weigh heavily in the choices made. For a hypothetical site (Table 2) and for only these three representative processes, this seems neither warranted nor instructive. It is a matter of agonizingly strenuous judgement to set up such a numerical table for a specific case. Once this is done, processes can be consistently evaluated at the cost of further effort in assigning individual scores.

For the three processes considered in the general framework here, the Wellman-Lord/Allied Chemical process has the advantage of being the best demonstrated. The Catalytic/IFP process is nearly as well demonstrated, uses less energy and produces less solid waste. The Atomics International ACP process is still under development, but has the potential to use coal as a direct reductant, to use the least energy of the three processes and to produce the least solid waste. Thus, incentives exist to continue to move both the Catalytic/IFP and Atomics International ACP processes toward commercialization.

REFERENCES

- (1) McGlamery, G.G., et al, "Detailed Cost Estimates for Advanced Effluent Desulfurization Processes", EPA-600/2-75-006, January, 1975.
- (2) Bierbower, R.G. and Van Sciver, J.H., "Allied's SO₂ Reduction Systems", Chem. Eng. Prog., 70, August, 1974.
- (3) Mann, E.L. and Christman, R.C., "Status of Demonstration of the Wellman-Lord/Allied FGD System at NIPSCO's D.H. Mitchell Generating Station. Part I", FGD Symposium Sponsored by U.S. EPA, New Orleans, March, 1976.
- (4) Ennis, C.E., "APCI/IFP Regenerative FGD Ammonia Scrubbing Process", FGD Symposium Sponsored by U.S. EPA, New Orleans, March, 1976.
- (5) Gehri, D.C. and Oldenkamp, R.D., "Status and Economics of the Atomics International Aqueous Carbonate Flue Gas Desulfurization Process", FGD Symposium Sponsored by U.S. EPA, New Orleans, March, 1976.

TABLE 2

SAMPLE SITE CHARACTERISTICS

Plant Capacity:	500 MW
Capacity factor:	7,000 hrs/yr
Heat rate:	9,000 Btu/kwh
Flue gas rate:	3,100 ACFM/MW
Flue gas temperature:	310 ⁰ F
Eastern coal characteristics:	3.5% sulfur
	11,600 Btu/lb (as received)
Plant location:	Central U.S.
Plant characteristics:	Sufficient water
	No natural gas
	Petroleum coke available at a premium over coal
SO ₂ Emissions Limit:	1.2 lb/MM Btu (NSPS)

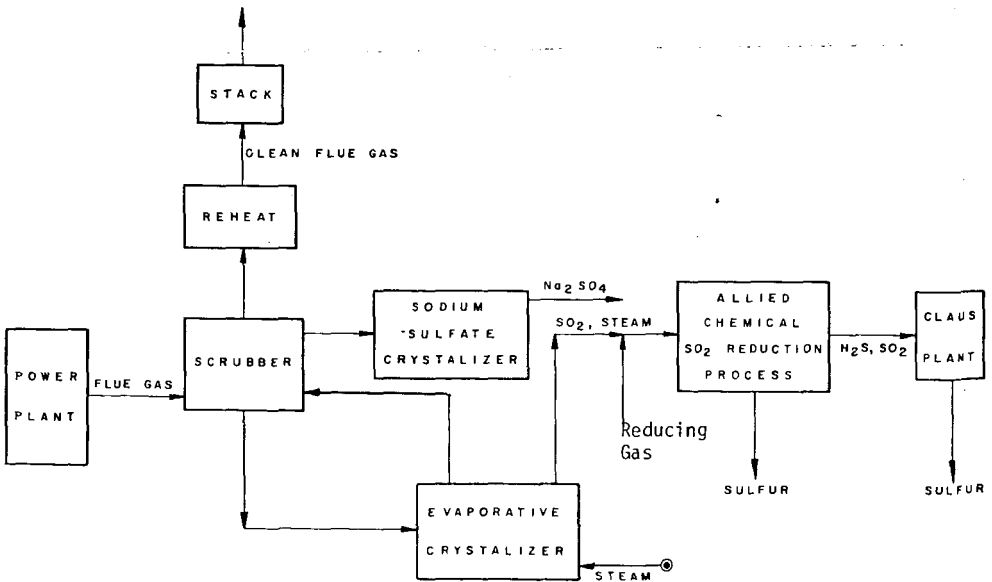


Figure 1. Wellman-Lord/Allied Chemical Process

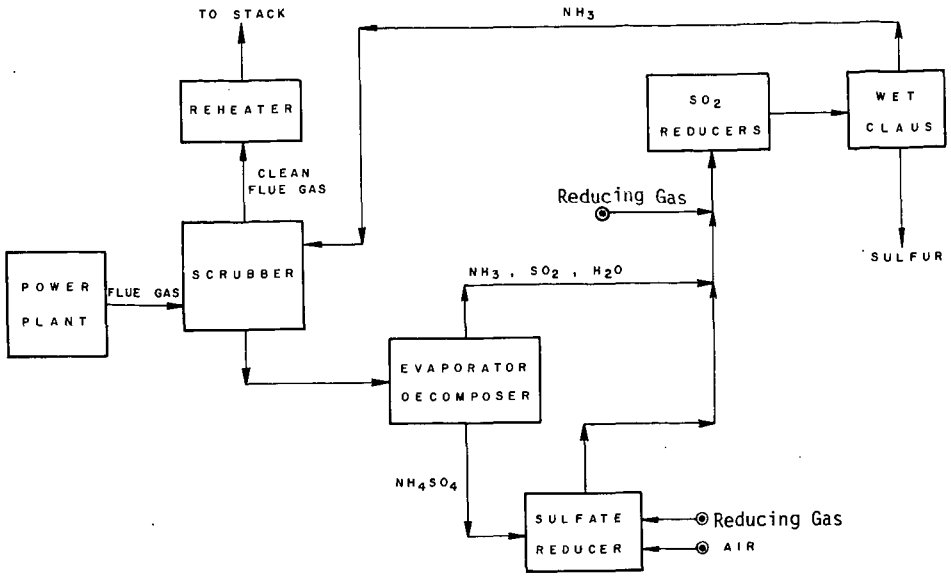


Figure 2. Catalytic/IFP Process

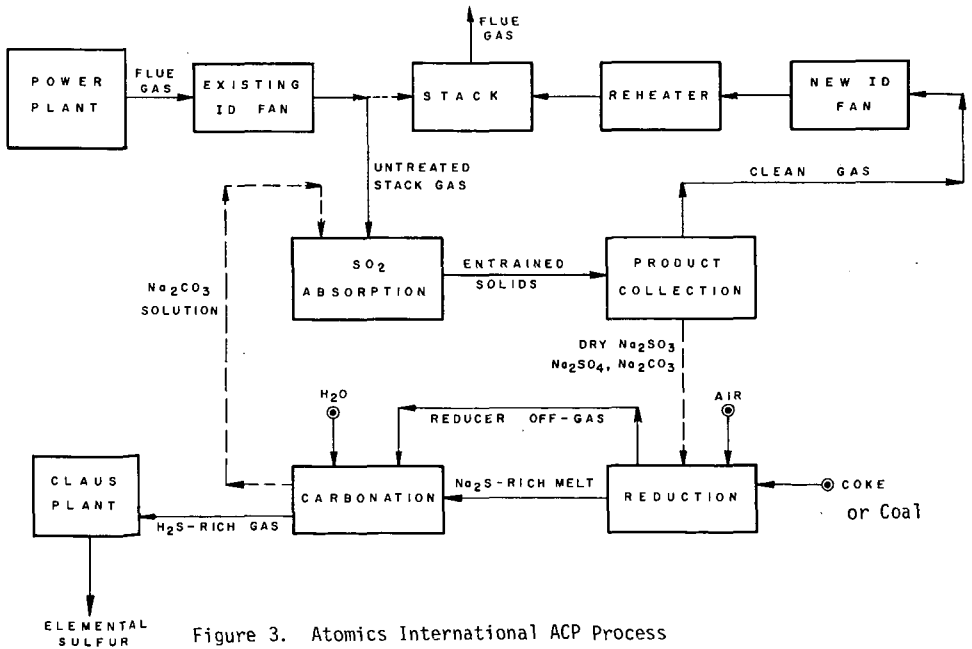


Figure 3. Atomics International ACP Process

Thermal cracking of ethylene, propylene and
light hydrocarbon mixtures

Froment G.F., Van De Steene B.O.

Laboratorium voor Petrochemische Techniek, Rijksuniversiteit,
Gent, Belgium.

Goossens A.G.

Kinetics Technology International, B.V., The Hague, The Netherlands.

1. Introduction

There are quite a few publications dealing with the thermal cracking of ethylene, of propylene and of their mixtures with alkanes (1,2,3,4,5), but most of them are confined to rather narrow ranges of the process variables. Further, there is little agreement as to the product distribution and the kinetics of the overall reaction, although it would seem that a gradual transition between polymerization and decomposition processes could explain some of the contradictions.

The thermal cracking of ethane, propane, n and i-butane has been investigated rather intensively, but the thermal cracking of binary and ternary mixtures has received far less attention. Although industrial practice generally deals with mixtures, there are no guiding lines to day for the prediction of reaction rates and product distributions of mixtures cracking from data on the cracking of individual components. The question whether or not the reaction partners significantly interact to alter the product distributions from those calculated from pure additivity has not been settled yet.

The work reported in the present paper aimed at determining kinetics and product distributions of the thermal cracking of ethylene, propylene, of mixtures of ethane-propylene and of binary and ternary mixtures of ethane, propane, n- and i-butane from an experimental program covering wide ranges of process variables and carried out in a pilot plant. Further, it aimed at reconciling some of the above mentioned contradictions in olefins cracking and at deriving some general rules for mixtures cracking.

2. Experimental program

The pilot plant has been described in detail by Van Damme et al (6) and Froment et al (7).

A. Ethylene

The ethylene was high purity grade (Air Liquide CH25) and contained less than 0.2 wt % C_2H_6 .

The process variables were varied over the following ranges :

Variable	Range
ethylene flow rate (kg/hr)	0.5 - 3
dilution (kg steam/kg hydrocarbon)	0.4 - 4
Reynolds number	4,500-8,000
exit temperature (°C)	625-850
exit pressure (atm.abs.)	1.2-2.3
pressure drop (atm.)	0.1-0.5

The majority of the 150 experiments were grouped into 5 classes depending upon the partial and the total pressure.

class	exit pressure (atm.abs.)	dilution (kg/kg)	inlet partial pressure (atm)
1	1.5	0.4	0.92
2	1.5	1	0.59
3	2.0	0.4	1.36
4	2.0	1	0.77
5	1.5	4	0.235

B. Propylene

The propylene was also high purity grade, containing less than 0.2 wt % C_5^+ . The operating conditions were similar to those described above, except for the inlet partial pressure, which was varied between 0.164 and 1.16 atm.abs. and for the temperature range, which extended from 625 to 870°C.

C. Binary and ternary hydrocarbon mixtures

Ethane-propylene mixtures containing from 25 to 75 wt % of propylene were investigated under class 1 conditions in a temperature range from 675 to 850°C and with hydrocarbon flow rates ranging from 2 to 3.6 kg/hr. Similar conditions were chosen for the investigation of ethane-propane, n.butane-propane, n.butane-i.butane and ethane-n.butane mixtures.

Finally, the following ternary mixtures were investigated under these conditions :

ethane	propane	n.butane (wt %)
20.81	67	11.65
41.39	37.53	20.78
30.63	11	58.32
42.23	18.40	39.35
70.61	18.45	10.93

3. Product Distributions.

A. Thermal cracking of ethylene.

The main products of ethylene cracking are H_2 , CH_4 , C_2H_2 , C_2H_6 , C_3H_6 , $1,3C_4H_6$ and a C_5^+ -fraction.

Figures 1 to 5 show the yields of some of these products. The results are plotted versus the ethylene conversion with the partial pressure of the hydrocarbon and the total pressure as parameters. Plotted in this way, there is practically no influence of temperature. From these figures it is clear that the range of investigated partial pressures has to be split in an area with $p_{C_2H_4} < 0.6$ atm, i.e. the class 5 experiments, and an area with $p_{C_2H_4} > 0.6$ atm, i.e. the experiments of the classes 1 to 4. This will be explained in the last section, in which the location of the border line between polymerization and decomposition zone is discussed. Table 1 summarizes the influences of partial and total pressure on the product yields. The C_5^+ yield is favored by an increase in partial and total pressure, but there was also a strong influence of the temperature : high temperatures lead to high C_5^+ yields. At temperatures below 800°C most of the C_5^+ formed were heavier than toluene, but at the higher temperatures the product spectrum shifts towards lighter C_5^+ products.

TABLE 1

Influence of the partial pressure of ethylene and the total pressure on the yields.

component	increase of partial pressure		increase of total pressure
	p < 0.6 atm	p > 0.6 atm	
H ₂	↓	↓	↓
CH ₄	↑	↓	none
C ₂ H ₂	↓	↓	↓
C ₂ H ₆	↑	no	none
C ₃ H ₆	↑	no	none
1,3C ₄ H ₆	↑	little or none	slight decrease

B. Thermal cracking of propylene

Figures 6 to 11 show the yields of the different products in propylene cracking.

The primary products of propylene cracking are H₂, CH₄, C₂H₄, 1,3C₄H₆ and C₅⁺. Considering only classes 1 to 4, the initial selectivities of these products are independent of partial and total pressure. The following values were found: H₂=.05; CH₄=.15; C₂H₄=.15; 1,3C₄H₆=.05; C₅⁺=.6.

In the class 5 experiments the initial C₅⁺ and 1,3C₄H₆ selectivities are lower and the initial H₂ selectivity is higher, however. Table 2 summarizes the influence of partial - and total pressure on the product spectrum.

TABLE 2

Influence of partial pressure of the hydrocarbon and of the total pressure on product yields for propylene cracking.

component	increase of partial pressure	increase of total pressure
H ₂	none	none
CH ₄	none	none
C ₂ H ₄	none	none
C ₂ H ₆	↑	↑
C ₂ H ₂	↓	↓
C ₃ H ₈	↑	↑
1C ₄ H ₈	none	none
1,3C ₄ H ₆	↑	↑
C ₅ ⁺	↑	↑

C. Thermal cracking of binary and ternary hydrocarbon mixtures

Figure 12 shows the experimental selectivities for the different products in ethane-propylene mixtures, versus the feed composition.

The selectivity of a component I in the cracking of a mixture A-B is defined as :

$$y_I = \frac{\text{mols of I from A} + \text{mols of I from B}}{\text{mols of A cracked} + \text{mols of B cracked}} \quad 1)$$

When there is no interaction, Froment et al (7) showed that equation 1 is identical with :

$$y_I = \frac{y_{I,A} x_{A,M} \psi'_A + y_{I,B} x_{B,M} \psi'_B}{x_{A,M} \psi'_A + x_{B,M} \psi'_B} \quad 2)$$

This predicted value of the selectivity will be called the non-interaction selectivity.

The pure additivity selectivity : $y_I = y_{I,A} \psi'_A + y_{I,B} \psi'_B$ 3), used in the literature so far, is obviously a very special case of 2) valid only for $x_{A,M} = x_{B,M}$.

It is clear from Figure 12 that 2) allows a far better prediction of the experimental results than 3). Analogous figures were plotted for different conversions and for all binary mixtures mentioned in the experimental program. From all these curves, the following rule can be deduced : "The experimental selectivities deviate from the pure additivity lines in the same direction as the non-interaction selectivities". This means that the effect of interaction can be predicted when the selectivities from the individual components and the relative rates of cracking are known.

The selectivities for cracking of ternary mixtures may be represented in diagrams of the type shown in figure 13. In this figure the ethylene selectivity at conversions $x_{E,M}=40\%$, $x_{P,M}=73\%$;

$x_{N,M}=88\%$ is plotted with respect to the ternary feed composition. With ternary mixtures the pure additivity, non interaction and experimental lines of Fig. 12 become surfaces. Here too the experimental selectivities deviate from the pure additivity surface in the same sense as the non-interaction surface.

4. Kinetics

The kinetics of the cracking of a component E, are derived from the experiments by means of its continuity equation. For ethane in a binary mixture ethane-propylene e.g., cracked in a tubular reactor with plug flow conditions, the continuity equation may be written :

$$F_{E,0} dx_{E,P} = A \exp\left(-\frac{E}{RT(z)}\right) \cdot (C_{E,P})^n dV \quad 4)$$

with :

$$C_{E,P} = \frac{1-x_{E,P}}{(1-x_{E,P}) + \gamma(1-x_{P,E}) + \xi(x_{E,P} + \gamma x_{P,E}) + \delta(1+\gamma)} \cdot \left(\frac{p_t(z)}{RT(z)}\right)$$

$$\xi = \text{expansion} = \frac{(\text{total molar flow rate})_{\text{exit}} - (\text{mols } C_2H_6 + \text{mols } C_3H_6)_{\text{exit}}}{\text{mols } C_2H_6 \text{ cracked} + \text{mols } C_3H_6 \text{ cracked}}$$

γ = molar ratio propylene/ethylene

λ = dilution factor : mols H₂O/mol hydrocarbon

In 4) the experimental temperature and total pressure profile are also accounted for.

The kinetics can now be derived from 4) as such or by making use of the equivalent reactor volume concept.

A. The equivalent reactor volume concept

In this approach, the non-isothermal, non-isobaric data are first reduced to isothermality and constant pressure. This leads to an equivalent reactor volume V_p rather than the physical volume V in 4), while $T(z)$ is replaced by a reference temperature and $p_t(z)$ by a reference pressure (6,7,8). The kinetic parameters of the thermal cracking of individual alkanes were determined by means of this concept. Figure 14 shows the Arrhenius plot of the first order rate constants for ethane, propane, n.butane and i.butane. The concept was also used to calculate the kinetic coefficients of the cracking of the individual components in the mixture, assuming first order. The integration of 4) then requires a relation $x_{p,E} = f(x_{p,p})$. From the experimental data, this relation was found in all cases to be parabolic, so that equation 4 could be integrated analytically. Figure 15 shows the value of $k_{p,p}$ versus the feed composition. The inhibiting effect of propylene on the ethane rate coefficient is very pronounced. The same procedure was followed to calculate the individual rate coefficients for all the components of the different feed mixtures.

Table 3 summarizes the relative influences, caused by cocracking.

TABLE 3

Effect of the addition of various components on the rate coefficient for the cracking of ethane, propane, n.butane, i.butane and propylene.

Addition of	Effect on rate coefficient				
	$k_{C_2H_6}$	$k_{C_3H_8}$	$k_{n C_4H_{10}}$	$k_{i C_4H_{10}}$	$k_{C_3H_6}$
C_2H_6	-	↑	↑	no data	↑
C_3H_8	↓	-	↓	no data	↑
$n C_4H_{10}$	↓	↓	-	↓	no data
$i C_4H_{10}$	no data	no data	↑	-	no data
C_3H_6	↓	↓	no data	no data	-

The individual rate coefficients in the ternary mixture ethane-propane-n.butane were calculated in an analogous way. Figure 16 shows the effect on the rate coefficient for ethane cracking of the addition of one or two components in various ratios. Analogous diagrams could be shown for $k_{p,M}$ and $k_{N,M}$. All three of them clearly illustrate the effect on the rate coefficients of interaction between reaction partners.

B. Determination of the kinetics from the non-isothermal, non-isobaric data as such.

The equivalent reactor volume concept requires an initial guess of the activation energy, valid over the whole range of investigated temperatures. This is no problem with alkanes but, as will be discussed in the next section, the ethylene and propylene cracking experiments cover a transition zone in which polymerization processes with activation energies of ± 35 kcal/mol and decomposition processes with activation energies of ± 70 kcal/mol simultaneously occur. In such cases it is preferable to resort

to the non-isothermal non-isobaric approach used by Van Damme et al (6). Equation 4, with the experimental temperature and pressure profile included, was integrated numerically and the residual sum of squares, $\sum(x_{\text{exp}} - x_{\text{calculated}})^2$ was minimized with A, E and n as parameters, using Marquardt's search routine (22). The results are shown in Table 4,5,6 and 7 respectively, from which it follows that there is a strong influence of temperature, partial and total pressure on the kinetic parameters in both ethylene and propylene cracking.

TABLE 4
Influence of the temperature on the kinetic parameters of the overall ethylene disappearance.

T(°C)	A	E(kcal/mol)	n
725	1.707 10^8	39.600 ± .984	1.61 ± 0.025
750	6.56 10^{13}	65.420 ± 7.090	1.46 ± 0.122
775	3.71 10^{17}	84.330 ± 1.690	1.43 ± 0.042
800	1.39 10^{13}	60.150 ± 2.520	1.19 ± 0.034
825	4.05 10^{15}	77.295 ± 5.890	1.22 ± 0.042

TABLE 5
Influence of the temperature on the kinetic parameters of propylene cracking

T	A	E(kcal/mol)	n
725	5.69 10^7	36.310 ± 1.200	1.33 ± 0.16
750	9.42 10^7	36.400 ± 5.500	1.46 ± 0.035
775	4.43 10^{12}	60.030 ± 11.000	1.24 ± 0.18
800	1.62 10^{11}	54.990 ± .280	1.10 ± 0.075
825	2.99 10^{11}	57.530 ± 3.800	0.95 ± 0.048

TABLE 6
Influence of inlet partial pressure and total pressure on the kinetic parameters of ethylene cracking.

	A	E(kcal/mol)	n
Class 1	2.48 10^{11}	54.220 ± 1.260	1.29 ± 0.046
Class 2	1.11 10^{17}	81.910 ± 1.340	1.54 ± 0.01
Class 3	1.65 10^{11}	54.430 ± 2.170	1.27 ± 0.023
Class 4	5.47 10^{13}	66.400 ± .211	1.35 ± 0.023
Class 5	1.50 10^{15}	72.840 ± .191	1.36 ± 0.018
All classes	2.51 10^{13}	60.400 ± .975	1.30 ± 0.027

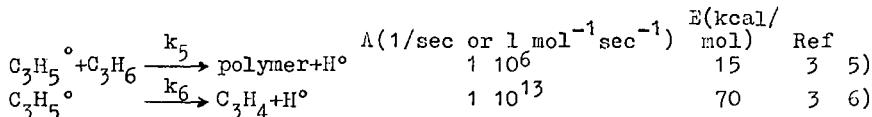
TABLE 7
Influence of inlet partial pressure and total pressure on the kinetic parameters of propylene cracking.

	A	E(kcal/mol)	n
Class 1	2.80 10^{10}	51.320 ± 2.600	1.02 ± 0.035
Class 2	1.86 10^{13}	66.020 ± 28.000	1.02 ± 0.37
Class 3	2.44 10^{11}	56.690 ± 2.900	1.05 ± 0.028
Class 4	1.89 10^{13}	63.960 ± 1.080	1.18 ± 0.040
Class 5	5.18 10^9	47.710 ± 2.150	1.15 ± 0.063
All classes	2.43 10^{10}	50.650 ± 1.600	1.08 ± 0.033

5. Decomposition and polymerization zones in olefines cracking

A. Propylene cracking

In the thermal cracking of propylene, polymerization and decomposition processes are in competition (1,2,3,12,13,14). Low temperatures and high partial pressures favor polymerization, high temperatures and low partial pressures favor decomposition. Allene and/or methylacetylene are obtained when decomposition is predominant, whereas they are not formed when only polymerization occurs. To account for both polymerization and for decomposition, all authors consider the following two reactions :



This means that the allyl radical acts as a β radical in the polymerization and as a μ radical in the decomposition processes. Combined with the termination : $C_3H_5^\circ + H^\circ \rightarrow C_3H_6$ and with the first order initiation : $C_3H_6 \rightarrow C_3H_5^\circ + H^\circ$, 5) leads to an overall order of 3/2 for polymerization and 6) to an overall order of 1 for decomposition.

From 5) and 6) and by setting $k_5(C_3H_6) = k_6$, Amano (3) calculated a border line between both zones in a temperature versus inlet partial pressure diagram. This is the dashed line in Figure 17. To permit a direct comparison with the literature, the propylene partial pressure is expressed in mm Hg. From Amano's border line, it follows that the present results would be completely located in the polymerization zone and indeed no allene is found. However, the order of the global disappearance reaction is not 3/2 but varies from 3/2 to 1 as the temperature is increased, while the activation energie varies from 36 to 66 kcal/mol. This suggests that the present data would be located in the transition area and this in turn requires the border line to be shifted towards the left of the figure. Such a shift could result from a decomposition of allyl into acetylene instead of allene :

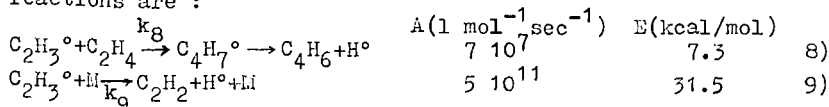


An isothermal, unsteady state radical simulation of the propylene experiments (10) led to a frequency factor of $1 \cdot 10^8$ and an activation energy of 32.4 kcal/mol for 7). These values are plausible, when compared with Allara's data (9) for the decomposition of C_5 radicals into C_2H_2 . When reaction 7 instead of reaction 6 accounts for the μ -behavior of the allyl radical, the border line between the two areas is calculated from : $k_5(C_3H_6) = k_7$. This is the full line on Figure 17. Both Kunugi's (2) and our experiments are now located in the transition zone. The experiments of Laidler (1) and Ingold (12) lie in the polymerization area and these of Szwarc (13) and Sakakibara (14) in the decomposition zone. This is in agreement with the fact that neither Laidler nor Ingold found acetylene, while Kunugi and Sakakibara did. The results of Szwarc are doubtful because of his rudimentary analytical technique. At 1200°C and higher, the decomposition of allyl into allene becomes more and more important, because of the high activation energy, so that Sakakibara, whose work is mainly situated in the temperature range 1200°C-1400°C, found more allene and methyl-

acetylene then acetylene.

B. Ethylene cracking

In complete analogy with propylene cracking, the two major initial reactions are :



The vinylradical acts as a β radical in 8) and as a γ radical in 9). The kinetic parameters of these reactions were derived from an extensive literature survey (11,15,16,17).

The border line between the two areas is now given by :

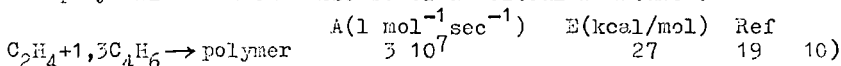
$$k_8(C_2H_3^\circ)(C_2H_4) = k_9(C_2H_3^\circ)(M)$$

This line is the full line in Figure 18. With a second order initiation like $2C_2H_4 \rightarrow C_2H_3^\circ + C_2H_5^\circ$ and a termination involving two vinylradicals ($2C_2H_3^\circ \rightarrow 1,3C_4H_6$), an order of 2 is predicted for conditions in the polymerization zone and an order of 1 for conditions in the decomposition zone.

Simon and Back (15) and Silcocks (18) observed second order kinetics, while Kolera and Stubbs (16) found second order kinetics in the region 3 of Figure 18 and first order kinetics in region 3', in agreement with the proposed border line. Kunugi's data (11) which are located in the transition area lead to an order of 3/2 for the global disappearance reaction.

The pilot plant experiments cover the transition zone. The order was shown in Tables 4 and 6 to evolve from 1.6 to 1.2 as the temperature is increased and the activation energy from 40 to about 75 kcal/mol.

The polymerization can also be of a molecular nature :



The ratio of the radical reaction and molecular condensation rates was calculated from an isothermal non steady state radical simulation of the ethylene experiments by Sundaram & Froment (10), to be 31 at 800°C and 1% conversion, 15 at 800°C and 3% conversion and 10 at 825°C and 8% conversion.

It follows that molecular condensation cannot be neglected at 800°C and higher. This explains why the experimental C_5^+ fraction was so strongly correlated with the temperature. In propylene cracking the ratios of the rates of the radical polymerisation and the molecular condensation at 800°C would be of the order of 1000 because the allyl radical is high and butadiene is low.

It is clear also from Figure 18 for ethylene and from Figure 17 for propylene that the influence of the partial and total pressure on the order and activation energy will be more or less pronounced depending upon the distance from the border line. The higher activation energies given in Tables 6 and 7 for the conditions of the classes 2, 4 and 5 may be related to this effect.

Finally, it should be added that even with an ethane content of less than 0.2 wt % in the ethylene feed, the initiation reaction $C_2H_6 \rightarrow 2CH_3^\circ$ cannot be neglected, as concluded already by

Kunugi (11) and by Towell and Martin (20).

From the mechanistic point of view the initiation then becomes of first order and the order of the global disappearance should vary between 3/2 and 1/2. On the other hand, the molecular reactions will increase the overall order. All these trends substantiate the variation of the order from 1.6 to 1.2 observed in the present work.

Notation

A	frequency factor	sec^{-1} or $l \text{ mol}^{-1} \text{ sec}^{-1}$
E	activation energy	kcal/mol
C	concentration	mol/l
C_T	concentration, total hydrocarbons	mol/l
F_0	molar flow rate of the cracked component at the inlet	mol/sec
k	rate coefficient	sec^{-1} or $l \text{ mol}^{-1} \text{ sec}^{-1}$
n	order of reaction	
P_t	total pressure	atm. abs.
R	gas constant	kcal/kmol $^{\circ}\text{C}$
r	rate of reaction	mol/l sec
T	temperature	$^{\circ}\text{K}$ or $^{\circ}\text{C}$
V_E	equivalent reactor volume	l
x	conversion	
y	selectivity	mol/mol
z	tube length	m
γ	mol ratio	mol/mol
δ	dilution ratio	mol steam/mol hydrocarbon
ϵ	expansion factor	mol products/mol hydrocarbon cracked
ψ	mol fraction	mol/mol

Subscripts

E	ethane
P	propylene
M	mixture
O	initial value
t	total
m	mean

Table captions

- Table 1 : Ethylene cracking. Influence of the total pressure and the partial pressure of ethylene on the yields of the different products.
- Table 2 : Propylene cracking. Influence of the total pressure and the partial pressure of propylene on the yields of the different products.
- Table 3 : Effect of the addition of various components on the rate coefficient for the cracking of ethane, propane, n-butane, i-butane and propylene.

- Table 4 : Influence of temperature on the kinetic parameters of the overall ethylene disappearance.
- Table 5 : Influence of temperature on the kinetic parameters of the overall propylene disappearance.
- Table 6 : Influence of inlet partial pressure and total pressure on the kinetic parameters of ethylene cracking.
- Table 7 : Influence of inlet partial pressure and total pressure on the kinetic parameters of propylene cracking.

Figure captions

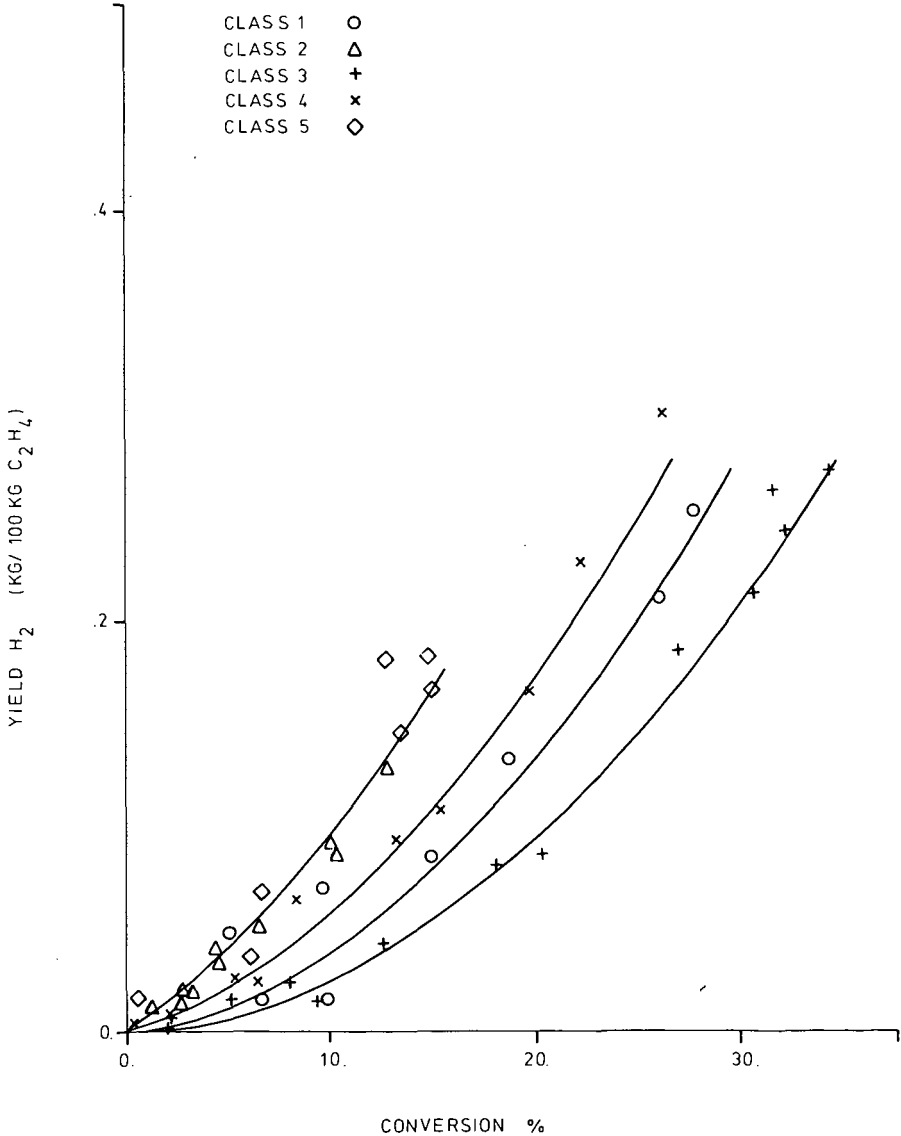
- Figure 1 : Ethylene cracking : hydrogen yield
 Figure 2 : Ethylene cracking : methane yield
 Figure 3 : Ethylene cracking : acetylene yield
 Figure 4 : Ethylene cracking : propylene yield
 Figure 5 : Ethylene cracking : butadiene yield
 Figure 6 : Propylene cracking : hydrogen yield
 Figure 7 : Propylene cracking : methane yield
 Figure 8 : Propylene cracking : acetylene yield
 Figure 9 : Propylene cracking : ethylene yield
 Figure 10 : Propylene cracking : butadiene yield
 Figure 11 : Propylene cracking : C_5^+ yield
 Figure 12 : Selectivity of H_2 , CH_4 and C_2H_4 versus mol fraction propylene in the mixture
 Figure 13 : Selectivity of C_2H_4 versus feed composition in the ternary mixture ethane-propane-n.butane
 - - lines on non-interaction surface ; + non interaction points ; . experimental
 Figure 14 : Arrhenius plot of rate coefficients for the cracking of light hydrocarbons
 Figure 15 : Rate coefficient for the cracking of ethane in an ethane-propylene mixture versus feed composition
 Figure 16 : Rate coefficient for the cracking of ethane in ternary mixtures of ethane-propane and n-butane
 Figure 17 : Polymerization and decomposition zones in propylene cracking
 Figure 18 : Polymerization and decomposition zones in ethylene cracking.

References

- 1) Laidler K.J., Wojciechowski B.W., Proc.Roy.Soc. (London), A259, 257 (1960)
- 2) Kunugi T., Sakai T., Soma K. and Sasaki Y., Ind.Eng.Chem. Fundam., vol.9, N°3 (1970).
- 3) Amano A., Uchujama M., J.Phys.Chem., 68, 1133 (1964).
- 4) Sakai T., Soma K., Sasaki Y., Tominaga H. and Kunugi T., Refining Petroleum for Chemicals, 68 (1970).
- 5) Kallend A.S., Purnell J.H., Shurlock B.C., Proc.Roy.Soc. (London), A300, 120 (1967).
- 6) Van Damme P.S., Narayanan S. and Froment G.F., A.I.Ch.E. Journal, vol.21, N°6, 1065 (1975).

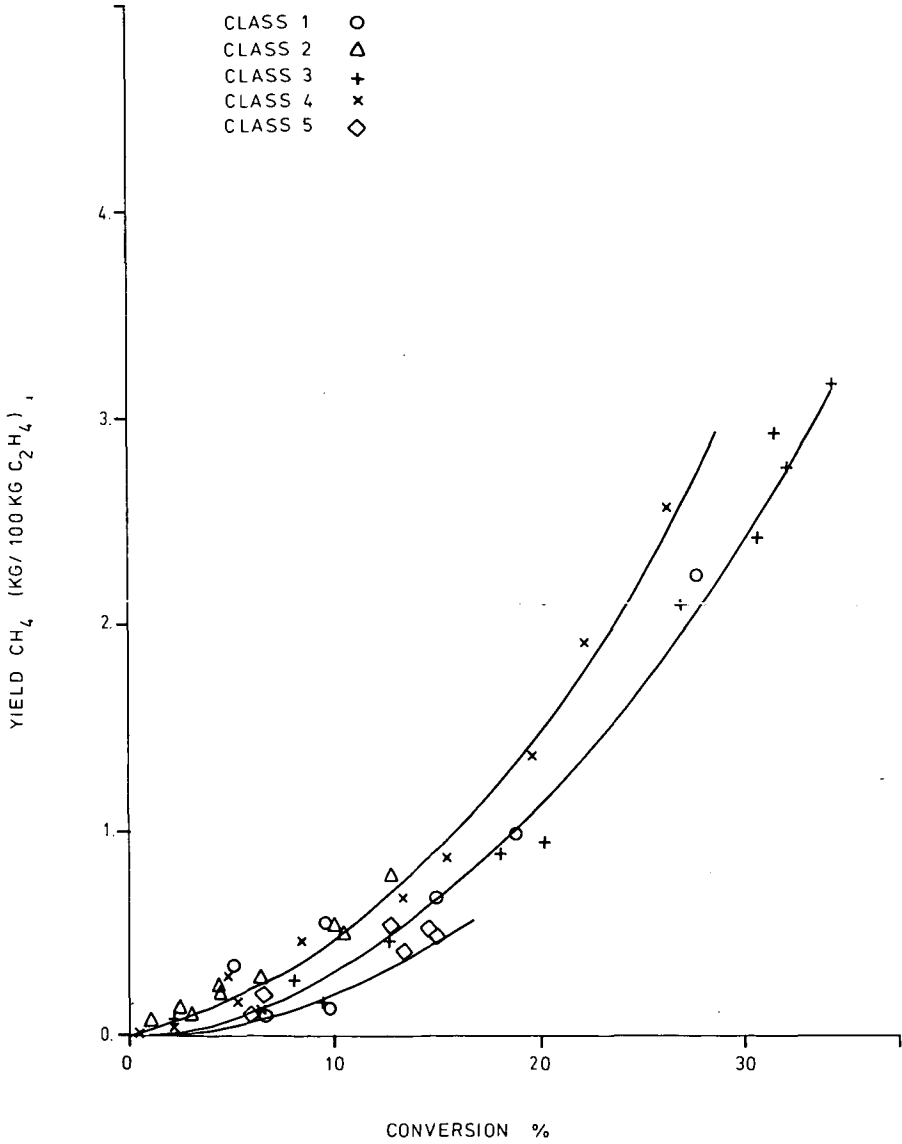
- 7) Froment G.F., Van de Steene B.O., Van Damme P., Narayanan S. and Goossens A.G., Ind.Eng.Chem.Process Des.& Develop. (to be published)
- 8) Froment G.F., Pycke H., Goethals G., Chem.Eng.Sci.,13, 173, 180 (1961)
- 9) Allara D.L., A compilation of kinetic parameters for the thermal degradation of n-alkane molecules
- 10) Sundaram M., Froment G.F., (to be published)
- 11) Kunugi T., Sakai T., Soma K., Sasaki Y., Ind.Eng.Chem.Fundam. Vol.8, 374 (1969)
- 12) Ingold K.U., Stubbs F.J., J.Chem.Soc., 1749 (1951)
- 13) Szwarc M., J.Chem.Phys., 17, 284 (1949)
- 14) Sakakibara Y., Bull.Chem.Soc. Japan, 37, 1262 (1964).
- 15) Simon M., Back M.H., Can.J.Chem., 47, 251 (1969)
- 16) Molera M.J., Stubbs F.J., J.Chem.Soc., 381 (1952)
- 17) Benson S.W., Hougen G.R., J.Phys.Chem., 71, 1735 (1967)
- 18) Silcocks C.G., Proc.Roy.Soc., A233, 465 (1955)
- 19) Bowley D., Steiner H., diss.Trans.Faraday Soc., 10,198(1951)
- 20) Powell G.D., Martin J.J., A.I.Ch.E. Journal, vol.7,N°4,693(1961)
- 21) Froment G.F., Van De Steene B.O. and Goossens A.G. (to be published)
- 22) Marquardt D.W., Soc.Ind.Appl.Math.J., 11, 431 (1963).

Figure 1.



THERMAL CRACKING OF ETHYLENE

Figure 2.



THERMAL CRACKING OF ETHYLENE

Figure 3.

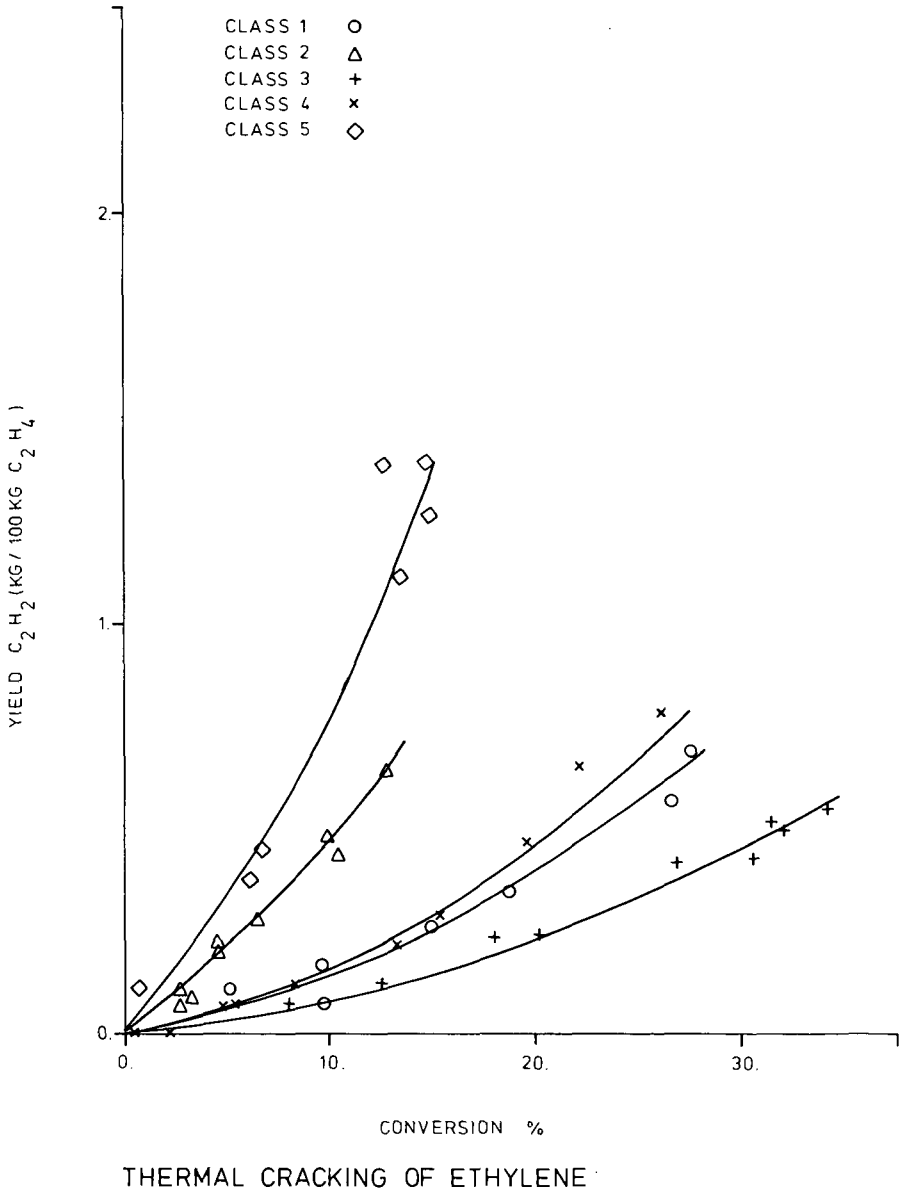
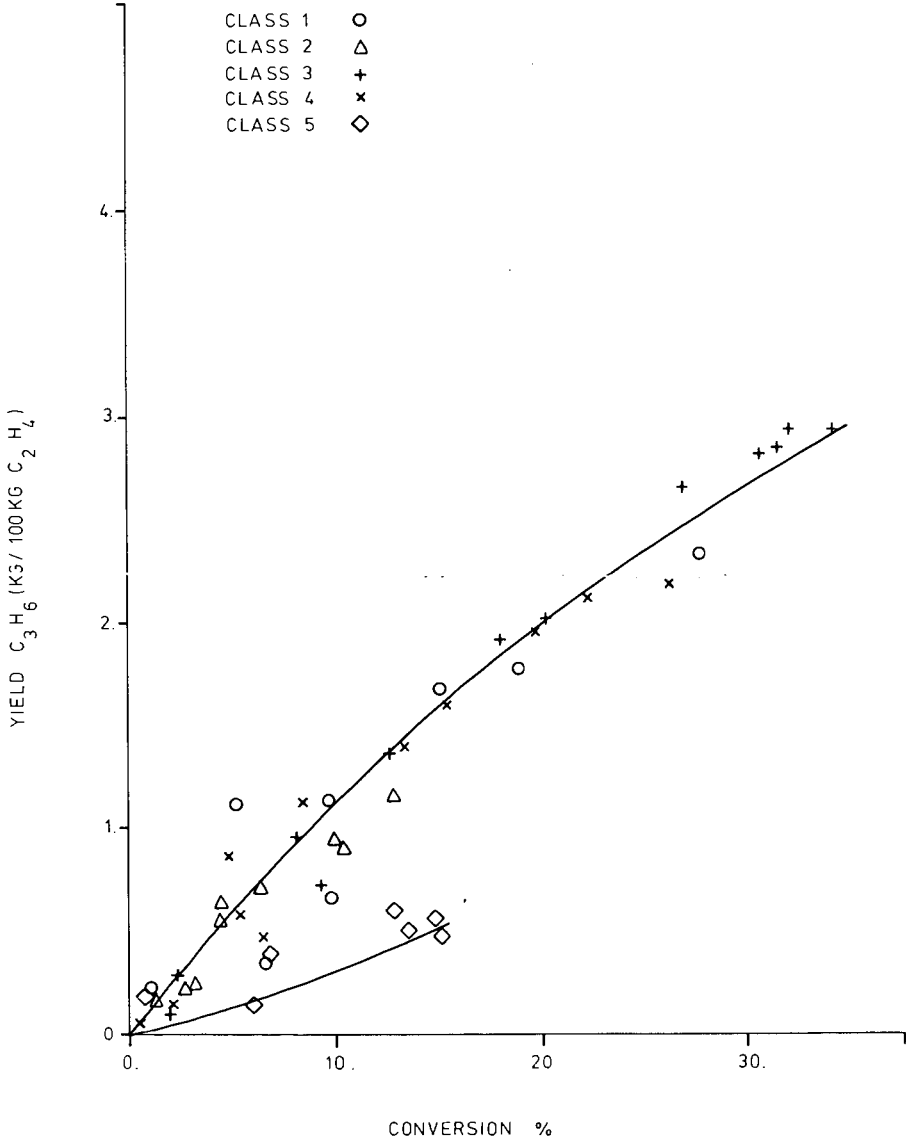
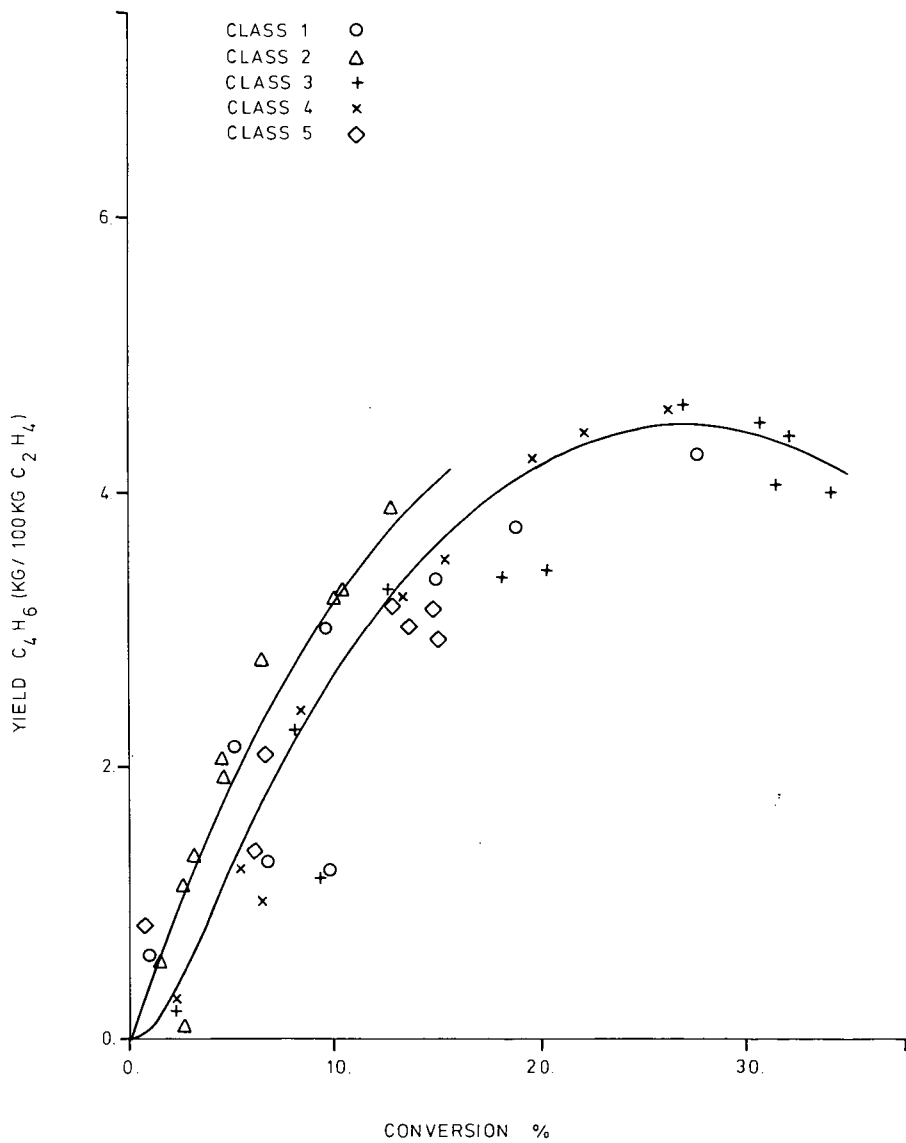


Figure 4.



THERMAL CRACKING OF ETHYLENE

Figure 5.



THERMAL CRACKING OF ETHYLENE

Figure 6.

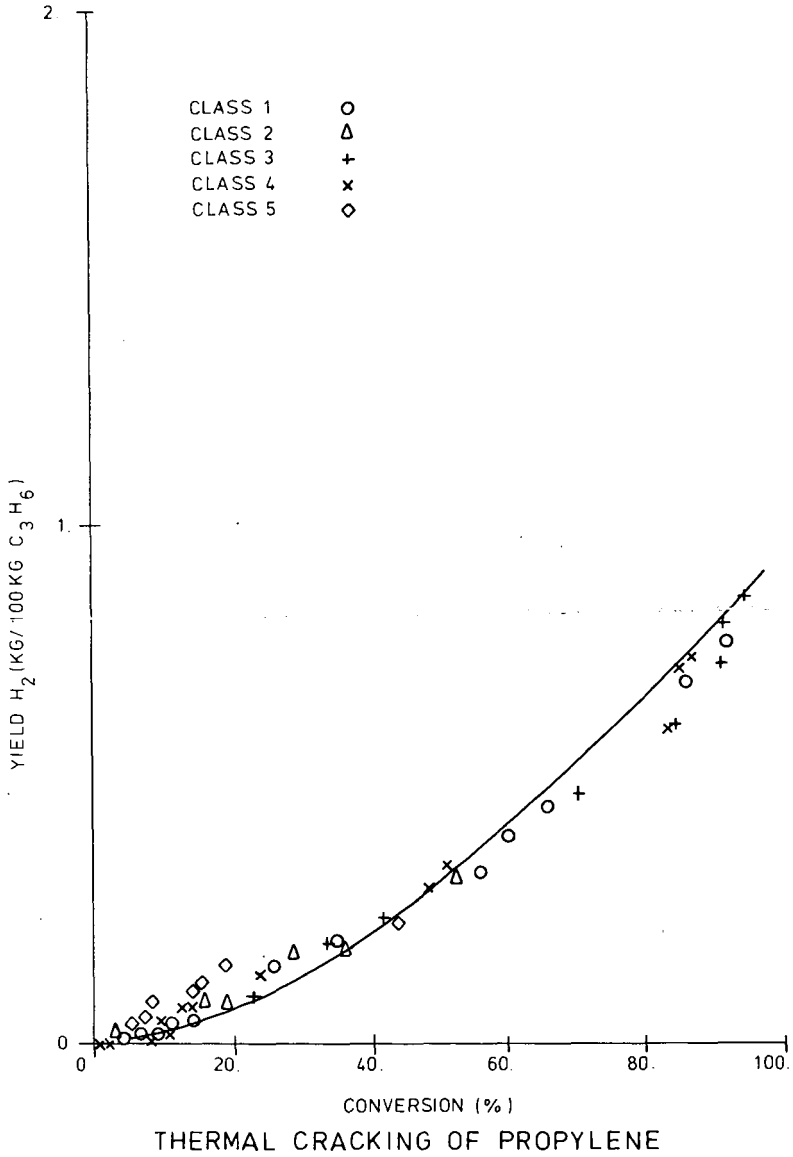


Figure 7.

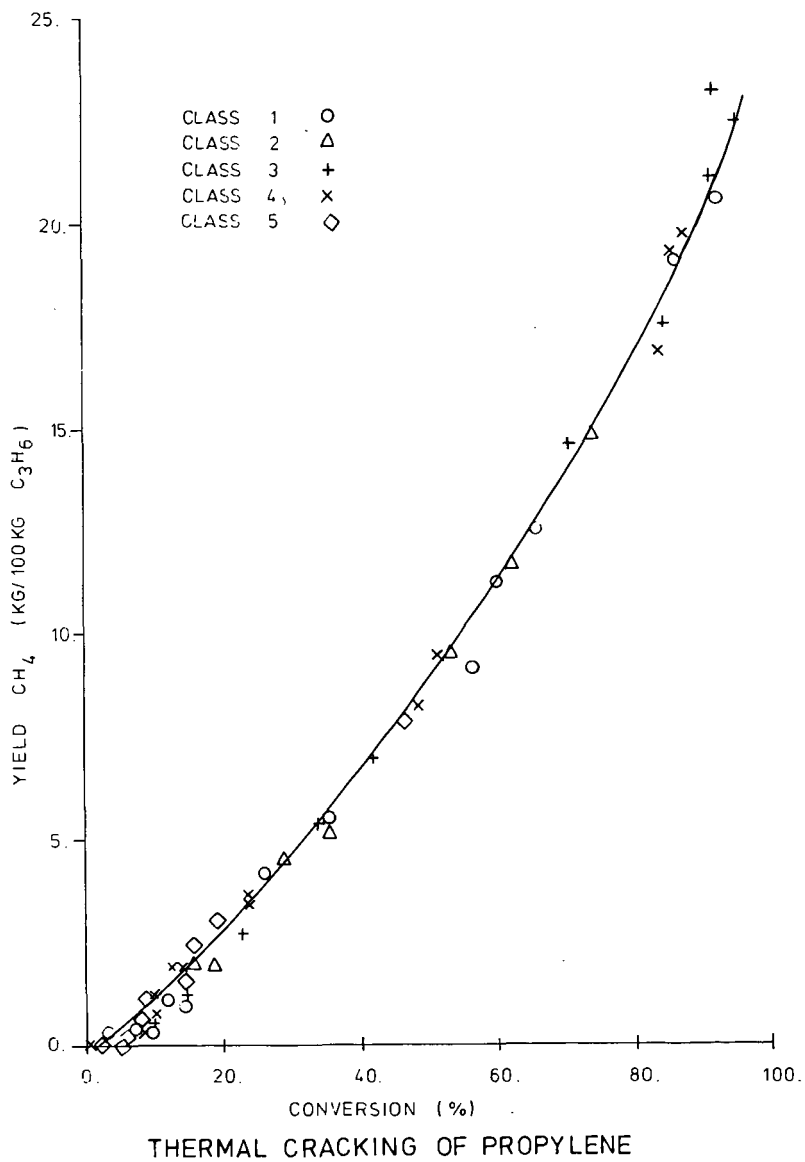


Figure 8.

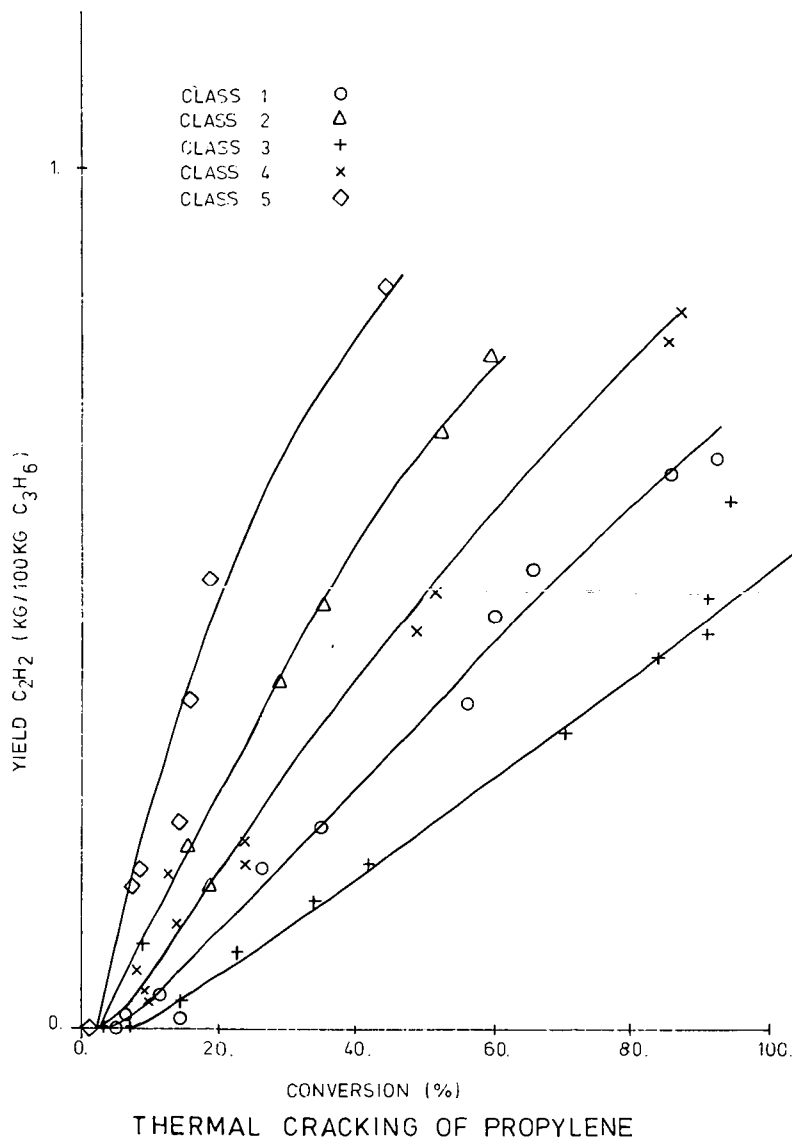


Figure 9.

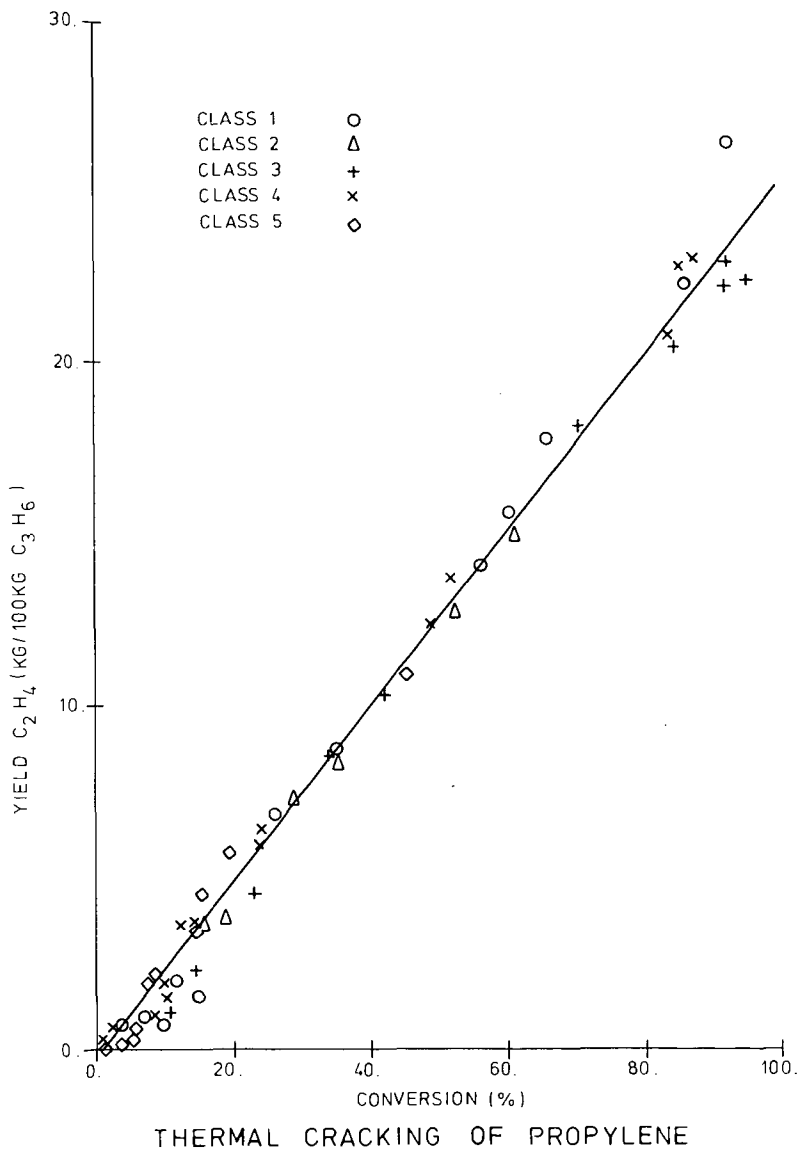


Figure 10.

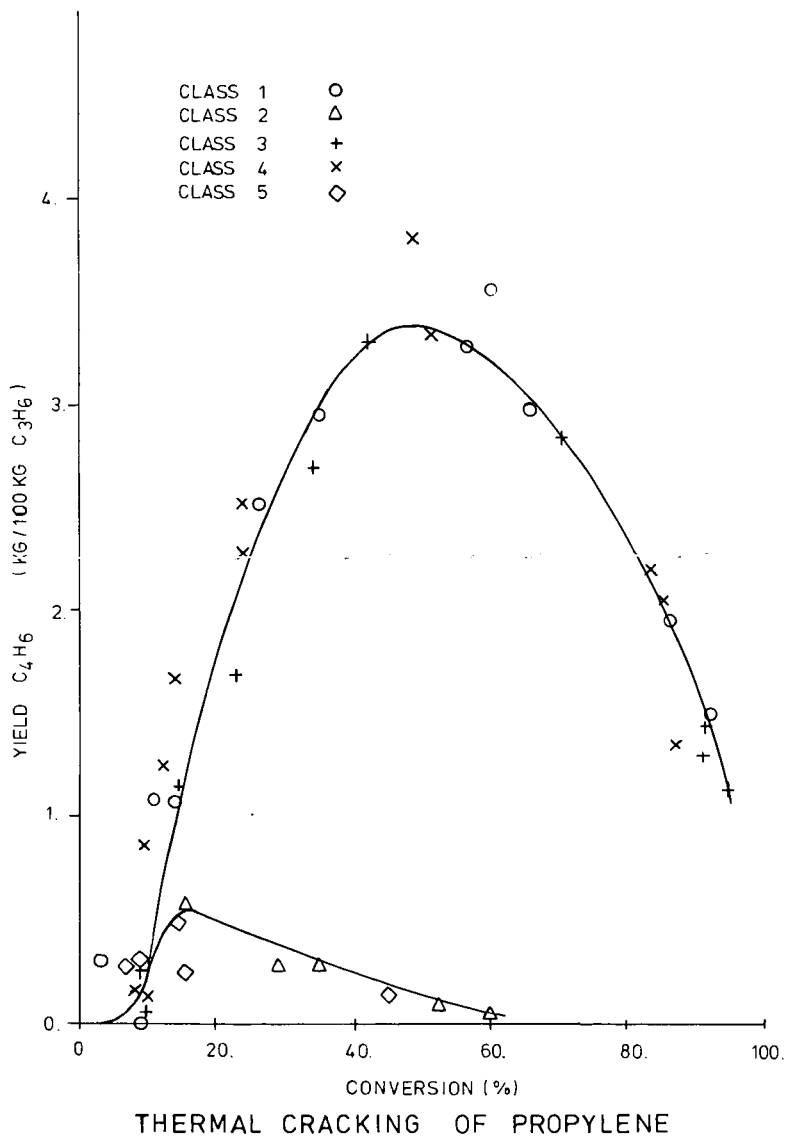


Figure 11.

CLASS 1	○
CLASS 2	△
CLASS 3	+
CLASS 4	x
CLASS 5	◇

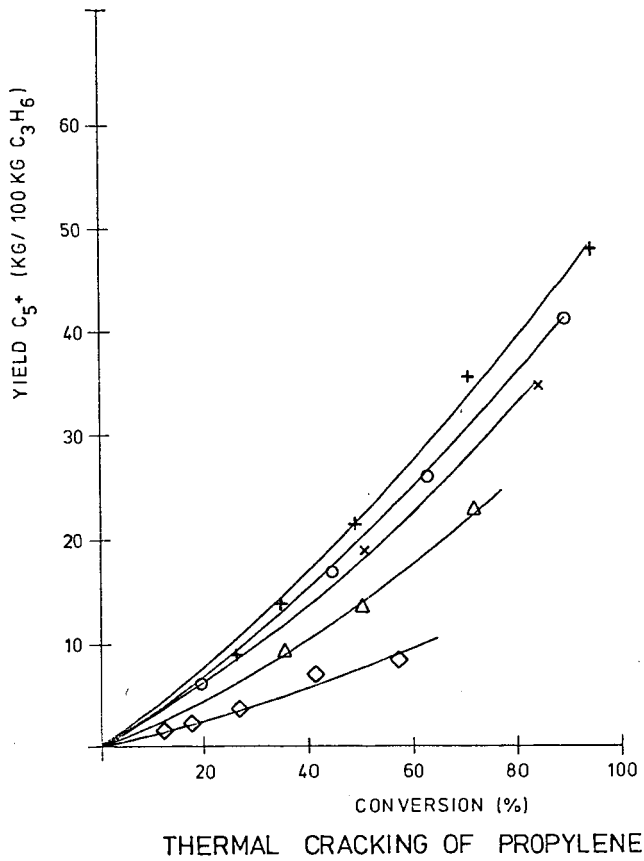


Figure 12.

ETHANE-PROPYLENE MIXTURES

CLASS 1

$X_E = 49\%$

$X_P = 70\%$

SELECTIVITY

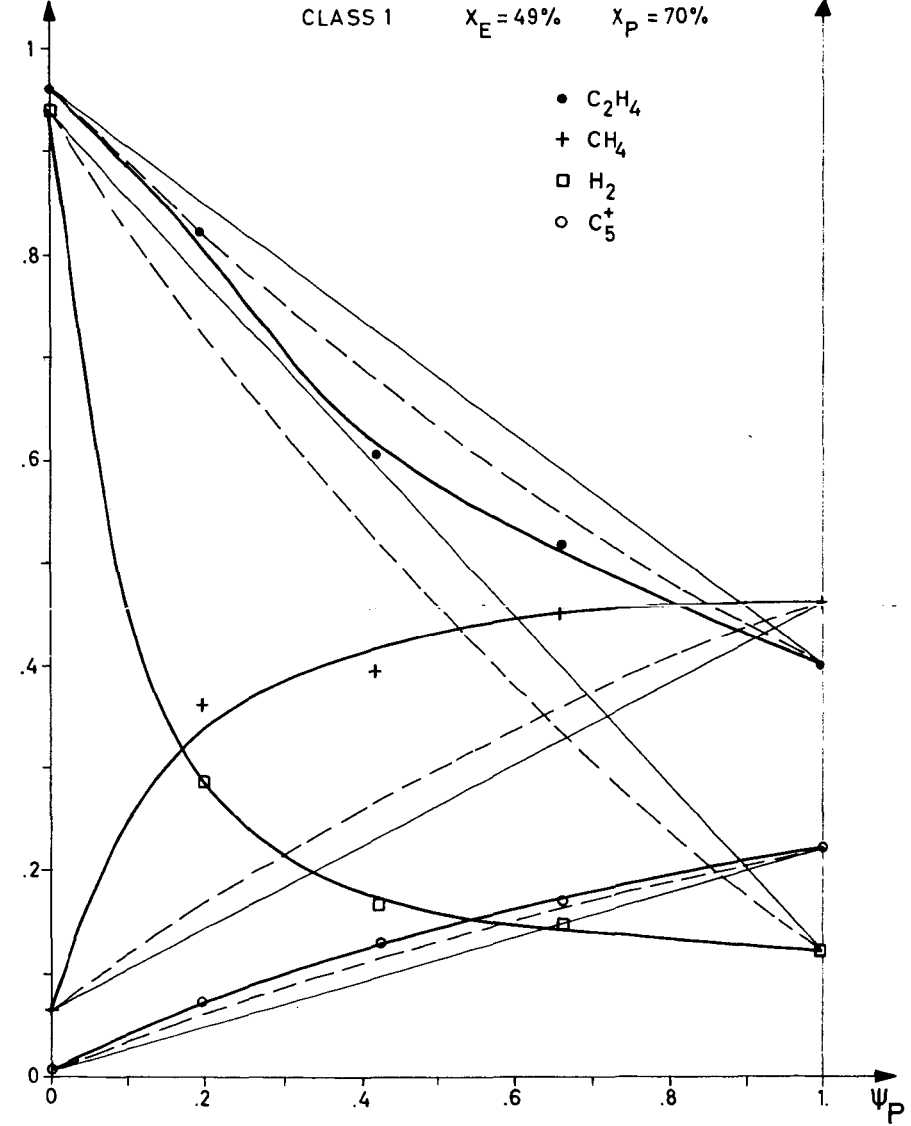
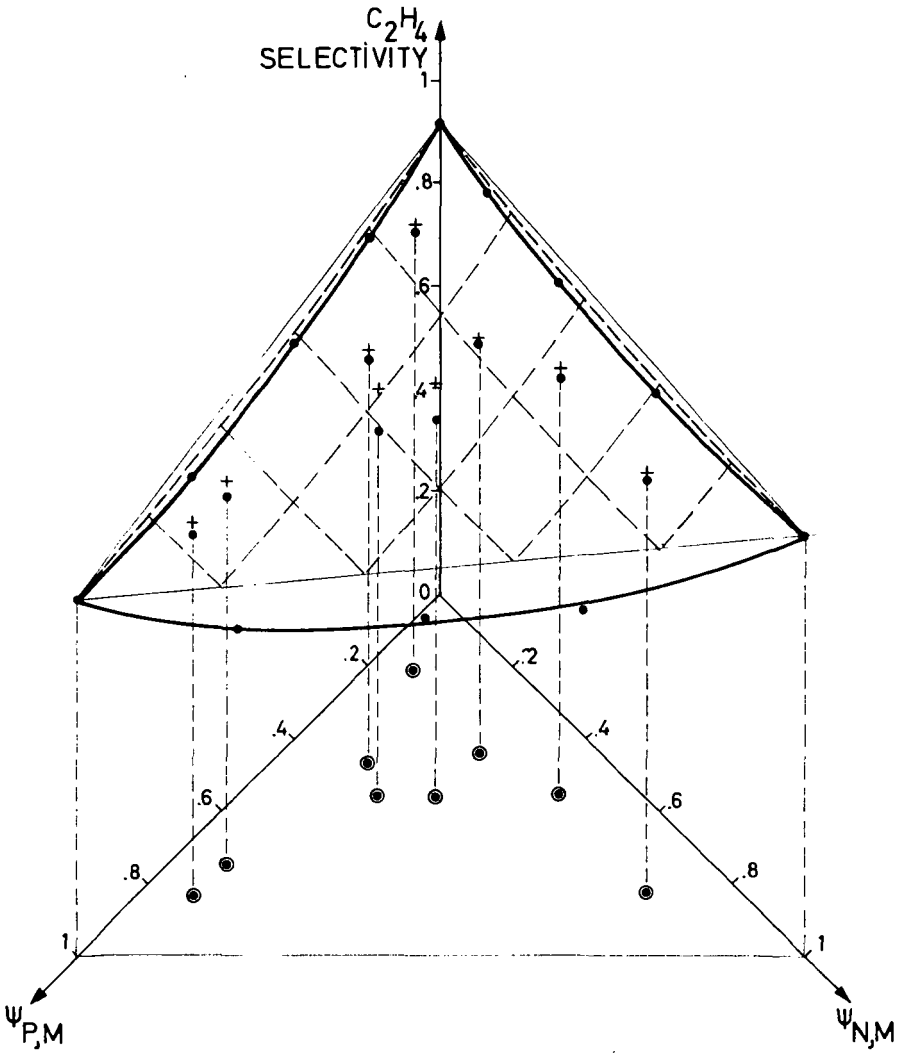


Figure 13.

TERNARY MIXTURES
ETHANE - PROPANE - N. BUTANE

CLASS 1 $X_{E,M} = 40\%$ $X_{P,M} = 73\%$ $X_{N,M} = 88\%$



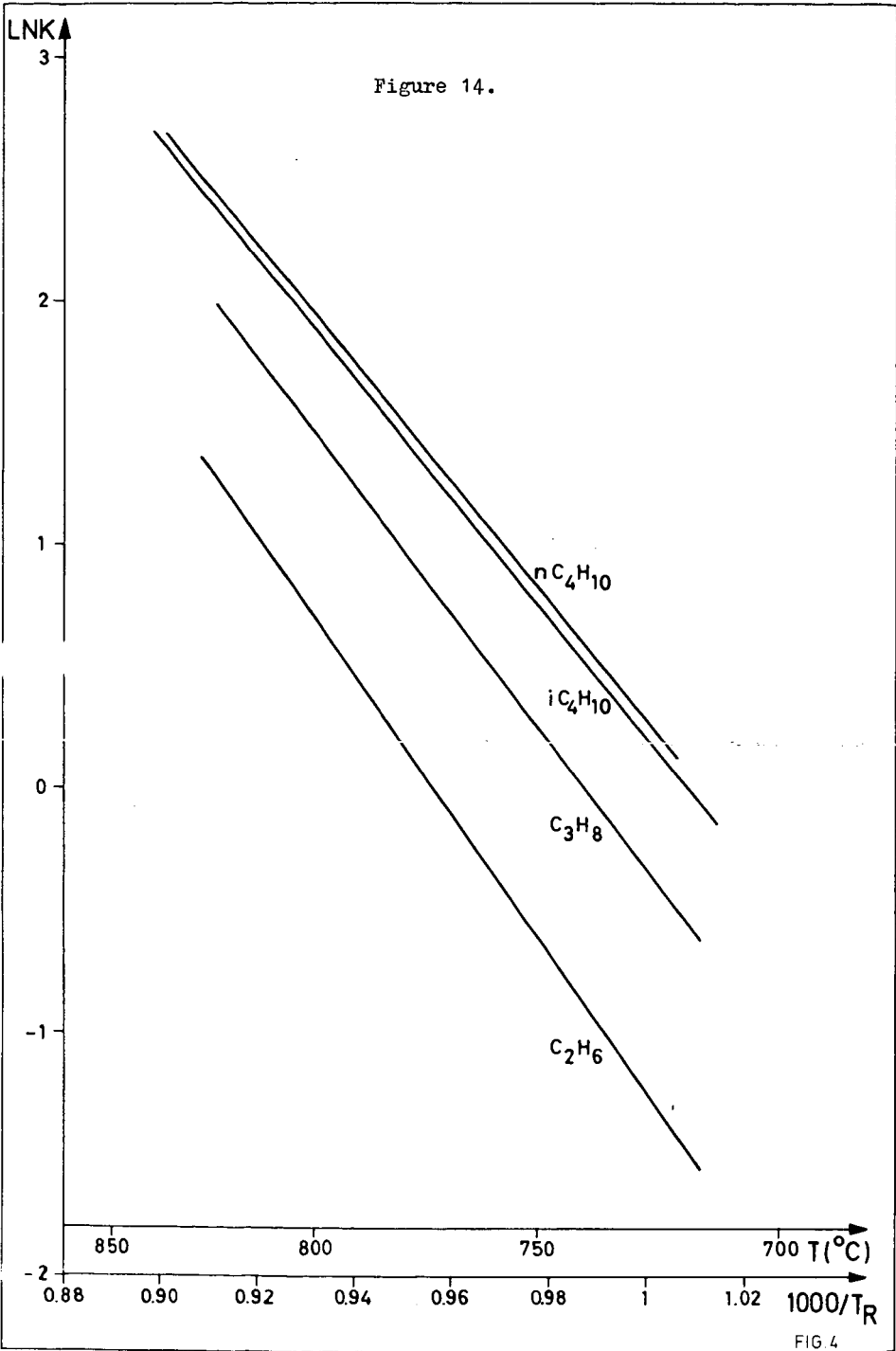


FIG. 4

Figure 15.

ETHANE - PROPYLENE MIXTURES

CLASS 1

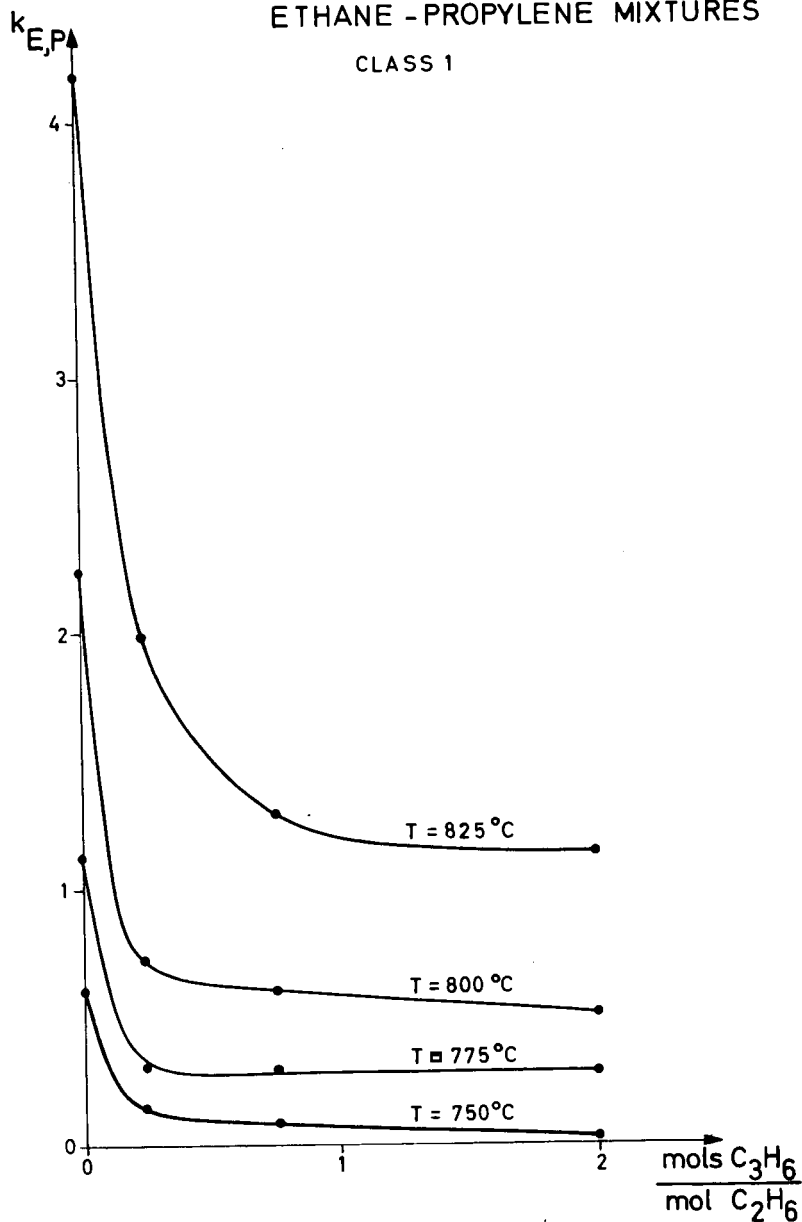
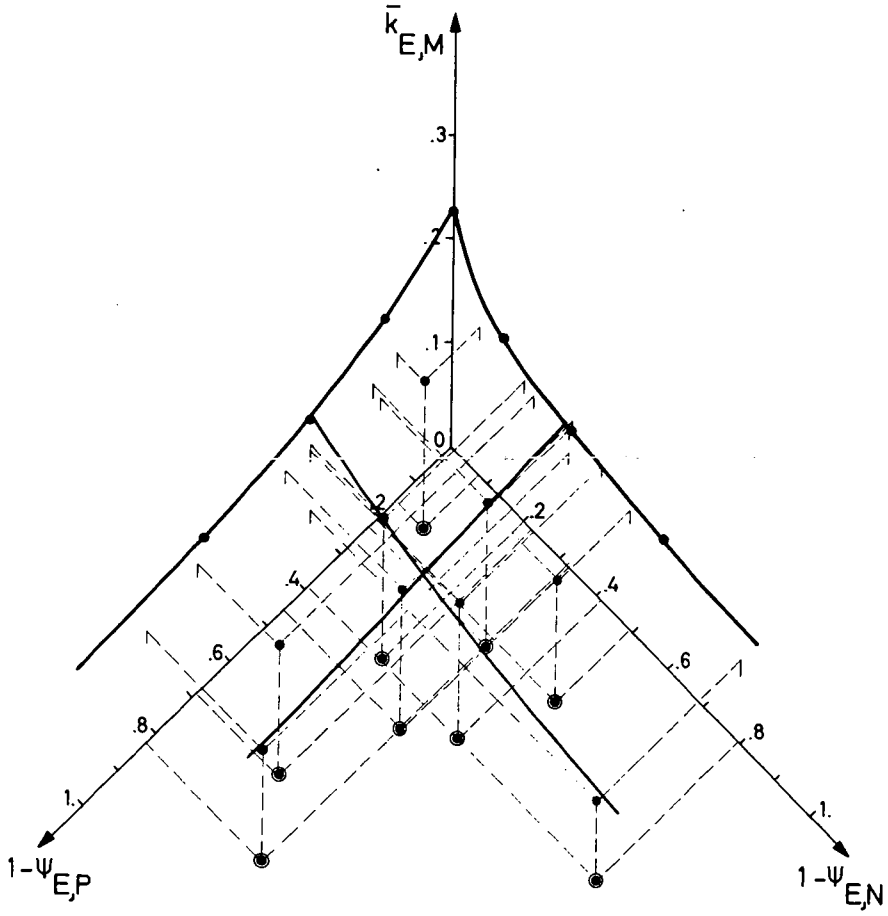


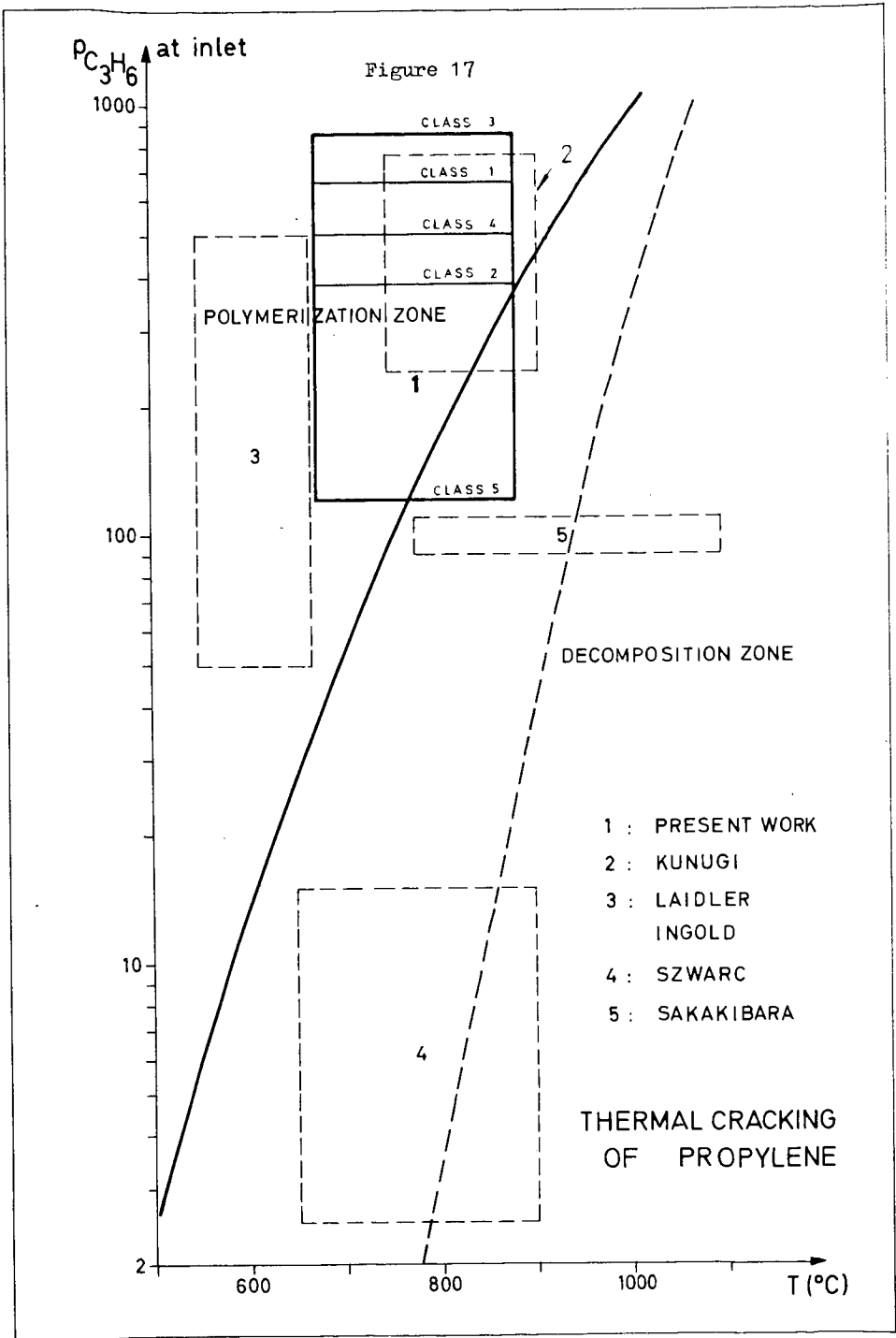
Figure 16.

TERNARY MIXTURES
N.BUTANE - PROPANE - ETHANE

CLASS 1

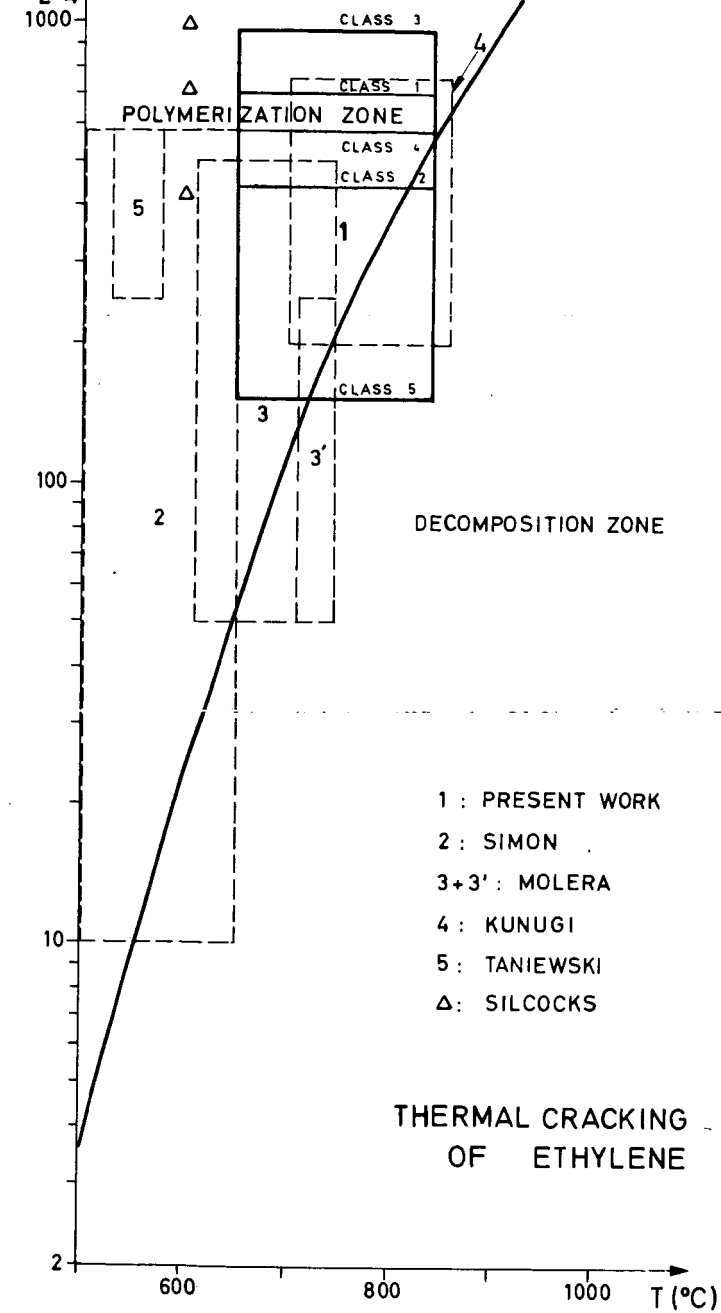
T = 800°C





PC_2H_4 at inlet

Figure 18.



PRODUCTION OF HYDROGEN VIA CATALYTIC
DECOMPOSITION OF AQUEOUS ALKALI FORMATES

C. W. Zielke, W. A. Rosenhoover, and Everett Gorin

Research Division
Conoco Coal Development Company
Library, Pennsylvania 15129

Introduction

Yoneda, et al, ^(1,2) have published in the 1940's a series of studies on the use of aqueous potassium carbonate solutions as high-pressure water gas shift catalysts. They showed that the initial step consisted of the reaction of CO with K_2CO_3 to produce KOOCH as follows:



and that this reaction was relatively rapid at temperatures of the order of 250-300°C. The second step, the decomposition of KOOCH to produce hydrogen by reaction (2) below, was shown to be relatively slow, however, in the above temperature range.



The use of catalysts to accelerate the water gas shift and presumably reaction (2) was also studied.^(1b) A number of metal carbonates were studied wherein those of Cd, Al, Zn, Cr, Sn and Co were most effective.

The combination of reactions (1a) and (2) with the decomposition of $KHCO_3$ via reaction (3) below,



is equivalent to the water gas shift, reaction, i.e.,



Somewhat later Royen and Erhard⁽³⁾ made a similar study of a nonaqueous water gas shift catalyst which consisted of K_2CO_3 impregnated on activated carbon. They showed that the mechanism followed the same route outlined by Yoneda, et al for the aqueous system.

The reactions in the "dry" charcoal supported system proceeded under much milder conditions than in the aqueous system because of the higher surface area of the charcoal absorbent and because the charcoal apparently possesses some catalytic activity for decomposition of KOOCH.

Neither set of investigators discussed the possibilities of a cyclic system wherein the CO absorption step is separated from hydrogen generation via formate decomposition.

It is the purpose of this paper to describe in summary form the work carried out sporadically in the CCDC laboratories over a period of years to evaluate the potential of such a cyclic system.

There are a number of alternatives in the way that such a system can be conducted but considerations given here are limited to the use of aqueous potash solutions wherein the CO absorption step is carried out noncatalytically while the formate

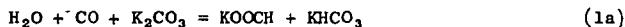
decomposition is conducted with the aid of a supported catalyst which has substantially no solubility in the aqueous reagent.

The system under consideration and experimental work to test its feasibility is described in what follows. Economic evaluation of the system is now underway at the CCDC laboratories, but no data on this question are available for presentation at this time.

Process Description

The system under consideration for removal of CO from a CO-rich gas and its conversion to a separate stream of hydrogen is illustrated schematically in Figure 1.

Formate synthesis is via noncatalyzed reactions (1a and 1b):



No distinction has been made in the discussion that follows between the rate of the two reactions. No experimental data to prove this equivalence are available, however.

The rationalization here is that the mechanism involves, as proposed by Royen and Erhard,⁽³⁾ the reaction of CO with hydroxyl ion. As long as the hydroxyl ion concentration is high enough to sustain mass transfer rate control, then the rate should be reasonably independent of the salt composition.

Various type of contacting devices for reactions (1a and 1b) have been investigated in a preliminary fashion as will be discussed below. A suitable device would be a gas sparged bubble column possibly packed with a catalytic inert packing to increase the gas-liquid interfacial area and accordingly the mass transfer rate. Suitable operating conditions will be discussed after the experimental data are presented.

It is essential to success of the system presented here that the formate synthesis via reactions (1a and 1b) proceed with a rate many fold greater than its noncatalytic decomposition via reaction (2). It will be shown below that this condition is readily achieved in practice.

The second essential step is the catalyzed decomposition of formate via reaction (2). The preferred system here is a fixed-bed catalyst, trickle-phase operation wherein steam is passed countercurrent to the descending stream of aqueous formate. The experimental system discussed, however, used a cocurrent system but this was done only for experimental convenience.

The gas leaving the formate decomposition will contain appreciable amounts of carbon dioxide and may contain in addition small but appreciable amounts of carbon monoxide. These must be removed from the final gas by conducting reactions (1a, 1b and the reverse of reaction 3). The reversal is effected by first partially decomposing the KHCO_3 in the effluent, liquid stream from the formate decomposition via steam stripping at a reduced pressure.

The K_2CO_3 enriched liquid is then used to absorb residual CO_2 and CO from the hydrogen-rich gas in a countercurrent column at a reduced temperature as shown.

Various types of CO-rich gas may be treated by the proposed process, but the discussion here is limited to treatment of a low hydrogen and methane content gas. A generic schematic system for generation of a CO-rich gas integrated with the formate system is shown in Figure 2.

The system shown in Figure 2 envisions generation of a low hydrogen and methane content gas via gasification of a hydrogen deficient fuel such as coal or char. A particularly suitable feedstock, for example, is a low temperature char produced by fluid bed carbonization of the residue from coal extraction or hydroextraction.

The hydrogen and methane contents are maintained low by operating at a relatively high exit temperature from the gasifier, i.e., at 1750°F or above, and by recycle of CO₂ to the gasifier rather than by use of steam.

The CO₂ is supplied either by recycle of the tail gas from the formate system or by CO₂ evolved from the KHCO₃ decomposition or both as illustrated in Figure 2.

The gasifier itself may be operated with air, oxygen-enriched air or relatively pure oxygen depending in part on the specific type of gasifier chosen. Various types of gasifiers may be used here including entrained phase, fluid bed or fixed bed systems but it is outside the scope of this paper to discuss the gasification step further.

The system shown in Figures 1 and 2 makes no special provision for removal of sulfur from the gas. When the system is applied to relatively low-sulfur subbituminous coals or lignites, the major fraction of the sulfur will be retained in the coal ash, at least when a fluid bed gasifier is used. A considerable amount of sulfur will also be rejected with the CO₂ in the KHCO₃ decomposition steps. The result should be that the residual gas would be low enough in sulfur after incineration for direct release to the atmosphere.

Experimental

The experimental procedure used in the course of this work will only be described in summary form because of the large number of different topics covered.

The noncatalytic synthesis of formate by reaction of CO with aqueous carbonate was studied by a number of different methods. A continuous reactor system using a 3" ID x 9" pool height, stirred reactor was previously described.⁽⁴⁾ Kinetic studies were likewise made using the same reactor operated batchwise with respect to the liquid but continuously with respect to the gas. Continuous studies were also made in a stirred pilot plant reactor. The reaction system and its operation was identical to that previously described in connection with its use for the analogous noncatalyzed reduction of K₂S₂O₃.⁽⁵⁾ with CO. The reaction was also studied in a 3" ID continuous gas-sparged bubble column.

The catalytic decomposition of aqueous formate was studied in both batch and continuous equipment. The batch apparatus used the same 3" ID stirred reactor employed for formate synthesis.⁽⁴⁾ The apparatus was used initially for screening studies of various metals and metal sulfides supported on activated carbon. Finally, the apparatus was used for equilibrium studies in the decomposition of formate via reaction (2). The best catalyst found from the screening study, i.e., 9% Mo as MoS₂ on 12 x 20 mesh Darco activated carbon, was used in this work. The apparatus was modified to permit sampling of both the gas and liquid phase at various times to determine steam partial pressures over the liquid phase. A pressure of 35-40 atmospheres of carbon dioxide was impressed on the system to eliminate complications due to decomposition of potassium bicarbonate. Equilibrium was assured in reaction (3) by approaching it from both sides, i.e., via synthesis as well as decomposition of formate.

The continuous unit studies of the decomposition of aqueous formate were conducted using a fixed-bed, trickle phase system. The same 12 x 20 mesh MoS₂ on carbon catalyst used in the equilibrium studies was also used in this work. The 1-1/4" ID reactor was constructed of Hastelloy C to eliminate stress corrosion. It was operated cocurrently

with respect to liquid feed and gas withdrawal. A schematic sketch of the equipment used is shown in Figure 3. The liquid feed was distributed evenly over the catalyst bed by means of a cup with holes in the perimeter. The catalyst bed was 26" high. The lower 22-1/4" of the reactor was packed initially with Cannon stainless steel packing. This was later replaced, because of corrosion, with the same height of mullite beads. The inert packing was operated at a temperature between 55 and 90°F below the catalyst section in order to partially reabsorb any carbon dioxide evolved via reaction (3). A three hour line-out period was universally used before initiation of the material balance operation to obtain the data reported here.

The catalyst was prepared by impregnation of the activated carbon with aqueous ammonium molybdate. The catalysts were dried and calcined in a nitrogen stream at 550°F for four hours, followed by sulfiding for four hours at 550°F with 15 mol % hydrogen sulfide in hydrogen.

Gas analyses were conducted by standard gas chromatography.

The liquid samples were analyzed for potassium formate via use of excess potassium permanganate as an oxidant followed by back titration with ferrous ammonium sulfate.

The bicarbonate content was determined by use of excess KOH to convert it to carbonate. The carbonate was converted to unreactive form by precipitation with barium chloride and the excess KOH determined by titration with HCl.

Total carbonate plus sulfide sulfur were determined by acidifying the sample with dilute sulfuric acid and removal of the H₂S and CO₂ by purging with nitrogen. Hydrogen sulfide was recovered and analyzed iodimetrically. Carbon dioxide was determined gravimetrically by absorption on Ascarite after drying the gas with magnesium perchlorate.

Rate of Formate Synthesis

The rate of formate synthesis via reactions (1a and 1b) was studied in a number of different types of experimental units as outlined above. The most extensive study was made in the 3' ID continuous stirred unit. A summary of results obtained in this study was presented previously.⁽⁴⁾

It is outside the scope of this paper to give detailed results of the formate synthesis. Only summarized conclusions will be presented.

The reaction at temperatures above 400°F has the characteristics of a liquid film mass transfer controlled process.⁽⁶⁾ The reaction rate has a low temperature coefficient of the order of 10 Kcal/mol of CO absorbed, the rate is first order with respect to CO pressure and increases at least linearly with agitator speed. The absolute formate synthesis rate is approximately equivalent to the rate of CO consumption in the noncatalyzed reduction of aqueous thiosulfate which were reported earlier.⁽⁵⁾

It also has been found more recently that the formate synthesis rate, like the thiosulfate reduction rate,⁽⁵⁾ increases markedly with decreasing salt concentration down to at least about 35 wt % salt concentration. The effect of salt concentration is probably related to the decreasing solubility of CO with increasing salt concentration⁽⁷⁾ which in turn would have the effect of decreasing the mass transfer rate, R, of CO, i.e.,

$$R = k_v \alpha P_{CO} \quad (5)$$

The reaction rate undergoes a transition to a chemical reaction rate controlled regime as the temperature is reduced to 400°F and below. The rate apparently is negligibly slow under conditions where the hot potassium carbonate process for removal of acid gases normally operates, i.e., at ca 200-240°F.

The reaction rates previously reported⁽⁴⁾ were relatively low. The specific rate at 482°F, for example, was 7×10^{-3} lb mols/hr-ft³-atm. One reason for the low rate was the high salt concentrations, i.e., 70 wt % employed. More recent data have shown specific rates at 450°F as high as 2×10^{-1} lb mols/hr-ft³-atm using more dilute, i.e., 35 wt %, salt solutions.

The above specific rates are based on unit volume of the aerated liquid, not as is often done, to base the rates on unit volume of unaerated liquid.

The commercial embodiment would preferably use a nonmechanically agitated contactor. A gas-sparged bubble column contactor (BCC) would be suitable for this purpose. Many investigators^(8,9) have studied mass transfer processes in BCC reactors. The rate is approximately proportional to the seven-tenths power⁽¹⁰⁾ of the superficial gas velocity (V_g). At highly turbulent conditions, i.e., $V_g \approx 0.7$ ft/sec, the rate in a BCC reactor⁽⁸⁾ approaches that of a vigorously mechanically stirred reactor.

The BCC has another advantage over a mechanically agitated reactor in that the gas flow pattern approaches piston flow.

A few experiments were carried out in the CCDC laboratories in a 3" ID BCC reactor but much more remains to be done. The preliminary data confirm expectations from the literature that high rates can be obtained in a BCC reactor.

Rate of Formate Decomposition

Formate decomposition via reaction (2) must obviously be minimized during synthesis via the noncatalyzed reaction with CO. The decomposition of formate is quite slow in the absence of a catalyst such that normally this is not a problem. Metal surfaces are usually readily poisoned for this reaction by treatment with hydrogen sulfide.

Conversion of CO to hydrogen was only of the order of one mol percent, for example, in the pilot plant stirred reactor operated at 540°F, 720 psig and 35 minutes residence time. Under the above conditions 88 mol % conversion of carbonate to formate was achieved.

Equilibrium Data

There are five equilibria which completely define the system as long as the only species present in the liquid phase are KOCH, KHCO₃, K₂CO₃ and H₂O, and the only species in the gas phase are CO, CO₂, H₂ and H₂O. The appropriate equilibria are the steam pressure over the salt solutions, equilibria in reactions (2, 3 and 4), respectively, and salt solubility relationships.

Steam Pressure

The steam equilibrium pressure decreases with increasing salt concentration. It is desirable, of course, to operate with as low a steam pressure as possible. It is not, however, entirely practical to do this by indefinitely increasing the salt

concentration. The use of more concentrated salt solutions incurs the disadvantages of decreased reaction rate, limited solubility of one of the components - usually KHCO_3 , and increased viscosity.

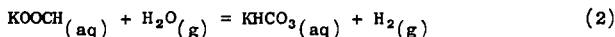
The steam partial pressure in the $\text{KOOCH-K}_2\text{CO}_3\text{-KHCO}_3\text{-H}_2\text{O}$ system was correlated against the parameter of mols K/1000 gm H_2O . The basic assumption here is that all salt solutions in the above system have the same vapor pressure at the same value of the above parameter. Insufficient experimental data were obtained to verify this assumption precisely. It is useful, however, as a means of roughly predicting the vapor pressure of steam over a given salt solution.

Experimental data are presented in Figure 4 for three series of salt solutions as a function of temperature on a semi-log plot of vapor pressure versus the reciprocal of the absolute temperature. The lines correspond to the least squares regression through the experimental points. The heats of vaporization calculated from the regression lines are reasonably close to that of pure water at this temperature, namely, 9.0-9.3 Kcal/mol.

Figure 5, is a cross plot of the data of Figure 4 with temperature as parameter.

Equilibrium in Formate Decomposition

The equilibrium in reaction (2),



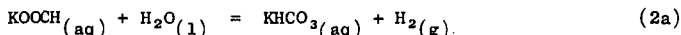
was studied using solutions equivalent to 40 wt % KOOCH or 9 mols K/1000 gm H_2O . Equilibrium was approached from both directions by use of the MoS_2 catalyst.

The "equilibrium constant" in the above reaction, i.e.,

$$K = \frac{(\text{KHCO}_3) P_{\text{H}_2}}{(\text{KOOCH}) P_{\text{H}_2\text{O}}}$$

is not independent of the concentrations and partial pressure ratios due to the large deviation from ideality, particularly of the salt components. Accordingly, the "equilibrium constant" of reaction (2) is plotted as a function of the molar ratio $(\text{KHCO}_3)/(\text{KOOCH})$ in Figure 6. Regression analysis was again used to locate the "best" straight lines to represent the data.

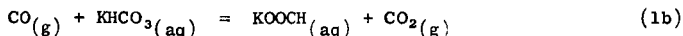
Figure 7 shows the partial pressure of hydrogen as a function of the fraction of KOOCH decomposed via reaction (2) with temperature as a parameter. It is immediately apparent that the hydrogen partial pressure is almost independent of temperature. Thus, if equilibrium in reaction (2) is expressed in the form,



it is immediately obvious that the heat of reaction (2a) is substantially zero.

Equilibrium in Formate Synthesis

Equilibrium in the formate synthesis reaction (1b),



may be expressed simply as the sum of the reverse of reaction (2) and the water-gas shift reaction (4), and accordingly,

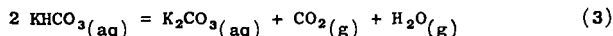
$$K_{1b} = K_4/K_2$$

The measured and equilibrium values for the water-gas shift ratio and the calculated equilibrium ratio PCO_2/PCO for reaction (1b) at a molar ratio of $KHCO_3/KOOCH = 1$, are given in Table I. It is immediately clear that the equilibrium in reaction (1) is highly favorable and there is little equilibrium limitation to prevent nearly complete absorption of CO .

The experimental values for the water-gas shift ratio obtained in the equilibrium study of reaction (2) were usually somewhat higher than equilibrium. This indicates that equilibrium was not quite achieved in the reverse of reaction (1b).

Equilibrium in Bicarbonate Decomposition

The equilibrium in reaction (3), i.e.,



is now needed for definition of the system. Unfortunately, the system described here operates at higher temperatures and higher salt concentrations than is usually employed in the "hot pot" process. The equilibrium relationships are further complicated by the presence of $KOOCH$. Thus, the data previously presented for reaction (3), in connection with the "hot pot" process by Tosh, et al.⁽¹¹⁾ and by Bocard and Mayland⁽¹²⁾ are of little value for the present case.

A limited equilibrium study for reaction (3) was, however, made in the course of the development of the CCDC Stack Gas Scrubbing Process⁽⁵⁾ in the $KHS-KHCO_3-KOOCH-H_2O$ system. The data have somewhat limited applicability to the present case because of the presence of KHS . Some data in the range of interest to the present process are shown in the curves given in Figure 8.

These data are compared with the data on the actual system in Figure 8 for two sets of experiments. The first set was obtained in the continuous unit where the effluent from the catalytic bed was run over an inert bed of packing at the temperature indicated. Equilibrium, accordingly, was not necessarily approached. It is noted that the partial pressure of CO_2 in the continuous unit series appears significantly lower than the values expected from the equilibrium data.

A possible explanation is that the continuous unit data are low due to further absorption of CO_2 in the effluent lines and receivers. The receivers were operated at a temperature usually about $100^\circ F$ lower than the inert packed bed, but relatively poor contact between gas and liquid was provided. It is, nevertheless, to be expected that some additional CO_2 absorption occurred. It should be noted also that the equilibrium pressure of CO_2 should be somewhat lower in the continuous unit series because of the higher water and $KOOCH$ contents. It is clear from the equilibrium data, for example, that the addition of $KOOCH$ at the same water content suppresses the CO_2 dissociation pressure.

Data from a second set of experiments in the batch unit are also indicated on Figure 8. These data were obtained by cooling the batch autoclave from the decomposition temperature to $437^\circ F$ and holding at this lower temperature for 30 minutes. The deviation from the equilibrium CO_2 pressure should, in contrast to the continuous series, be on the high side in these runs.

The batch data are somewhat scattered as shown, but are in the approximate range expected from the equilibrium data.

It is obvious that more data are required to elucidate the equilibrium pressures in the actual system more closely.

Salt Solubility Relationships

It is outside the scope of this paper to present any data on the above subject. However, due to the higher temperature at which this system operates as compared with the "hot pot" system, no problem is incurred because of the presence of insoluble salts as long as the total salt concentration is below about 50 wt % and the temperature is maintained above about 250°F.

Rate Data on Catalytic Decomposition of KOOCH

A screening study of various metal sulfides supported on activated carbon was made in the batch autoclave as catalysts for reaction (2). The best catalysts found were the group VI sulfides typified by MoS₂ and the noble metals.

The continuous unit studies were limited therefore to the uses of MoS₂ and Pt catalysts. It soon became obvious that the MoS₂ catalyst was much more active than the Pt catalyst and accordingly only results from the former catalyst will be presented.

The feed solution and catalyst used in the continuous unit runs presented here were of constant composition as given in Table II.

The liquid hourly space velocity (LHSV) was varied between 2 to 4 at two operating temperatures, i.e., 425 and 475°F. One run was made at 525°F at a space velocity of 3. The liquid and gas product compositions for the two series are given in Tables III and IV, respectively. It is immediately noted that high purity hydrogen is generated in the range of 96.5 to 99.5 mol %. The major impurity is CO₂.

The product composition expressed as the fraction $(\text{KHCO}_3) / [(\text{KHCO}_3) + (\text{KOOCH})]$, equivalent to fractional decomposition of KOOCH via reaction (2), is plotted as a function of LHSV in Figure 9 where it is compared with the equilibrium values. The equilibrium values are estimated from the product gas and liquid compositions without any correction for changes that occur on cooling. The hydrogen partial pressure used to estimate the decomposition parameter is arrived at from the dry gas composition and the steam partial pressure obtained from Figures 4 and 5. It is noted that at 475°F, equilibrium is closely approached as the LHSV is reduced to a value of 2. The one run at 525°F showed a higher than equilibrium conversion which is obviously impossible. The product liquid and gas compositions were actually those measured after cooling to 435°F. Thus, the KHCO₃ content at the reaction temperature of 525°F was undoubtedly somewhat lower due to partial decomposition via reaction (3). The hydrogen partial pressure is also slightly lower at the higher temperature. These factors would cause the experimental decomposition ratio to shift downward and the calculated ratio to shift upward slightly. It would appear, in any case, that true equilibrium is closely approached at 525°F and LHSV = 3.

Catalyst Life

Studies not reported here with more concentrated salt solutions indicated a very short catalyst life. The major reason for the catalyst activity decline was traced to the deposition of insoluble salts, probably KHCO₃, blocking the catalyst pores. A major improvement in catalyst life was achieved by use of the more dilute solution shown in Table II.

The results of a prolonged run are given in Figure 10. It is noted that after a brief relatively rapid decline, that the activity decline with time is relatively slight. The experimental data on the rate of decline after 35 hours onstream was fitted by a linear regression equation:

$$y = 52.92 - 0.0075 t.$$

where y is the percent formate decomposed and t is the time in hours.

The above equation cannot realistically be used beyond the range of the data, i.e., 121 hours. It is obvious that longer runs are required to establish a realistic value for catalyst life.

Process Operating Conditions

Considerably more data are required to establish optimum operating conditions for the process than has been presented here.

It is clear, however, that the salt concentration should be below 60 wt %, because of the adverse effect of high salt concentration on the rate of formate synthesis, but probably above 35 wt %. The operating temperature in the formate synthesis reactor should be above 400°F, but preferably below 500°F to avoid excessive steam vapor pressures. A suitable temperature is approximately 450°F.

Approximate sizing of the formate synthesis reactors may be obtained by considering the simplest case where synthesis is via reaction (2), i.e., no change in gas volume occurs, and a BCC type reactor is used such that piston flow of gas may be assumed.

The appropriate rate equations in differential and integrated forms are:

$$-dF_{CO} = \frac{k_G \pi F_{CO} dV}{F} \quad (6)$$

$$2.303 \log \left(\frac{1}{1-\alpha} \right) = \frac{k_G \pi V}{F} \quad (7)$$

A hypothetical case was considered using equation (7) in a BCC reactor for production of 25,000 lb mols H_2 /hr from dry producer gas containing 35 mol % CO . The conditions used are illustrated in Table V. The basic assumption on reaction kinetics is that the maximum rate realized in a mechanically agitated contactor, i.e., $k_G = 0.2$ lb mols/hr-ft³-atm at 450°F can also be achieved in a BCC contactor at a superficial velocity of 0.75 ft/sec. This has not been demonstrated as yet and may very well prove to be optimistic. Obviously more experimental work is required. Under the conditions specified in Table V, three 12' diameter vessels with a liquid pool height of 50' would be required. To maintain the desired superficial gas velocity, the reactors would have to be operated in parallel.

It is clear from the data in Table V, that the minimum operating pressure for the formate synthesis reactor when operated with producer gas is of the order of 60 atm. The operating pressure may be reduced somewhat if the gasifier is operated with oxygen or oxygen-enriched air, but obviously must always substantially exceed the vapor pressure of the salt solution which at 450°F amounts to 24 atm.

The catalytic formate decomposition reactor should operate generally at temperatures somewhat higher, i.e., 25-100°F, than the synthesis reactor. Countercurrent flow of steam versus the formate solution will permit operation at maximum pressure with minimum steam consumption. The total operating pressure should be at least equal to that in the formate synthesis reactor. The data of Figure 7, for example, indicates that pressures as high as 100 atm are practical at 525°F in a countercurrent system.

The gas leaving the catalytic decomposition zone will contain appreciable amounts of carbon dioxide. This must be removed by scrubbing with the K_2CO_3 enriched reagent as discussed previously. The scrubbing temperature must be below 400°F, but desirably above 250°F to prevent deposition of insoluble salts.

Conclusions

The aqueous formate process for treating a CO-rich gas, with separation and conversion of the CO to a separate stream of pure hydrogen has been shown to be technically feasible. More experimental work is required to ascertain optimum operating conditions. The economic potential also remains to be determined.

The process is limited in scope to treatment of gases at relatively high pressure, i.e., above about 40 atmospheres.

Acknowledgment

Appreciation is expressed to Conoco Coal Development Company for permission to publish this paper.

Many other individuals than the authors have made contributions to the material presented here. They include: R. T. Struck, E. B. Klunder, G. P. Curran, P. J. Dudt of CCDC as well as P. M. Yavorsky and N. J. Mazzocco formerly associated with CCDC. Appreciation is herein expressed for their efforts.

Nomenclature

k_G = mass transfer rate, lb mols/hr-ft³-atm.

k_V = volumetric mass transfer rate, hr⁻¹.

α = CO solubility, lb mols/ft³-atm.

P_{CO} , P_{H_2} , etc. = partial pressure of gas, atm.

(KOOCH), (KHCO₃), etc. = mols of salt in question/unit volume.

V = volume of aerated liquid, ft³.

π = total pressure, atm.

F_{CO} = carbon monoxide flow rate, ft³/hr.

F = total gas flow rate, ft³/hr.

α = fractional absorption of carbon monoxide.

References

1. Yoneda, K, Kondo, S., and Abe, R., Jour. Chem. Soc., Japan
 - a. 44, 385 (1941).
 - b. 44, 388 (1941).
 - c. 46, 667 (1943).
 - d. 47, 5 (1944).
 - e. 47, 7 (1944).
2. Yoneda, K., Honda, Y, Momiyama, N, and Abe, R., Jour. Chem. Soc., Japan 46, 554 (1943).
3. Royen, P., and Erhard, F.,
Erdol und Kohle 6, 195 (1953).
Ibid 9, 19 (1956).
4. Yavorsky, P.M., Mazzocco, N.J., Rutledge, G.D., and Gorin, Everett,
Environ. Science & Tech. 4, 757 (1970).
5. Struck, R.T., Gorin, Everett, and Clark, W.E.,
Paper presented at 68th AIChE Annual Meeting,
Los Angeles, Calif., Nov. 16-20, 1975.
6. Higbie, R., Trans. AIChE, 31, 365 (1935).
7. Wise, D.L., and Houghton, G., Chem. Eng. Science, 23, 1211 (1968).
8. Braulick, W.J., et al., AIChE, J. 11, 73 (1965).
9. Juvekar, V.A., and Sharma, M.M., Chem. Eng. Sci., 28, 825 (1973).
Ibid , 28, 977 (1973).
10. Mashelkar, R.A., Brit. Chem. Eng., 15, (10) 1297 (1970).
11. Tosh, J.S., et al., Bureau of Mines Reports of Investigations, 5484 (1959).
12. Bocard, J.P., and Mayland, B.J.,
Hydrocarbon Proc. & Pet. Ref., 41, 128 (1962).

TABLE I

Estimated Equilibria in Reaction 1b
 $\text{CO} + \text{KHCO}_3 = \text{KOOCH} + \text{CO}_2$

Temp., °F	Water-Gas-Shift Ratio,		Equilibrium Values at $(\text{KHCO}_3)/(\text{KOOCH}) = 1$	
	$\frac{P_{\text{CO}_2}}{P_{\text{H}_2}}$ Equilibrium	$\frac{P_{\text{H}_2}/P_{\text{H}_2\text{O}}}{P_{\text{CO}}}$ Expt'l Range	$\frac{P_{\text{H}_2}}{P_{\text{H}_2\text{O}}}$ (expt'l)	$\frac{P_{\text{CO}_2}}{P_{\text{CO}}}$ (calc'd)
425	141	150-280	1.7	83
475	87	88-101	0.92	95
525	56	53-74	0.64	88

TABLE II

Composition of Feed Solution and Catalyst in
Continuous Formate Decomposition Experiments

Solution

KOOCH	38.90 Wt %	$\frac{\text{Mols K}}{1000 \text{ gms H}_2\text{O}} = 12.45$
K ₂ CO ₃	10.60 Wt %	
KHS	0.45 Wt %	
H ₂ O	50.05 Wt %	$\frac{\text{Mols KOOCH}}{1000 \text{ gms H}_2\text{O}} = 9.25$

Catalyst

9% Mo as MoS₂ on 12 x 20 mesh Darco activated carbon.

TABLE III

Product Compositions in Continuous
Catalytic Decomposition of KOCH

Catalytic Decomposition Temp., °F CO ₂ Absorption Temp., °F	←————— 475 —————→			
	400	415	414	415
LHSV	3	3	2	4
<u>Liquid Product</u>				
<u>Mol Fraction of K as</u>				
KOCH	0.372	0.389	0.329	0.466
K ₂ CO ₃	0.278	0.284	0.285	0.231
KHCO ₃	0.350	0.327	0.386	0.303
Mol Fraction K ₂ CO ₃ Converted to KHCO ₃	0.558	0.535	0.577	0.567
<u>Dry Exit Gas, Mol %</u>				
H ₂	96.72	96.83	96.65	97.90
CO ₂	3.11	3.00	3.22	1.98
CO	0.13	0.13	0.11	0.11
H ₂ S	0.02	0.04	0.02	0.01
CH ₄	0.02	0.00	0.00	0.00
Total Pressure, atm	←————— 52.65 —————→			
Est. Partial Pressure H ₂ O at 475°F, atm	←————— 32 —————→			
Est. Partial Pressure H ₂ O at 415°F, atm	←————— 15.0 —————→			
Partial Pressure CO ₂ at 415°F, atm	1.17	1.13	1.21	0.75

TABLE IV

Product Compositions in Continuous
Catalytic Decomposition of KOOCH

Catalytic Decomposition Temp., °F	←----- 425 -----→		
CO ₂ Absorption Temp., °F	365	370	370
LHSV	3	2	4
<u>Liquid Product</u>			
<u>Mol Fraction of K as</u>			
KOOCH	0.576	0.613	0.657
K ₂ CO ₃	0.207	0.204	0.206
KHCO ₃	0.217	0.183	0.137
Mol Fraction K ₂ CO ₃ Converted to KHCO ₃	0.513	0.472	0.400
<u>Dry Exit Gas, Mol %</u>			
H ₂	98.88	99.21	99.58
CO ₂	1.05	0.75	0.39
CO	0.05	0.03	0.02
H ₂ S	0.02	0.01	0.01
CH ₄	0.00	0.00	0.01
Total Pressure, atm	←----- 44.5 -----→		
Est. Partial Pressure H ₂ O at 425°F, atm	←----- 17.6 -----→		
Est. Partial Pressure H ₂ O at 370°F, atm	←----- 9.2 -----→		
Partial Pressure CO ₂ at 370°F, atm	0.37	0.26	0.14

TABLE V

Sizing of Formate Synthesis Reactor

Operating Conditions for Production - 25,000 lb mols/hr H₂

Temperature	450°F	
Total Pressure	80 atm	
Salt Concentration	<u>10 mols K</u> 1000 gms H ₂ O	- equivalent to 46 wt % salts as KOOCH
Steam Partial Pressure	24 atm	
Mol Fraction CO in Dry Producer Gas	0.35	
CO Mass Transfer Rate	0.2 lb mols/hr-ft ³ -atm	
Percent Absorption CO	91.2	
Superficial Gas Velocity	0.76 ft/sec	
No. of 12' ID x 50' Vessels	3	

FIGURE 1
 HYDROGEN PRODUCTION FROM CO-RICH GAS
 VIA
 FORMATE SYSTEM

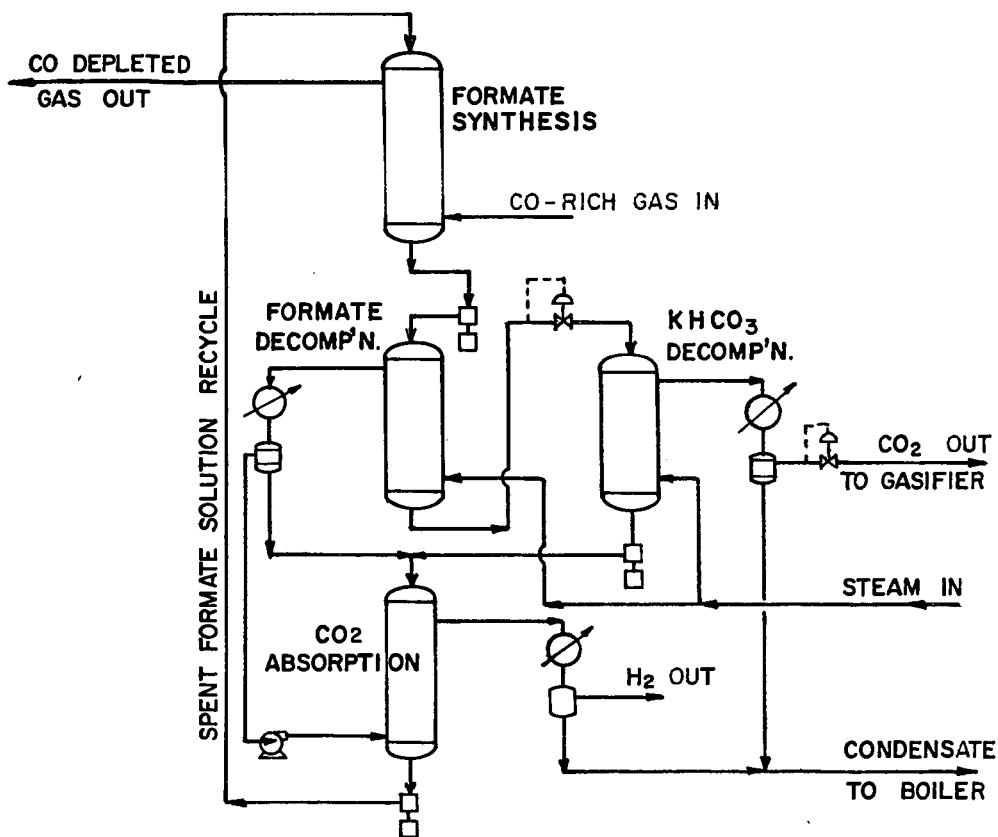


FIGURE 2
 GENERATION OF CO-RICH GAS
 SCHEMATIC SYSTEM

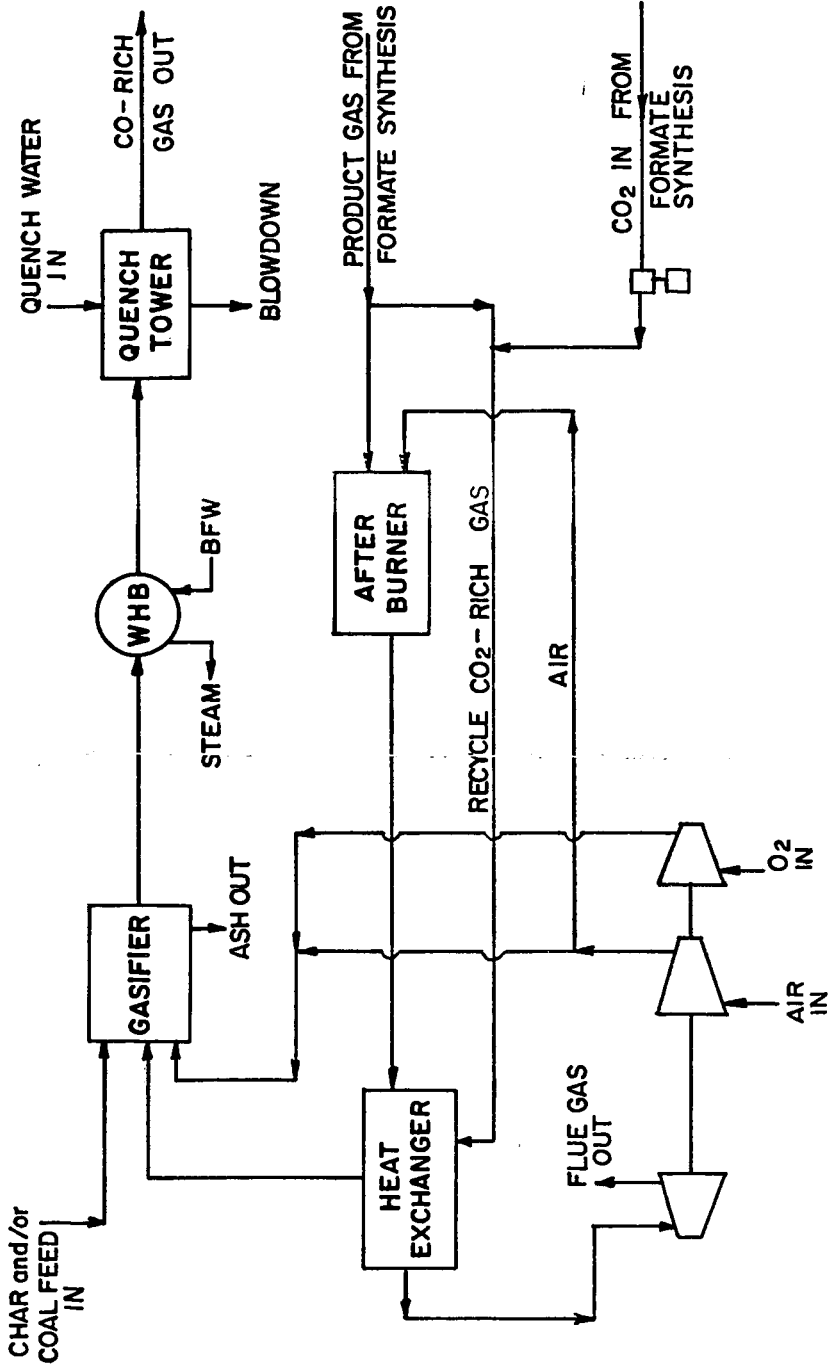


FIGURE 3

SIMPLIFIED SCHEMATIC FLOW SHEET
CONTINUOUS UNIT FOR CATALYTIC DECOMPOSITION
OF AQUEOUS FORMATE

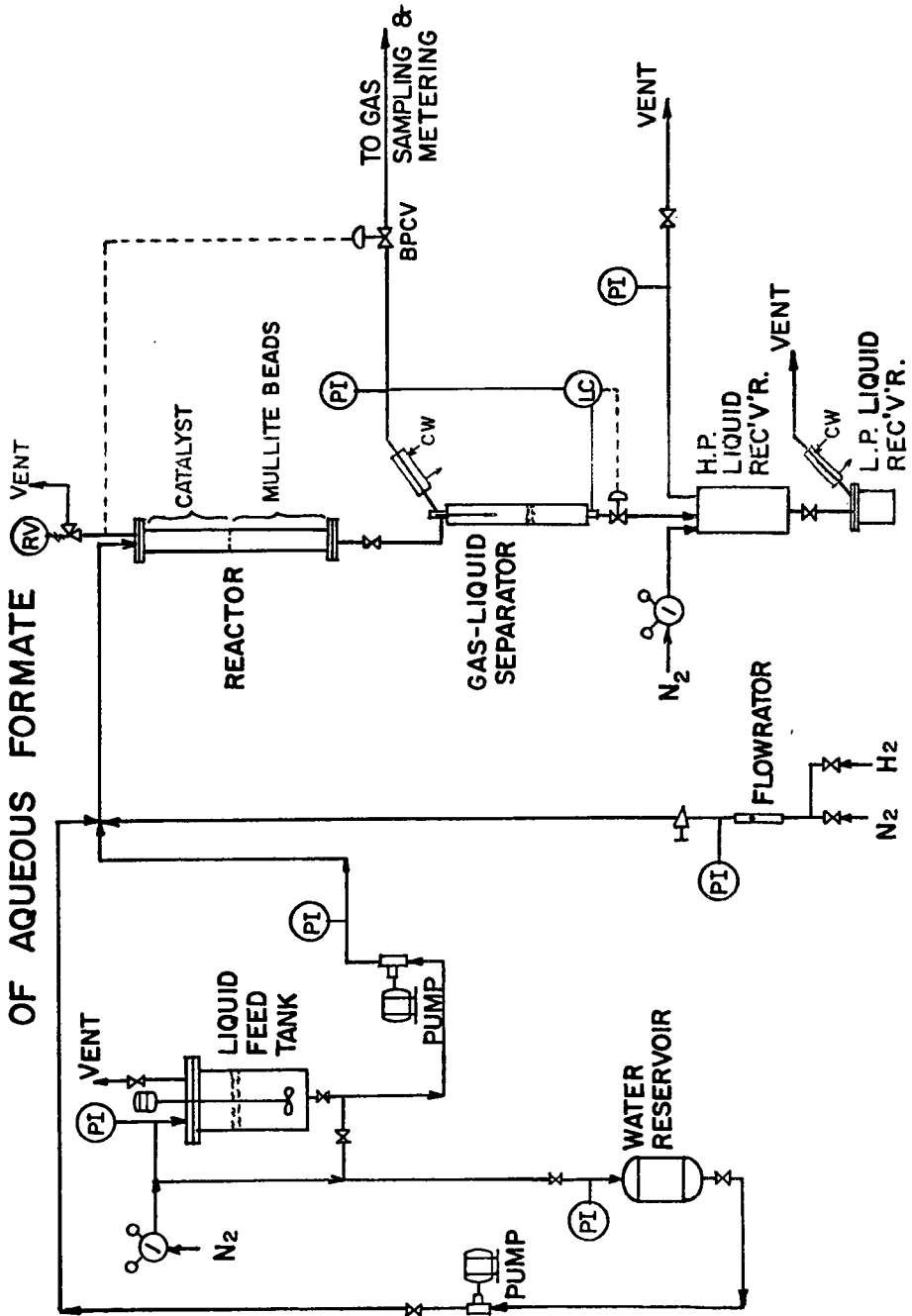


FIGURE 4

STEAM PARTIAL PRESSURE OVER
 $\text{KOOCH} - \text{K}_2\text{CO}_3 - \text{KHCO}_3 - \text{H}_2\text{O}$ SOLUTIONS

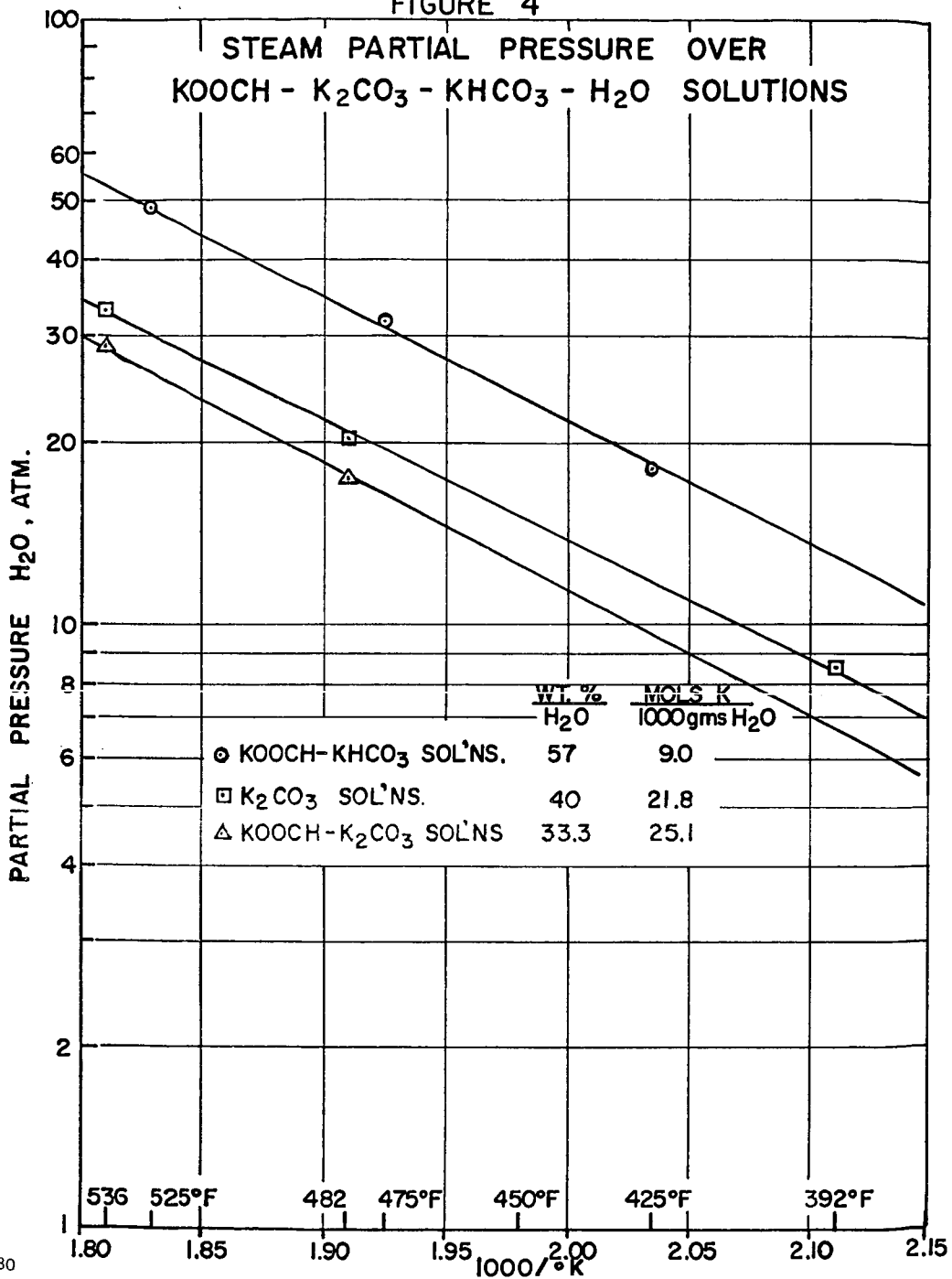


FIGURE 5
STEAM PARTIAL PRESSURE
vs SALT CONCENTRATION

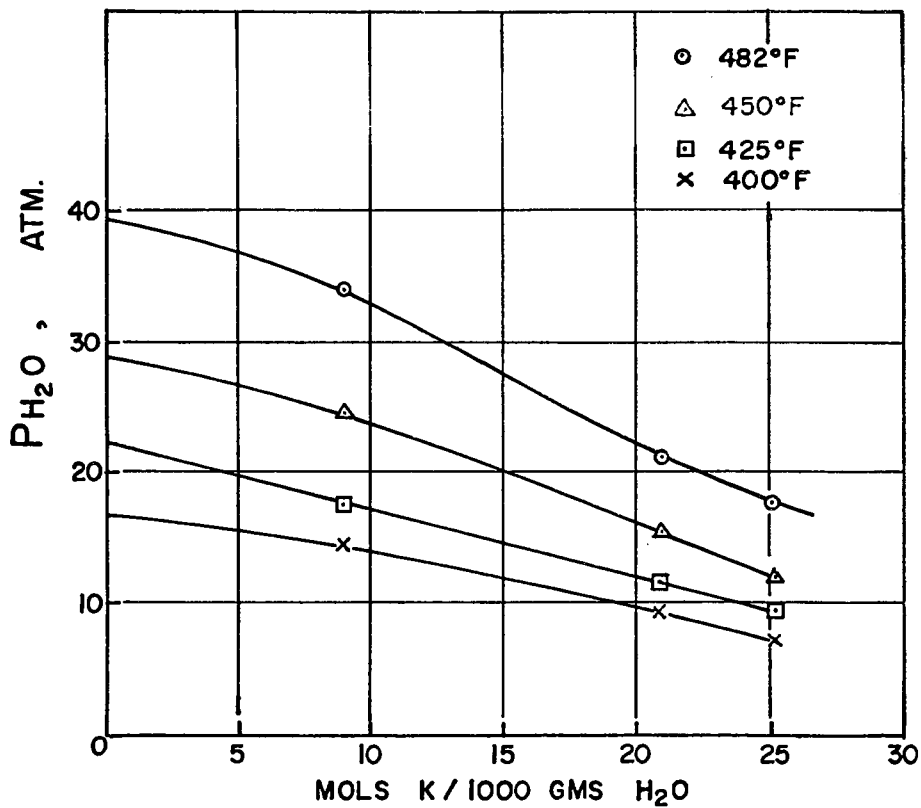


FIGURE 6
EQUILIBRIUM DATA
DECOMPOSITION AQUEOUS KOOCH

$$\frac{\text{Mols K}}{1000\text{gms H}_2\text{O}} = 9.0$$

$$\text{WT. \% H}_2\text{O} \cong 57$$

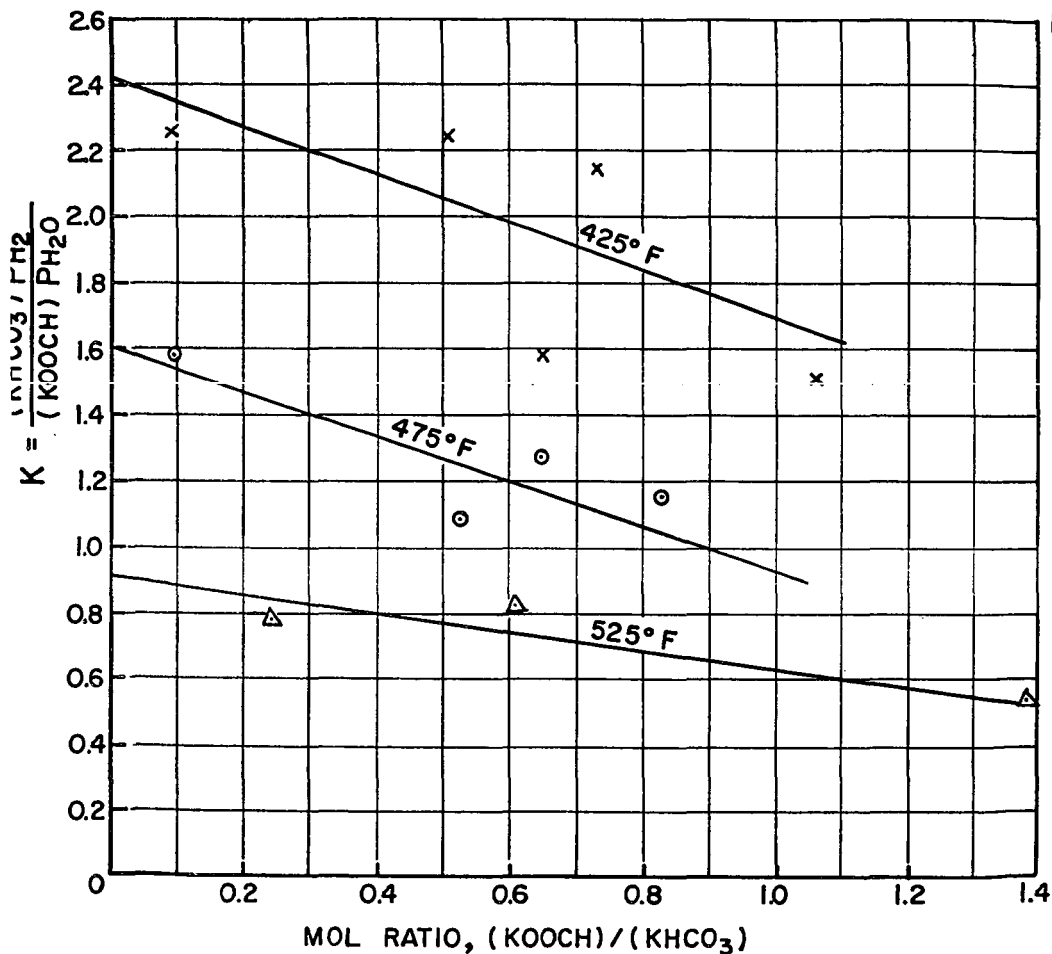


FIGURE 7
EQUILIBRIUM HYDROGEN PRESSURE
VS FRACTION KOOCH DECOMPOSED

		SMOOTHED DATA POINTS	
		TEMP. °F	P _{H₂O} -ATM
WT. % H ₂ O ≈ 57	△	525	48.9
$\frac{\text{Mols K}}{1000 \text{ gms H}_2\text{O}} = 9.0$	○	475	32.0
	x	425	17.8

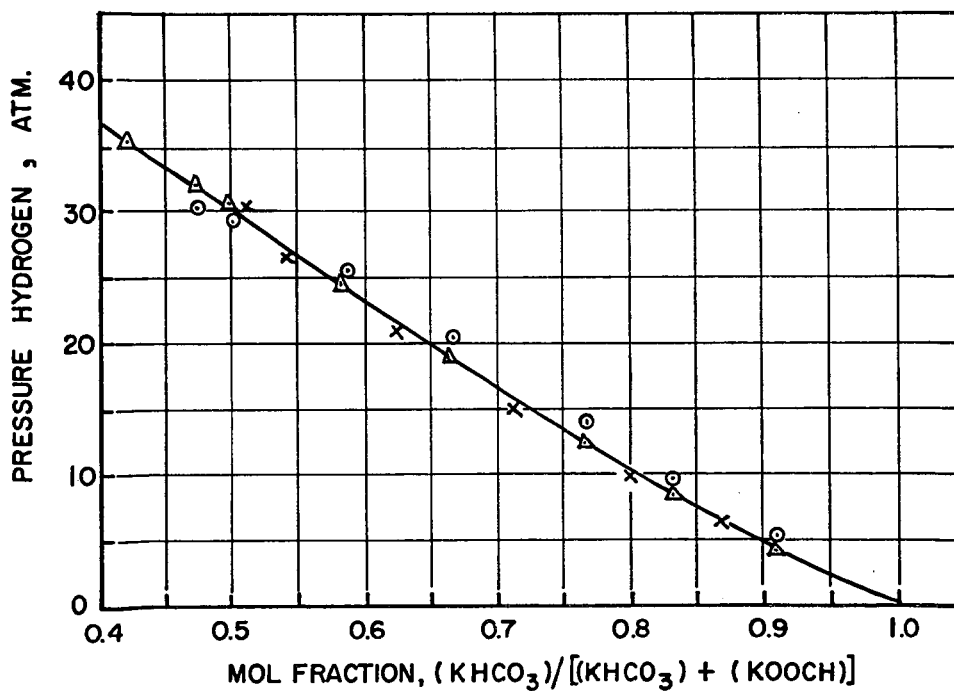


FIGURE 8

COMPARISON OF DATA ON PARTIAL
PRESSURE OF CO₂ OVER
POTASH SOLUTIONS

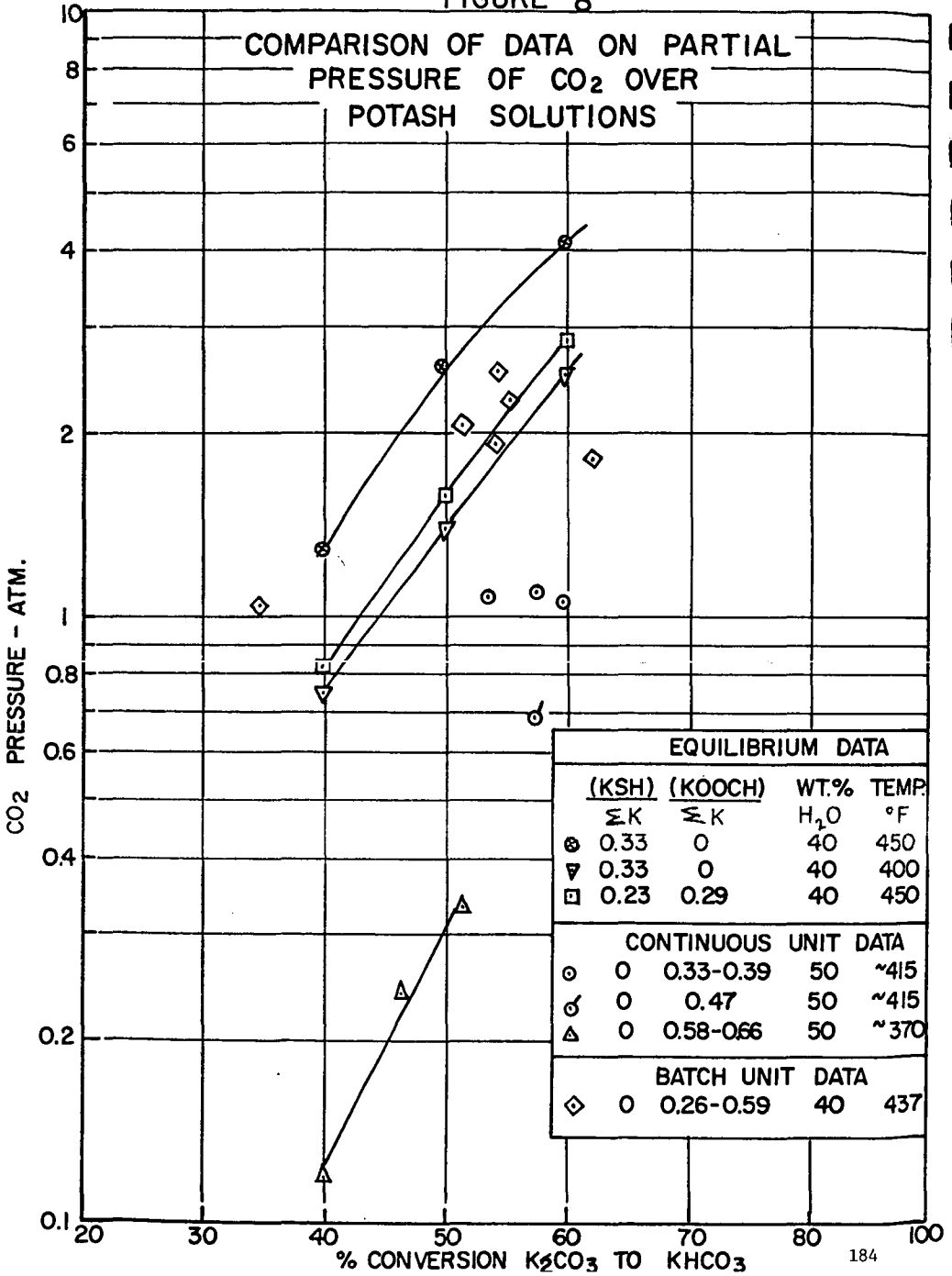


FIGURE 9
 APPROACH TO EQUILIBRIUM IN CATALYTIC
 DECOMPOSITION OF AQUEOUS KOOCH

$\frac{\text{MOLS K}}{1000 \text{ GMS H}_2\text{O}} = 12.5$		<u>TEMP. °F</u>	<u>P_{H₂O}-ATM.</u>	
	△	EQUIL. LINE	525	22.2
	○	" "	475	24.6
	⊙	" "	425	27.7
		EXPTL. POINTS		
	△		525	22.2
	○		475	24.6
	x		425	27.7

WT. % H₂O = 50.5

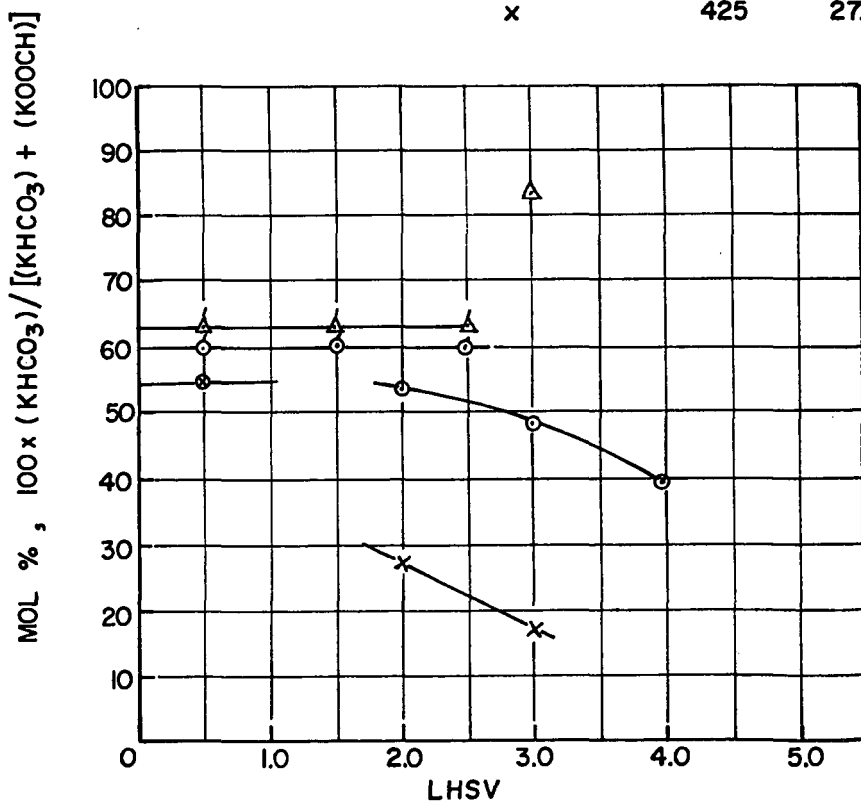


FIGURE 10
 CATALYST LIFE IN KOOCH DECOMPOSITION

TEMP. 475°F LHSV = 3 OP. PRESS. = 774 PSIA

$\frac{\text{MOLS K}}{1000 \text{ GMS H}_2\text{O}} = 12.5$ WT. % H₂O = 50.5

